THE GEOCHEMISTRY AND GEOCHRONOLOGY OF THE SHELBURNE DYKE OF NOVA SCOTIA AND THE MESSEJANA DYKE OF SPAIN

Andrew McKenzie Dunn

Submitted in Partial Fulfilment of the Requirements
for the Degree of Bachelor of Sciences,
Department of Earth Sciences
Dalhousie University, Halifax, Nova Scotia
March 1994

Dalhousie University

Department of Earth Sciences
Halifax, Nova Scotia
Canada B3H 3J5
(902) 494-2358
FAX (902) 494-6889

DATE April 25, 1994

AUTHOR Andrew McKenzie Dunn

TITLE THE GEOCHEMISTRY AND GEOCHRONOLOGY OF THE SHELBURNE DYKE OF NOVA SCOTIA AND THE MESSEJANA DYKE OF SPAIN.

Degree B.Sc. Convocation May Year 1994

Distribution License

DalSpace requires agreement to this non-exclusive distribution license before your item can appear on DalSpace.

NON-EXCLUSIVE DISTRIBUTION LICENSE

You (the author(s) or copyright owner) grant to Dalhousie University the non-exclusive right to reproduce and distribute your submission worldwide in any medium.

You agree that Dalhousie University may, without changing the content, reformat the submission for the purpose of preservation.

You also agree that Dalhousie University may keep more than one copy of this submission for purposes of security, back-up and preservation.

You agree that the submission is your original work, and that you have the right to grant the rights contained in this license. You also agree that your submission does not, to the best of your knowledge, infringe upon anyone's copyright.

If the submission contains material for which you do not hold copyright, you agree that you have obtained the unrestricted permission of the copyright owner to grant Dalhousie University the rights required by this license, and that such third-party owned material is clearly identified and acknowledged within the text or content of the submission.

If the submission is based upon work that has been sponsored or supported by an agency or organization other than Dalhousie University, you assert that you have fulfilled any right of review or other obligations required by such contract or agreement.

Dalhousie University will clearly identify your name(s) as the author(s) or owner(s) of the submission, and will not make any alteration to the content of the files that you have submitted.

If you have questions regarding this license please contact the repository manager at dalspace@dal.ca.

Grant the distribution license by signing and dating below.

_____ _____

Name of signatory Date

Abstract

This paper is a geochemical and geochronological study of two rift-related Mesozoic basaltic dykes. The Shelburne Dyke of Nova Scotia and the Messejana Dyke of Spain are extensive vertical sheets of intrusive rock that are over 100 kilometres in length, average 100 metres in thickness, and strike northeast-southwest at a latitude of 44°N. An outcrop of the Shelburne Dyke crops out in Little Harbour, where it intrudes metawackes and metapelites of the Cambro-Ordovician Meguma Group. The Messejana Dyke crops out in Cabezuela de Valle and intrudes a body of sillimanite-bearing, two-mica granite belonging to the Tournaisian and Lower Visean Volcanic-Siliceous Complex. The two dykes contain plagioclase and pyroxene, with minor biotite, olivine, and opaque minerals, and have subophitic to ophitic textures. Chemical classification plots show that the Shelburne and Messejana Dykes are tholeiites and, according to the CIPW normative tetrahedron, they are quartz normative. Major elements such as Fe and Mg show little or no effects of chemical variation, whereas many compatible and incompatible trace elements show fractional crystallization. The removal of Ni and Cr from the melt in olivine and chrome spinel causes passive enrichment of other trace elements such as Sr, Ba, and Rb. The REE patterns for the two dykes show low La/Yb_N (2.9-3.7) values and small Eu/Eu* (0.89-1.08) anomalies. Tectono-magmatic discriminator diagrams suggest the Shelburne and Messejana Dykes are within-plate basalts transitional to ocean floor basalts, however, some discriminator diagrams suggest the involvement of a subduction-derived component. The $^{40}Ar/^{39}Ar$ dating method shows that the intrusion of the Shelburne and Messejana Dykes straddles the Triassic-Jurassic boundary (208 Ma). Three models to explain the relationship between the two dykes are: one-dyke model, two parallel dyke model, and two dyke perpendicular model. The simplest model that fits all the analytical data is the two parallel dykes model, i.e. the Shelburne and Messejana Dykes were two contemporaneous dykes on opposite sides of the principal rift that formed the North Atlantic Ocean.

Keywords: Shelburne, Messejana, tholeiite, rift, within-plate basalts, ocean floor basalts, $^{40}Ar/^{39}Ar$, Triassic-Jurassic, Atlantic Ocean

TABLE OF CONTENTS

TABLE OF FIGURES

TABLE OF TABLES

ACKNOWLEDGEMENTS

I would like to recognize and thank the following people who provided assistance and support during all stages of work on this thesis; Dr. D.B. Clarke for suggesting the topic and supervising every step of the way, Dr. R. Jamieson for all the constructive criticism, Andy Henry for the help preparing the samples for analysis and all help with the geochemical diagrams, Dr. P.H. Reynolds and Keith Taylor for all the work done in the lab and help with the interpretation of the geochronological data, Professor J.M. Ugidos of the University of Salamanca for maps and field descriptions of the Messejana Dyke, and last but certainly not least my parents and C.A. Britten for the help in putting the entire thesis together. Without their support completion of this thesis would not have been possible.

CHAPTER 1: INTRODUCTION

1.1 Introduction

This paper presents a study of two Mesozoic, rift-related dykes: (1) the Shelburne Dyke of southern Nova Scotia, as exposed at Little Harbour, Latitude 44°10'6" and Longitude 64°29'; and (2) the Messejana Dyke of western Spain, as exposed at Cabezuela de Valle, Latitude 44°12' and Longitude 5°48'. This chapter provides the background information necessary to understand the rest of the report, and also includes a statement of the purpose and a definition of the scope of the thesis. Following these is a brief section discussing the relationship between magmatism and crustal extension. The final section outlines the organization of the entire paper.

1.2 Purpose

The purpose of this paper is to compare the Shelburne Dyke with the Messejana Dyke in Spain on the basis of whole-rock geochemistry and $^{40}Ar/^{39}Ar$ geochronology. Both of these types of investigations have been the topics of previous studies, but with less precise analytical techniques, and with no direct comparison between the dykes of the two areas.

1.3 Scope

The principal tools used in this comparison are whole-rock geochemistry (major elements, trace elements, and rare earth elements) and geochronology ($^{40}Ar/^{39}Ar$ release

patterns on minerals and whole rocks). This study does not include mineral chemistry, other than the composition of the biotites used for age determination.

Samples come from only one locality in each of Nova Scotia and Spain; thus, a comparison of the two assumes that they fairly represent the entire dykes.

1.4 The Relationship Between Magmatism and Crustal Extension

1.4.1 Definitions

Previous work on the Shelburne and Messejana Dykes shows that they are related to an early phase of the opening of the Atlantic Ocean. However, before discussing the tectonics of extension in general and the Eastern Canadian and Iberian margins in particular, this section defines some of the structures and magma types used throughout this thesis.

A graben, according to Mohr (1982), is a simple, parallel-sided, downfaulted valley with a width ranging from a few hundred metres to as much as ten kilometres (Figs. 1.1, 1.2). A rift valley is a large (tens to hundreds of kilometres wide), parallel-sided, downfaulted valley whose floor may contain a complex of grabens and faults. These valleys are commonly asymmetric about their horizontal axes and, where a faulted margin faces a downfaulted valley, a half-graben forms (Mohr, 1982) (Figs. 1.1, 1.2).

Three types of magma emplacement are important in extensional environments. The first, which is most directly related to this paper, is the dyke. A dyke is a discordant (cuts across structures in the country rock), tabular or sheet-like body of intrusive rock that forms when magma moves into planar fractures in surrounding rock.

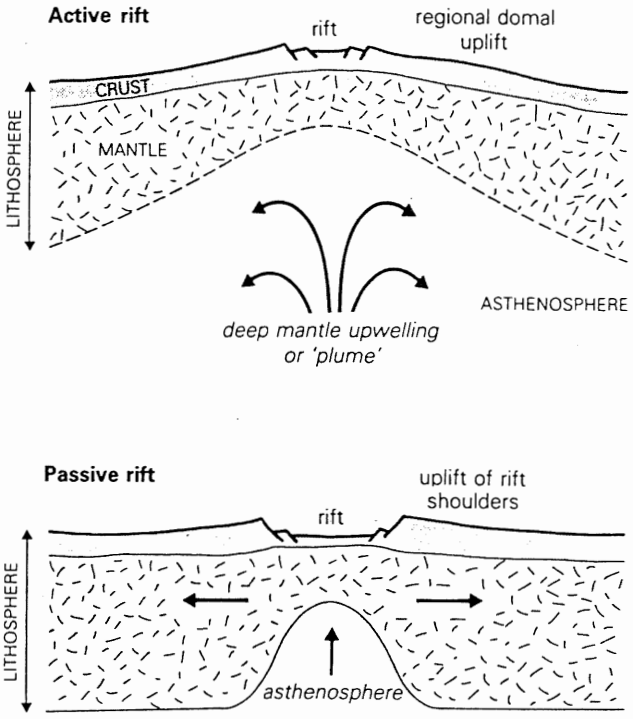

FIGURE 1.1 Active vs. passive rifting (from Wilson 1989). In active rifting, asthenospheric upwelling thins and causes uplift of the lithosphere and controls rift formation. In passive rifting, the mantle is forced to rise as the continents are pulled apart during the lithospheric stretching.

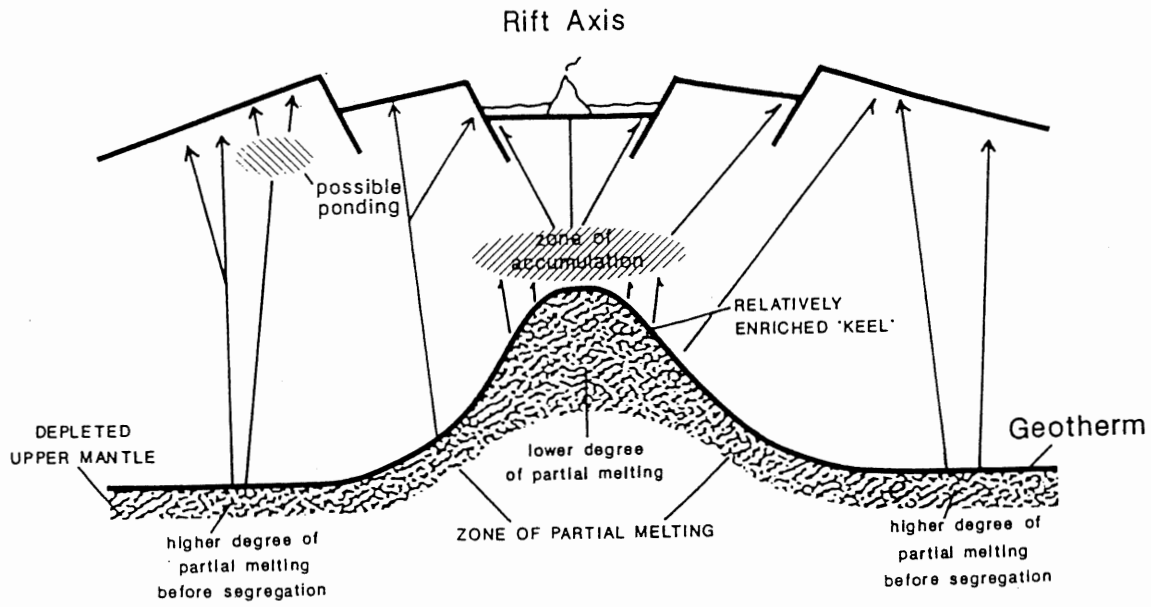

FIGURE 1.2 Conceptual picture for Mesozoic basaltic magmatism along Eastern North America (from Cummins et al. 1992). This cross-section shows a fully developed rift-basin setting and follows the description of the passive model of continental rifting.

A sill is a concordant (does not cut across bedding or structures in the country rock), tabular or sheet-like intrusive body. A basaltic lava flow may form a plateau of extrusive rocks when magma erupts onto a subhorizontal surface from fissures at the Earth's surface.

1.4.2 Continental Rift Zone Magmatism

Basaltic magmatism is a common product of extensional tectonics, both in oceans and in continents. Extension of the plates forms graben structures where the magmatic activity concentrates. Continental rift zones are areas of localized lithospheric stretching characterized by a central depression, uplifted flanks, and a thinning zone of the underlying crust (Wilson 1989). High heat flow and regional uplift also occur in continental rift structures.

Continental rifting may be the precursor to the formation of new ocean basins (e.g., the Red Sea). Many rift valleys, both active and inactive, occur on continents world-wide. Some of these rifts may eventually form new ocean basins, but many stop after only minor extension (failed rifts). The Bay of Fundy is an example of a rift that failed to open at the time the Atlantic Ocean was forming (Pe-Piper et al. 1992).

The question now is, what are the mechanisms that lead to the formation to continental rift zones? Two hypotheses that attempt to explain the process are active rifting and passive rifting (Fig. 1.1). Active rifting involves the ascent of the asthenosphere. This upwelling thins and raises the lithosphere, and also controls rift formation (Wilson 1989). The upwelling can be two-dimensional, associated with mid-

ocean ridges, or one-dimensional, associated with mantle plumes. In active rifting, volcanism and doming precede rifting. On the other hand, passive rifting involves differential stresses in the lithosphere, i.e. rising magma forces the continents to pull apart during lithospheric stretching (Wilson 1989). In this example, the rift forms first and, as a result of small-scale convection cells, uplift of the rift flanks follows.

1.4.3 Tectonics and Magma Types of Eastern Canada

Igneous rocks in eastern Canada formed during the late stages of early Mesozoic rifting prior to the opening of the central Atlantic Ocean (Pe-Piper et al. 1992). Because of the extent of lithospheric stretching, the style is consistent with the passive model of extensional rifting (Fig. 1.2). According to Pe-Piper (1992), three distinct tectonic and igneous phases related to the emplacement of the rocks on the eastern Canadian margin are:

1) Basins formed by extension along normal faults, during the Anisian to early Hettangian (242-200 Ma) (Fig. 1.3) filled with up to 2 kilometres of terrigenous clastics and evaporites. Associated with this first phase is minor magmatism, in the form of dykes.

2) Rapid subsidence of the central rift zone occurred during the late Hettangian to Bajocian (200-180 Ma) and resulted in tilting of the hinge zone. This tilting formed an unconformity in the sediments accumulating in the rift. This post-rift unconformity (build-up of younger sediments, after rifting, on top of a tilted surface of older rocks) is not a breakup unconformity (deposition of sediments during the rifting).

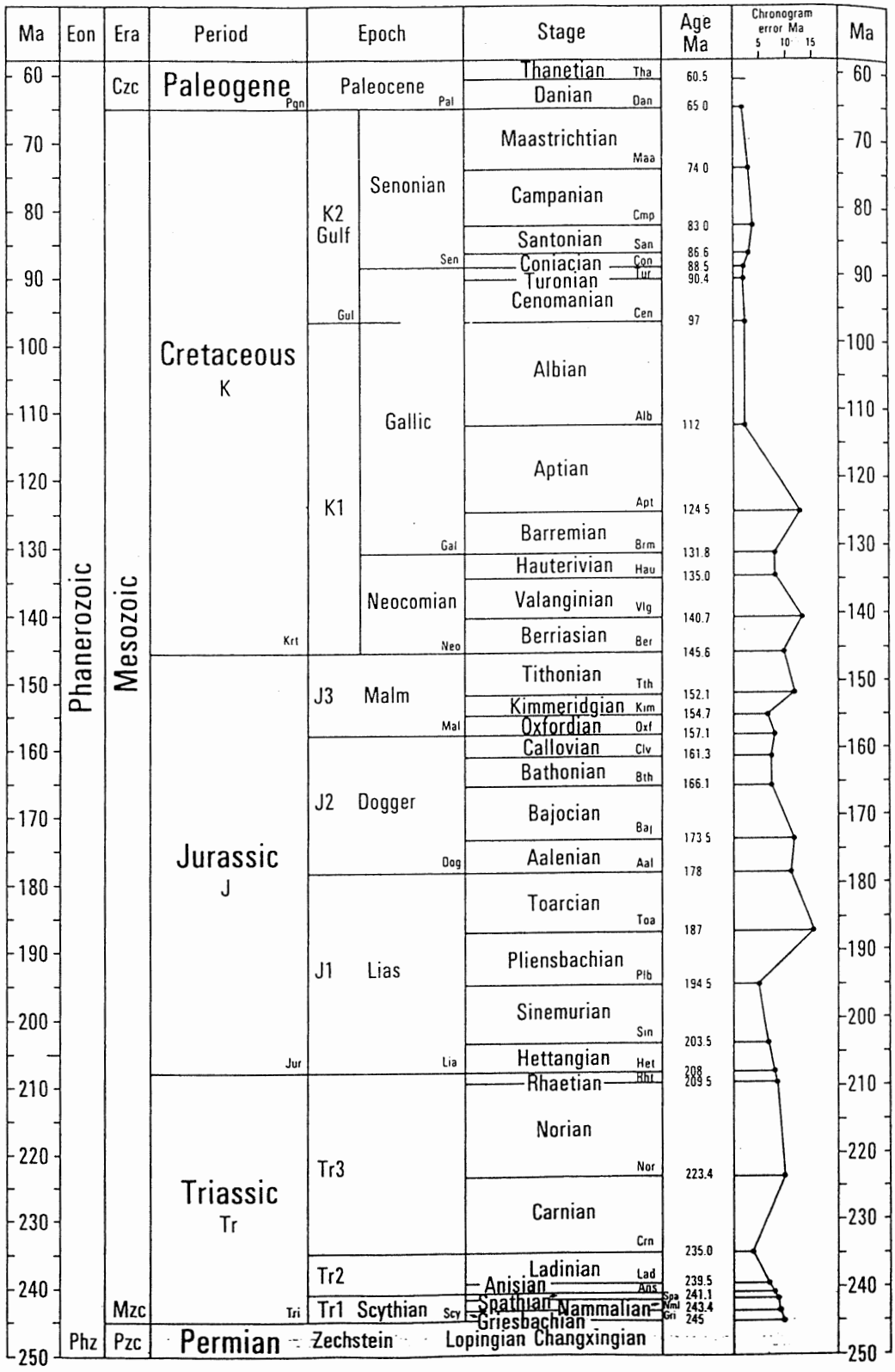

FIGURE 1.3 Mesozoic Time Scale (from Harland et al. 1990)

Magmatic activity along eastern Canada accompanied the tilting of the hinge. The total volume of igneous rock is small and, therefore, was probably emplaced over a relatively short period of time. This emplacement history indicates the importance of suitable tectonic pathways to permit the magma to rise to the surface.

3) The final phase occurred 180 My ago, during the Bajocian, and represented the first creation of oceanic crust and separation of the continental plates.

The rift-related Mesozoic basaltic rocks occur in a variety of modes along the margin of eastern Canada (Cummins et al. 1992). They occur as flows, sills, and dykes (Fig. 1.4). The basaltic flows occur around the Bay of Fundy, on the Scotian Shelf, and on the Grand Banks. Sills predominate in the eastern section of the United States. The dykes, found throughout the Atlantic provinces, tend to be large. The Avalon, Caraquet, and Shelburne Dykes are examples of these linear intrusive bodies.

1.5 Tectonics of the Messejana Dyke

The Messejana Dyke was emplaced along the Messejana Fault system. The exact age of the fault is unknown, but as it is post-Hercynian it must have been formed sometime during the Late Carboniferous to Early Triassic Periods (Schermerhorn et al. 1978). It is parallel to the Central Atlantic rift between Northwest Africa and North America, but not to the rift between Iberia and the Grand Banks; therefore, Schermerhorn et al. (1978) inferred that the fault is related to the Central Atlantic rift and reflects stresses created during the initial rifting stage.

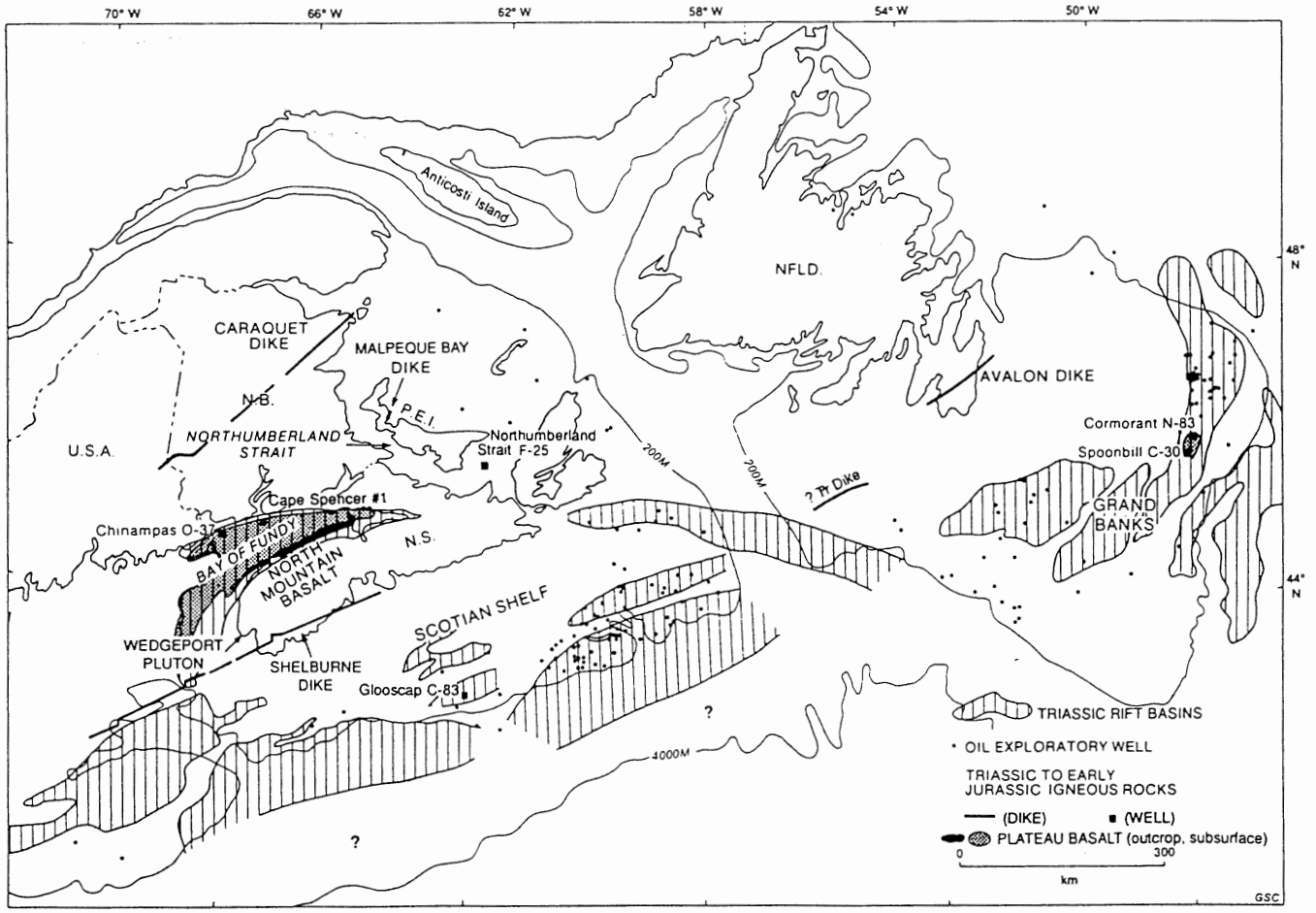

FIGURE 1.4 Location map showing onshore and offshore occurrences of Late Triassic-Early Jurassic igneous rocks and schematic outlines of Triassic rift basins (from Pe-Piper et al. 1990).

The magma that formed the Messejana Dyke intruded the fault when crustal tension opened a long fissure (Schermerhorn et al. 1978). The tholeiitic magma formed by partial melting in the upper mantle and ascended a major discontinuity extending through the crust (Schott et al. 1981).

The mechanism that led to the formation of the rifts on the European side of the Atlantic also is consistent with the passive style (Fig. 1.5). The upwelling of mantle material initiated and sustained plate separation from the continental breakup to the creation of oceanic lithosphere to seafloor spreading (Schermerhorn et al. 1978). Updoming caused crustal extension, and igneous activity started after the initial fracturing and rifting when fissures in the crust tapped the upper mantle.

Seafloor spreading, lithosphere separation, and the generation of oceanic crust began around 180 Ma, in the Early Jurassic (Schermerhorn et al. 1978). The North Atlantic Ocean began opening in the south, when North America split away from Africa (Ziegler 1989). Once detached, the continents moved away from each other and from the site of igneous activity along the mid-ocean ridge. Although the continental margins became passive trailing plate-edges, magmatic activity on them did not stop with the start of spreading on the east coast of North America or the west coast of Africa and Portugal, but continued until the Early Tertiary (Schermerhorn et al. 1978).

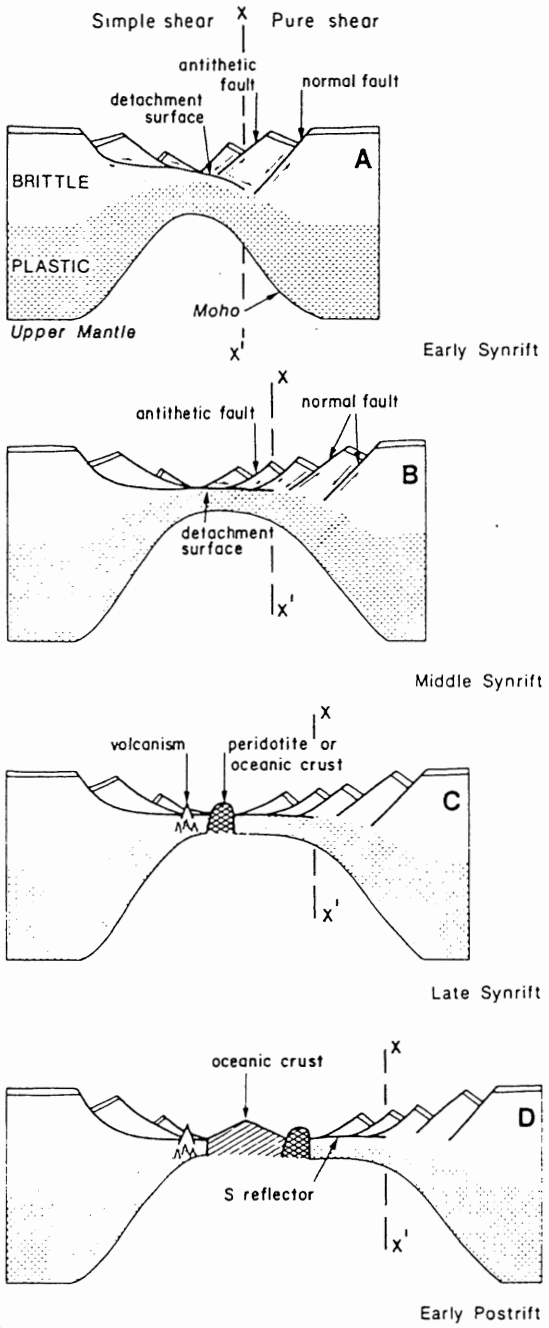

FIGURE 1.5 A four-step model of formation of rifts around Iberia (from Sibuet 1992) A. The detachment surface that has been active from the Canadian side to the Iberian side cuts the upper portion of the continental crust and merges at depth with the former brittle-plastic transition. B. The displacement along the detachment surface decreases eastward from the Canadian side to zero below the Iberian margin. C. At the end of the rifting phase, when the crust is thinned, upper mantle material rises. D. After the creation of oceanic crust, the continental lithosphere cools and the brittle-plastic transition sinks, leaving the former transition within the present-day, brittle upper crust.

1.6 Organization

The remainder of this paper consists of five more chapters. Chapter 2 deals with the locations and petrology of the two dykes. An understanding of the geological setting of the dykes, and of their mineralogy and textures, is important before determining geochemistry and geochronology, discussed in Chapters 3 and 4, respectively. Chapter 5 includes integration and discussion of all the new data, and the relationship between the Shelburne and Messejana Dykes and the evolution of the North Atlantic Ocean. The final chapter summarizes all the conclusions drawn throughout the paper.

CHAPTER 2: FIELD RELATIONS AND PETROLOGY

2.1 Introduction

This chapter begins the detailed investigation of the Shelburne and Messejana Dykes with descriptions of the geological setting, field relations, and petrology of the two dykes, based on a combination of previous work and current samples. This chapter ends with a summary and comparison of the two dykes.

2.2 Shelburne Dyke

The Shelburne Dyke extends from Lower West Pubnico to West Ironbound Island, a distance of 140 km (Papezik and Barr 1981). Faribault (1911, 1913, 1919) first mapped and described the Shelburne Dyke, and although it is mentioned in a few papers (Papezik et al. 1975, Hodych and Hayatsu 1980, Pe-Piper et al. 1992, Puffer 1992, and Cummins et al. 1992), the only other major investigations into the dyke are a paleomagnetic study by Larochelle and Wanless (1966) and a thesis by Lawrence (1966).

2.2.1 Geological Setting

The Shelburne Dyke cuts the metasedimentary rocks of the lower Paleozoic Meguma Group and some granitoid plutonic rocks of Devonian-Carboniferous age (Papezik and Barr 1981).

The Meguma Group was deposited during the Cambrian-Ordovician period and consists of a thick sequence of deep-sea turbidites (Schenk 1991). This sequence can be

divided into two formations: the Goldenville Formation, which consists of sandy marine sediments and the Halifax Formation, which consists of muddy or shaly marine sediments (Schenk and Lane 1982). These formations accumulated on the continental margin of Gondwana and constitute a proximal and distal turbidite fan sequence, respectively (Schenk and Lane 1982, Schenk 1991). The Acadian orogeny deformed and metamorphosed the rocks of the Goldenville and Halifax Formations (Keppie and Dallmeyer 1987, Muecke et al. 1988). At about 370 Ma (Clarke et al. 1993), a major magmatic event emplaced large volumes of peraluminous granite into the Meguma Group. The Shelburne Dyke intruded much later in Triassic-Jurassic time, during the early phases of the opening of the North Atlantic Ocean (Papezik and Barr 1981).

The age of the Shelburne Dyke, determined by several workers using various methods, lies in the 193-201 Ma range (Table 2.1). Chapter 4 presents new data on the age of the Shelburne Dyke.

2.2.2 Outcrop Description of the Exposure at Little Harbour

The present study area of the Shelburne Dyke is Little Harbour, Latitude 44°10'6" N and Longitude 64°29' W, in southern Nova Scotia (Fig. 2.1). The Shelburne Dyke at this locality is well exposed in coastal outcrop. Although the actual contacts between the Goldenville Formation and the dyke are not visible, the fine-grained rocks on the edges of outcrop indicate that the true contacts are about 10 cm from these edges. The width of the Shelburne Dyke in this area is approximately 100 m, and the strike is northeast-southwest (65°) with a vertical dip.

Location	Method	Date (Ma)	Reference
Shelburne	K/Ar i/c	201	Hodych and Hayastu, 1980
Shelburne	Paleomagnetism	179	Hozik, 1992
Shelburne	K/Ar wr i/c	193±3	Hodych and Hayastu, 1988
Shelburne Lat. 69° N Long. 98° W	K/Ar	197	Schott et al. 1981

Key:
K/Ar- Potassium/Argon
i/c- Isochron Method
wr- Whole Rock

TABLE 2.1 Previous geochronological work on the Shelburne Dyke

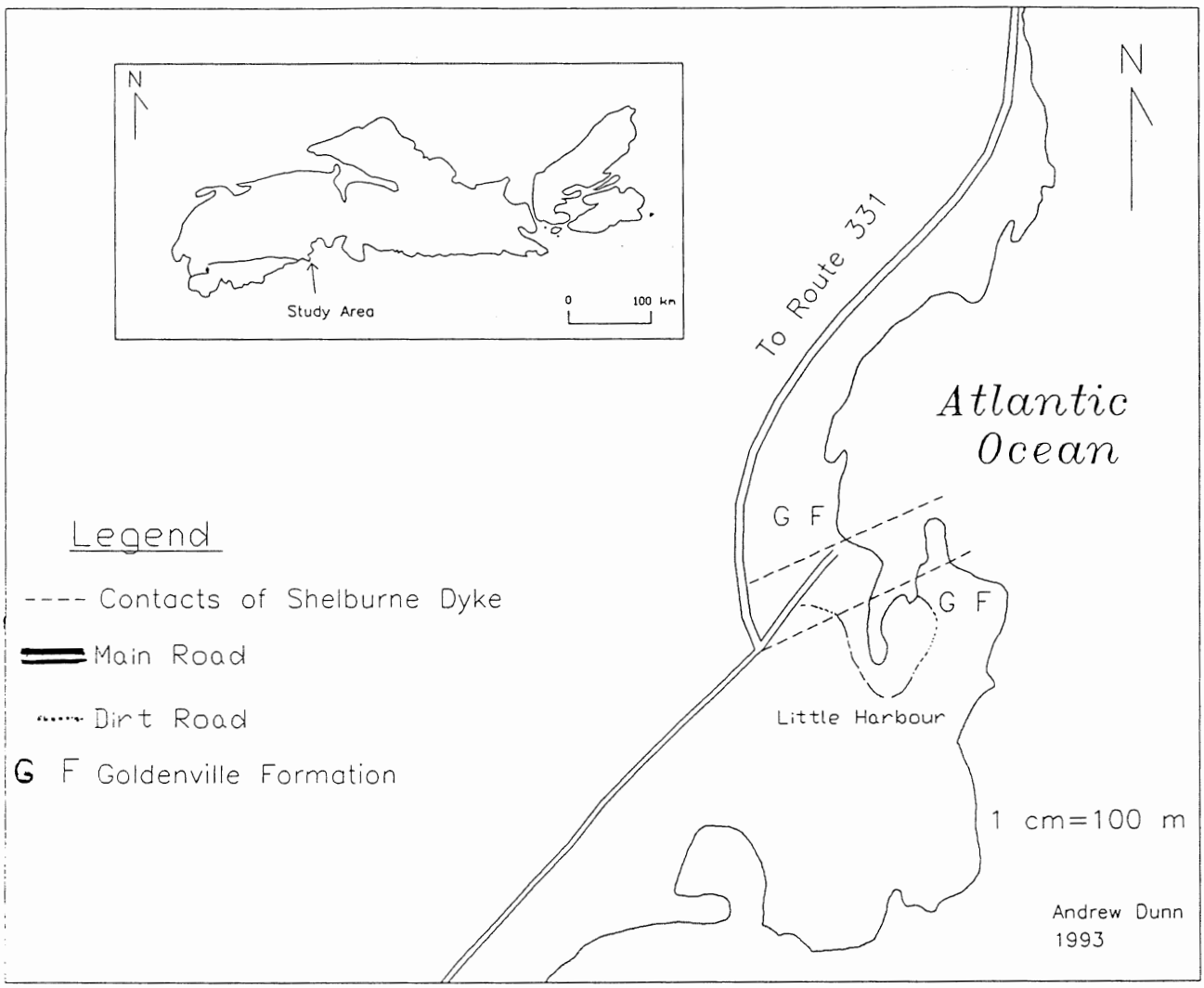

FIGURE 2.1 Location map of Little Harbour, Nova Scotia

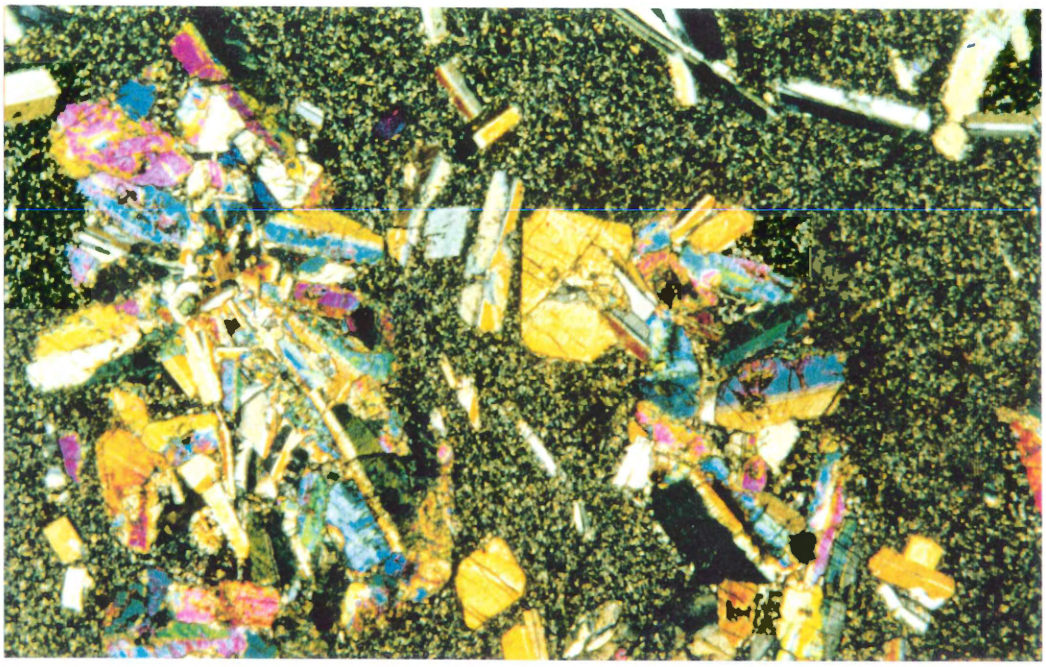

FIGURE 2.2 (SD93-1) Fine-grained margin of the Shelburne dyke showing plagioclase and pyroxene microphenocrysts set in cryptocrystalline groundmass. (width of photo is 2 cm.)

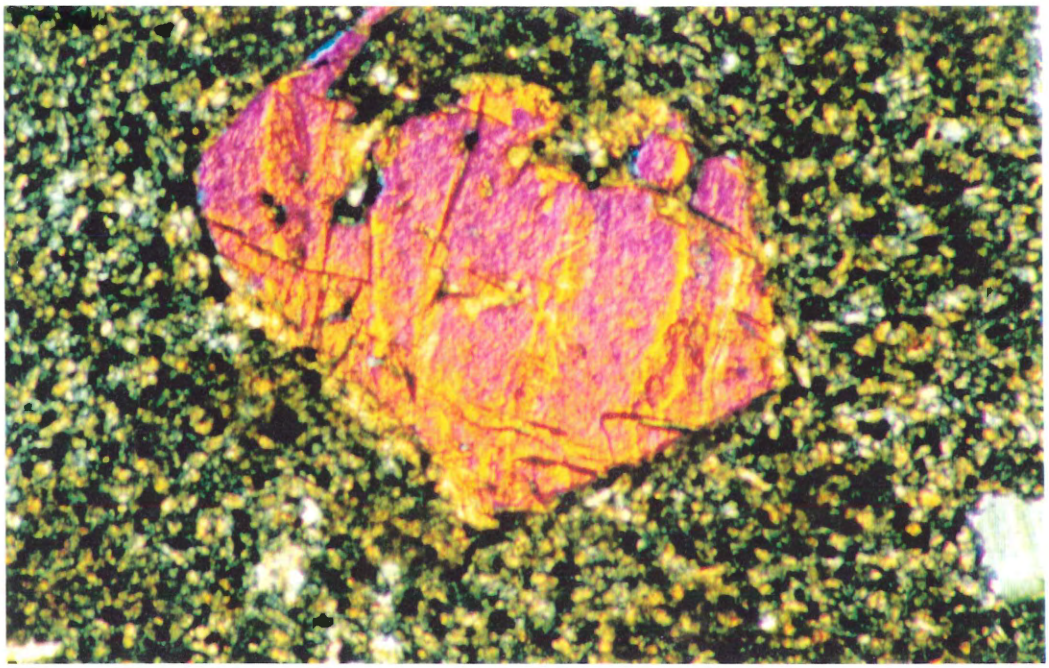

FIGURE 2.3 (SD93-7) Subhedral to skeletal orthopyroxene microphenocryst set in cryptocrystalline groundmass. (width of photo 1 cm.)

2.2.3 Petrological Description

According to Papezik and Barr (1981), the Shelburne Dyke is generally coarse-grained and diabasic in appearance. The dyke has fine-grained chilled margins and a coarser-grained interior. The chilled margins are several metres in width, and consist of a dense, fine-grained rock with microphenocrysts of plagioclase and pyroxene. The microphenocrysts are zoned labradorite, augite, and orthopyroxene. These microphenocrysts, according to Papezik and Barr (1981), comprise approximately 20-50% of the rock, the rest of which is a cryptocrystalline to intersertal groundmass.
The interior of the dyke consists mainly of labradorite and clinopyroxene in intergranular to subophitic texture. The pyroxenes have commonly reacted to chlorite, biotite and (or) amphibole. Opaque minerals (titanomagnetite and ilmenite), and interstitial granophyre (intergrowth of quartz and feldspar) occur in 10-20% of the rock.

The following petrological description is of samples and thin sections of the Shelburne Dyke from Little Harbour (Appendix A). The chilled margin of the dyke is a fine-grained rock that contains microphenocrysts of plagioclase, pyroxene, and minor olivine (Fig. 2.2). These microphenocrysts make up approximately 30-40% of the rock. The pyroxenes are predominantly orthopyroxene, with minor augite (Fig. 2.3). The olivine is commonly altered to iddingsite. The texture is inequigranular and glomeroporphyritic, with a subophitic relationship between the plagioclase and pyroxene (Fig. 2.2).

The center of the dyke is holocrystalline, coarse-grained, and equigranular. The minerals are plagioclase, pyroxene, biotite, opaques, and minor olivine (Fig. 2.4). The

pyroxenes are almost entirely clinopyroxene, commonly associated with late growths of biotite (Figs. 2.5-2.7). Minor amounts of micrographic intergrowths of quartz and feldspar (granophyre) occur interstitially. An ophitic to subophitic relationship occurs between the plagioclase and pyroxene.

The country rock, represented here only by a narrow pelitic band of the Goldenville Formation from the Meguma Group, contains abundant biotite and chlorite that comprise 30-40% of the rock, with minor muscovite, and opaque minerals that comprise only 10-20% (Fig. 2.8). Quartz and feldspar comprise the remaining 20-40% of the rock. The biotites generally occur as ovoid porphyroblasts (Fig. 2.9).

2.3 Messejana Dyke

The Messejana Dyke cuts diagonally across the Iberian Peninsula, from Odemira on the Atlantic coast of Portugal to Avila near the geographical centre of Spain (Schermerhorn et al. 1978) (Fig. 2.10), a distance of about 530 km (Schott et al. 1981). Study of the Messejana Dyke has taken place for more than seventy years.

Pereira first discovered the dyke in the 1920's. Torre de Assuncao (1949, 1951, 1957) provided a detailed description of the Messejana Dyke. Brak-Lamy (1949) provided the first chemical analyses of the dyke. In 1951 Fieo studied the geomorphology of the dyke in south Portugal. Zbyszewski and Freire de Andrade (1957) were the first to name the dyke the Messejana dolerite dyke. Quesada Garcia (1960) provided a detailed petrological description of the dyke.

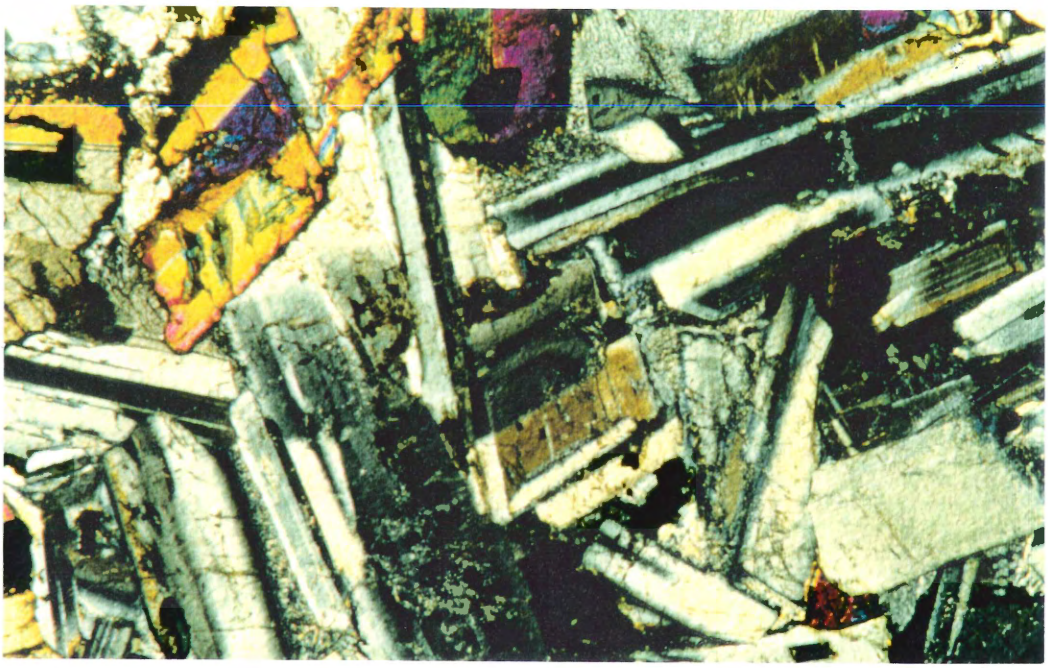

FIGURE 2.4 (SD93-6) Coarse-grained, equigranular centre of the Shelburne dyke showing plagioclase and clinopyroxene in subophitic relationship (width of photo 3 cm.).

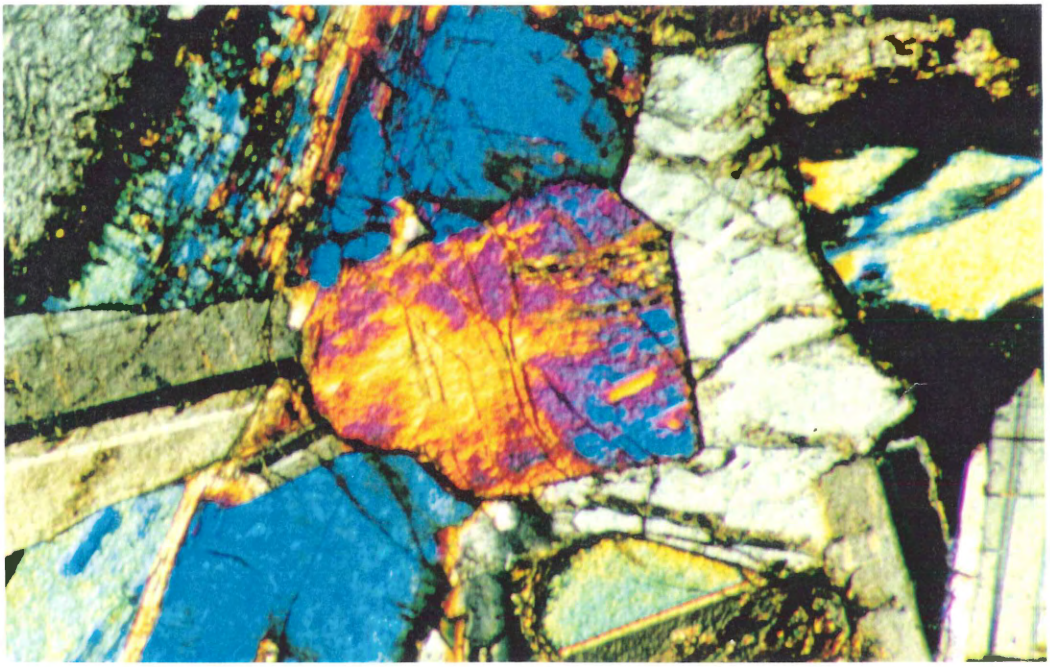

FIGURE 2.5 (SD93-6) Subhedral clinopyroxene microphenocryst showing subophitic relationship with plagioclase (width of photo 1.5 cm.).

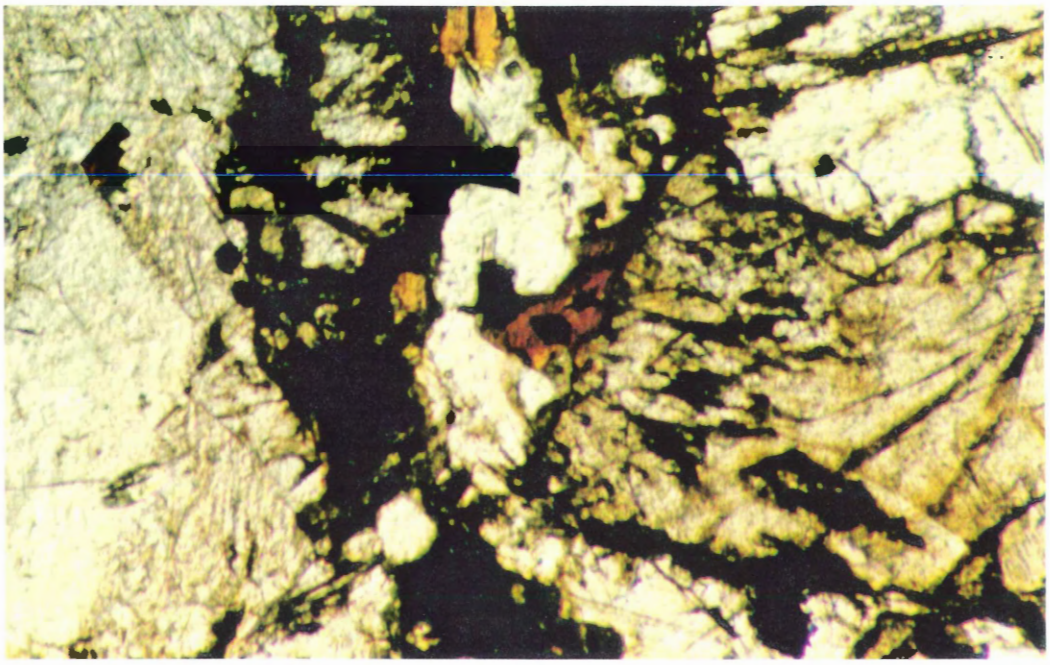

FIGURE 2.6 (SD93-6) Clinopyroxene with late overgrowth of biotite in plane polarized light (width of photo 1.5 cm.).

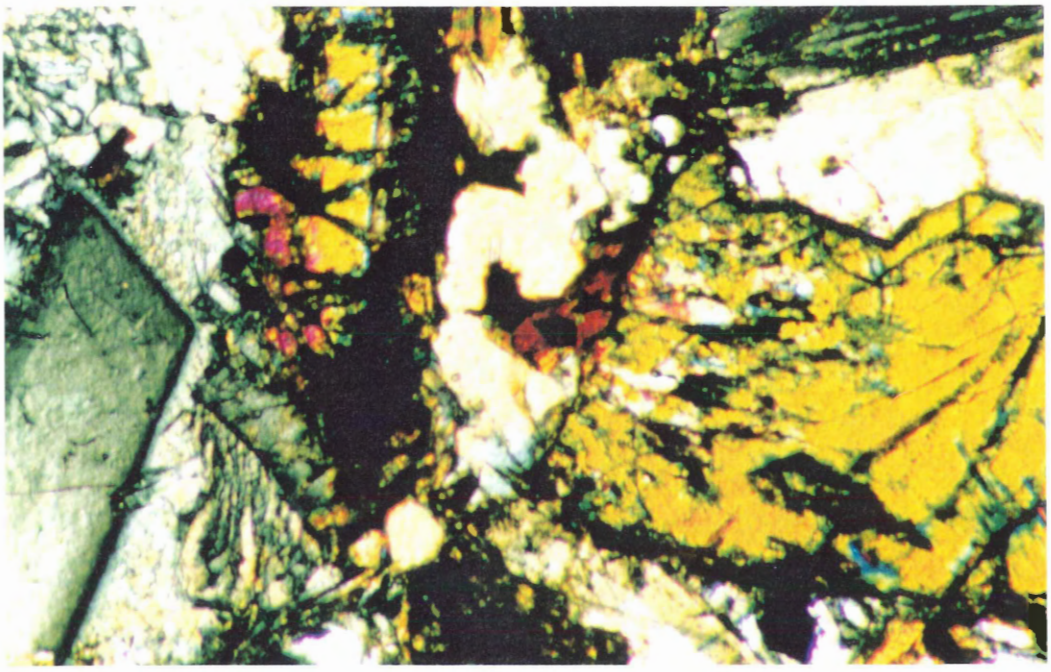

FIGURE 2.7 (SD93-6) Clinopyroxene with biotite growth in crossed polars (width of photo 1.5 cm.).

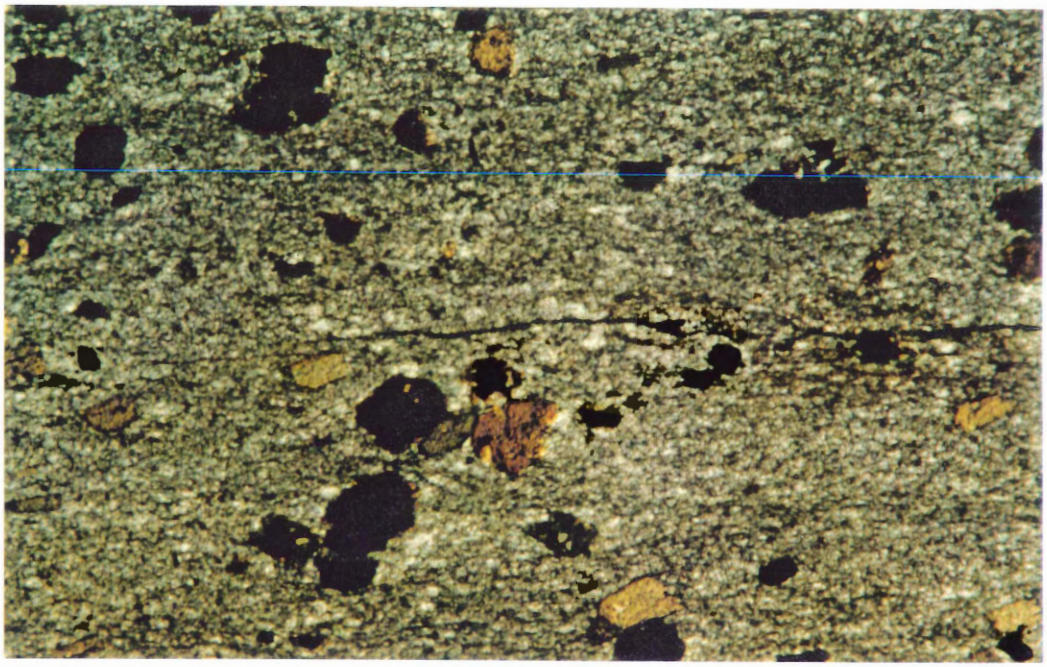

FIGURE 2.8 (SD93-4) Pelitic band in Goldenville metawacke. Shows ovoid porphyroblasts of biotite and chlorite, with minor opaque minerals in matrix of muscovite, quartz and feldspars (width of photo 4 cm.).

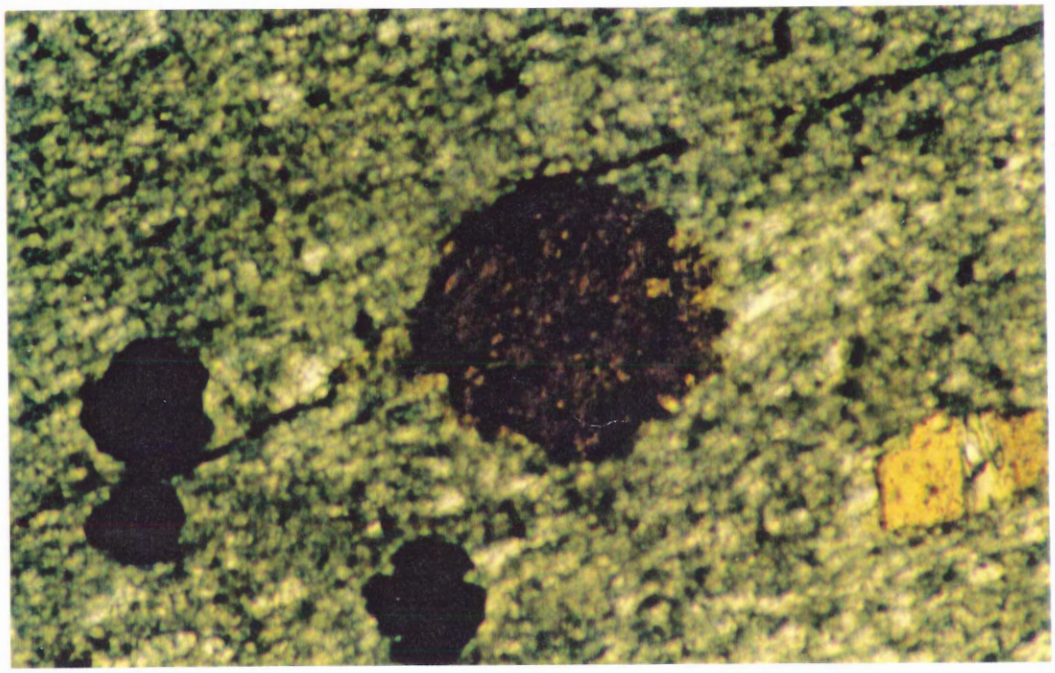

FIGURE 2.9 (SD93-4) Ovoid porphyroblast of biotite and opaque minerals in fine-grained matrix. (width of photo 1.5 cm.).

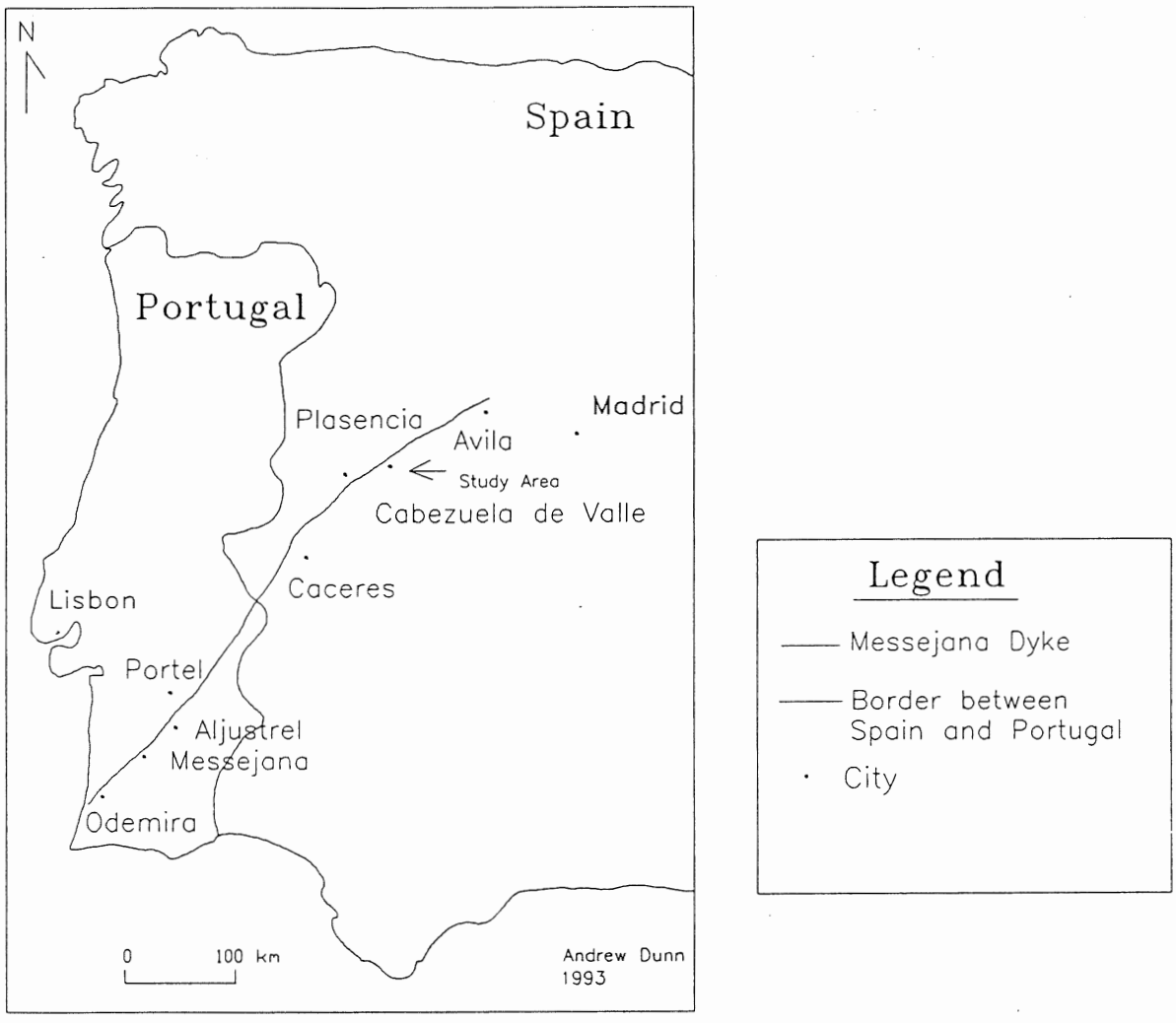

FIGURE 2.10 Location map of the Messejana Dyke

In 1972 Soares de Andrade provided the first whole-rock K-Ar date for the Messjana Dyke (274 ± 5 Ma), and Teixeria and Torquato (1975) added more K-Ar dates for the Messejana Dyke (Table 2.2). Recent studies include an investigation into the age and origin of the dyke by Schermerhorn et al. (1978), a paleomagnetic and K-Ar study by Schott et al. (1981), a Sr-Nd study by Alibert (1985), and a thesis on the K-Ar age of the dyke by Fukuzawa (1988).

2.3.1 Geological Setting

During the Tournaisian and Lower Visean epochs (Early Carboniferous), the so-called Volcanic-Siliceous Complex formed (Schermerhorn et al 1978). This complex consists of felsic tuffs, slates, siliceous slates, mafic to intermediate `spilite´ flows, and albite diabase sills. Overlying this complex is the Culm Group (Schermerhorn et al. 1978) consisting of greywacke-slate meta-turbidites. During the Hercynian orogeny, throughout the Lower Pennsylvanian period, these rocks were folded, locally overthrust, faulted and affected by very low-grade metamorphism (prehnite-pumpellyite facies or lower greenschist facies) (Schermerhorn et al. 1978). The Messejana dyke, also related to the early phases of the opening of the North Atlantic Ocean, intruded these strata during the Early to Middle Jurassic period. Chapter 4 discusses in detail the geochronology of the Messejana Dyke based on the sample obtained from Cabezuela de Valle.

Location	Method	Date (Ma)
Avila 1. Lat 40.68° Long 4.90°	K/Ar- plag.	205±6
Avila 2. Lat 40.05° Long 5.17°	K/Ar- plag.	179±5
Plasencia 1. Lat 39.82° Long 6.33°	K/Ar- plag.	157±4
Plasencia 2. Lat 40.05° Long 6.05°	K/Ar- plag.	164±5
Plasencia 3.	K/Ar- plag.	183±7
Caceres 1. Lat 39.65° Long 6.52°	K/Ar- plag.	195±5
Caceres 2. Lat 39.55° Long 6.63°	K/Ar- pyroxene	163±9

Key:
K/Ar- Potassium/Argon
plag.- Plagioclase

TABLE 2.2 Previous geochronological work on the Messejana Dyke (Schott et al. 1981)

Location	Method	Date (Ma)
Caceres 2.	K/Ar- plag.	171±5
CM Lat-39.07° Long-7.36°	K/Ar- pyroxene	160±9
CM	K/Ar- plag.	170±5
Aljustral Lat-38.68° Long-7.36°	K/Ar- plag.	188±5
Portel Lat-38.34° Long-7.68°	K/Ar- plag.	193±5
Odermia Lat-37.57° Long-8.66°	K/Ar- pyroxene	157±9
Odemira	K/Ar- plag.	134±4

Key:
K/Ar- Potassium/Argon
plag.- Plagioclase

TABLE 2.2 cont'd Previous geochronological work on the Messejana Dyke (Schott at al. 1981)

Location	Methods	Date (Ma)	References
Portel	K/Ar- wr	274.5±5	Soares de Andrade, 1972
Odemira	K/Ar- wr	156±2	Teixeira and Toquato, 1975
Monte De Derroca	K/Ar- wr	163±4	Teixeria and Toquato, 1975
Campo Maior	K/Ar- wr	199±18	Teixeria and Toquato, 1975
Araya River	K/Ar- plag.	220±13	Teixeria and Toquato,1975
Gaviao- surface sample	K/Ar- wr	148±8	Schermerhorn et al. 1978
Gaviao- borehole sample	K/Ar- wr	162±8	Schermerhorn et al. 1978
Gaviao- borehole sample	K/Ar- wr	171±8	Schermerhorn et al. 1978
Gaviao- borehole sample	K/Ar- wr	170±10	Schermerhorn et al. 1978

Key:
K/Ar- Potassium/Argon
plag.- Plagioclase
wr- Whole rock

TABLE 2.2 cont'd Previous geochronological work on the Messejana Dyke

Location	Method	Date (Ma)	References
Plasecia	K/Ar- wr	186±6	Schermerhorn et al. 1978
N.W. of Caceres	K/Ar- wr	182±10	Schermerhorn et al. 1978
Portugal 15.7.85-1	K/Ar- conv.	179±3.6	Fukuzawa, 1988
Portugal 15.7.85-2	K/Ar- conv.	188±3.8	Fukuzawa, 1988
Portugal 15.7.85-4	K/Ar- conv.	196±3.9	Fukuzawa, 1988
Portugal 15.7.85-5B	K/Ar- conv.	189±3.8	Fukuzawa, 1988
Spain 22.7.85-1	K/Ar- conv.	176±3.6	Fukuzawa, 1988
Spain 22.7.85-2	K/Ar- conv.	194±3.9	Fukuzawa, 1988
Spain 22.7.85-3	K/Ar- conv.	182±3.6	Fukuzawa, 1988
Spain 22.7.85-4	K/Ar- conv.	194±3.9	Fukuzawa, 1988

Key:
K/Ar- Potassium/Argon
wr- Whole rock
conv.- Conventional potassium/argon dating method
15.7.85-1- Sample number

TABLE 2.2 cont'd Previous geochronological work on the Messejana Dyke

2.3.2 Outcrop Location of Messejana Dyke in Spain

The study area for this investigation is an outcrop at Cabezuela de Valle, Latitude 44°12' and Longitude 5°48' (Fig. 2.10). The outcrop at Cabezuela de Valle is not as well-exposed as the outcrop of the Shelburne Dyke in Little Harbour. Many small faults and an abundance of recent fluvial and glacial sediment obscure the field relations in this area. The exposure consists of diabase with, fine-grained margins and a coarse-grained, gabbro-like interior zone. The host rock in Cabezuela de Valle is a sillimanite-bearing, two-mica granite. This granite is mainly porphyritic, but contains zones that are fine-grained with phenocyrsts. The width of the Messejana Dyke in this area is approximately 20 metres. The maximum reported thickness of the entire dyke is 300 metres. The sample used in this study was obtained by Dr. D.B.Clarke in the summer of 1993.

2.3.3 Petrological Description

Torre de Assuncao (1949) described the Messejana Dyke as a pigeonitic dolerite with micropegmatite, composed of labradorite and pigeonite in ophitic texture with interstitial micropegmatite and minor green amphibole, biotite, magnetite, ilmenite, and apatite. Further studies by Torre de Assuncao and Perdigao (1962), and Garcia de Figuerloa (1963, 1965) describe the dyke as varying from fine-grained, nearly basaltic, to coarse-grained, and nearly gabbroic. The Messejana Dyke contains plagioclase and pyroxene with minor olivine, hornblende, and biotite, with a subophitic to ophitic texture (Schermerhorn et al. 1978).

The following description of the Messejana Dyke is based on the sample and thin section from Cabezuela de Valle (Appendix A). The rock is medium- to coarse-grained, indicating that it is from the interior of the dyke. The thin section contains crystals of plagioclase and pyroxene with minor amounts of opaques, olivine, biotite, and chlorite (Fig. 2.11-2.14). The pyroxenes are mainly clinopyroxene and the olivine grains are generally altered to iddingsite. The texture of the rock ranges from subophitic to ophitic, with a late poikilitic texture involving clinopyroxene enclosing plagioclase (Fig. 2.15).

2.4 Summary

The Shelburne Dyke extends a distance of 140 km across southern Nova Scotia. It cuts through the Goldenville and the Halifax Formations of the lower Paleozoic Meguma Group. Intrusion of the Shelburne Dyke occurred at a time close to the boundary of the Triassic and Jurassic Periods, and was associated with the early stages of the spreading of the North Atlantic Ocean. A well-exposed coastal outcrop of the Shelburne Dyke occurs at Little Harbour. At this locality, a clear difference exists between the center of the dyke (coarse-grained) and the chilled margins (fine-grained). The Shelburne Dyke is a tholeiite with a subophitic to ophitic texture (Pe-Piper et al. 1992). A thin pelite bed intruded by the dyke contains abundant porphyroblasts of biotite.

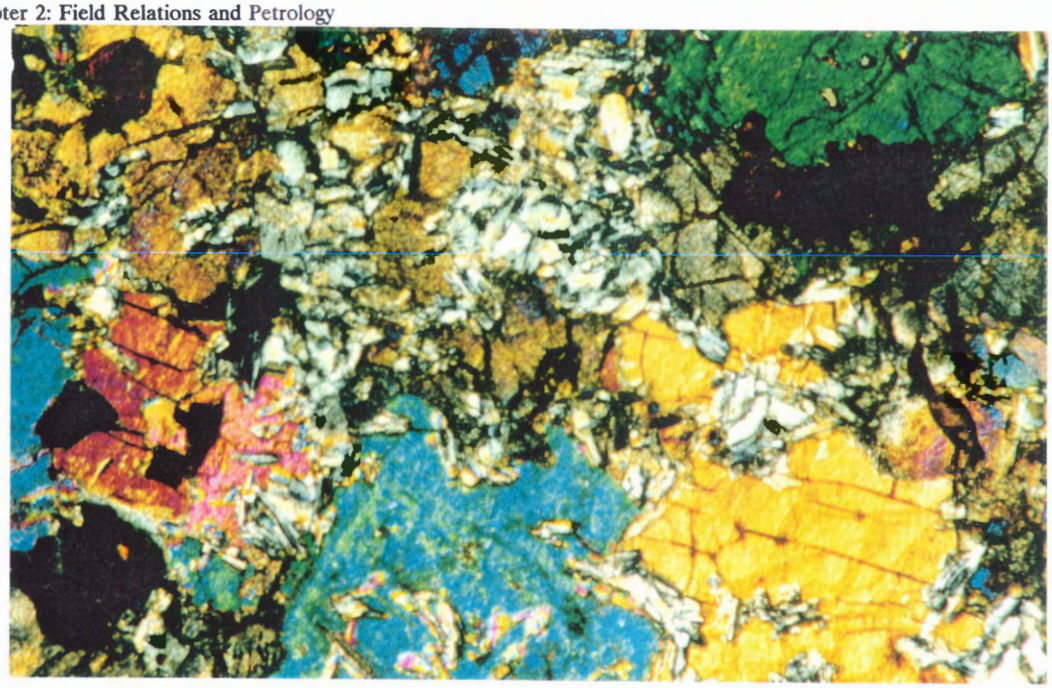

FIGURE 2.11 (MD93-1) Medium to coarse-grained interior of Messejana Dyke showing clinopyroxene enclosing plagioclase (poikilitic texture), opaque minerals, and biotite (width of photo 3 cm.).

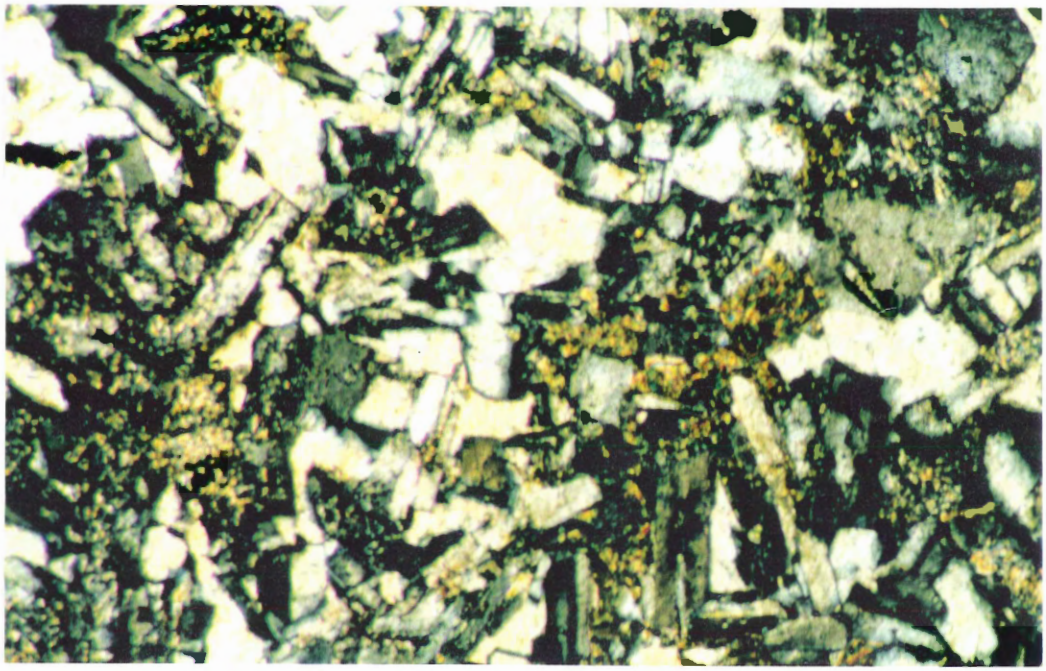

FIGURE 2.12 (MD93-1) Medium-grained plagioclase crystals. Euhedral to subhedral in shape with definite Carlsbad twinning (width of photo 1 cm.).

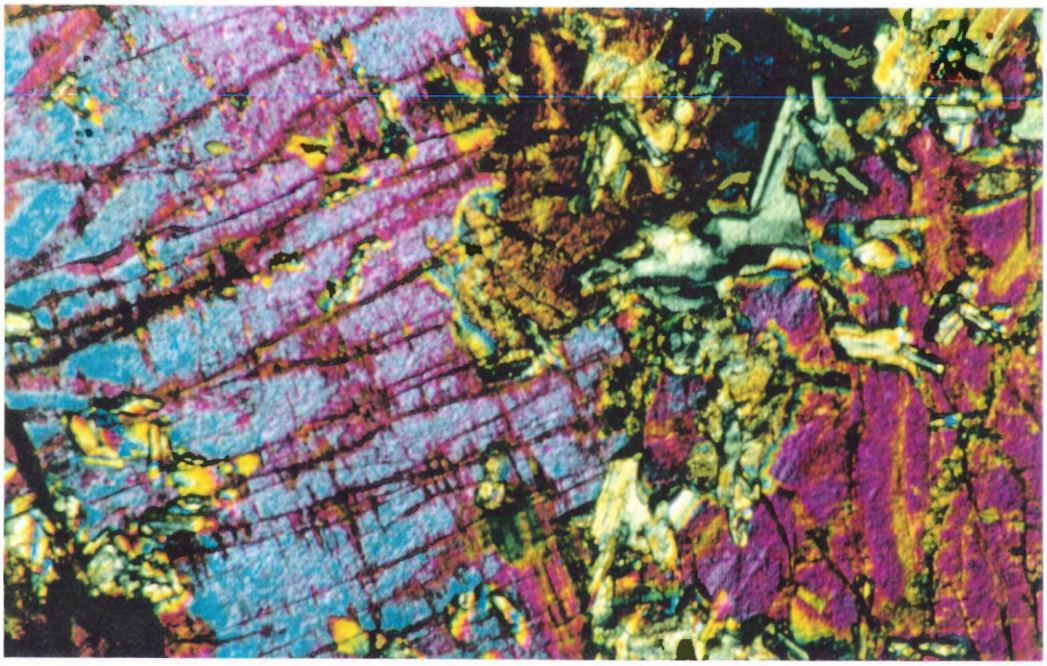

FIGURE 2.13 (MD93-1) Clinopyroxene crystals containing plagioclase crystals. Anhedral to subhedral in shape with a skeletal framework (width of photo 1.5 cm.).

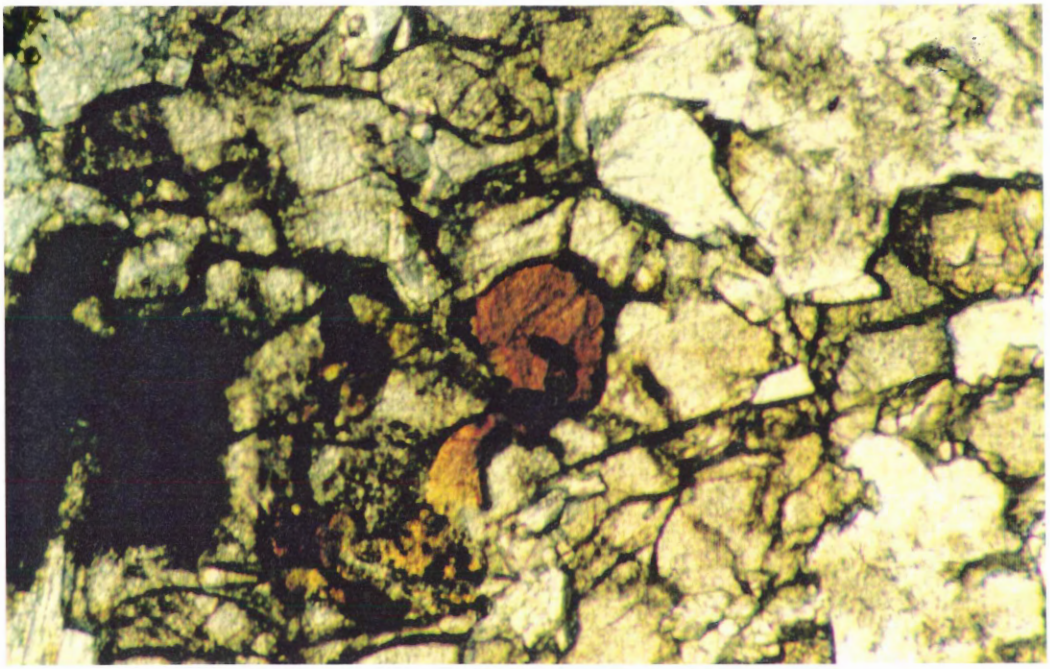

FIGURE 2.14 (MD93-1) High relief biotite crystal growth on clinopyroxene crystals (width of photo 1 cm.).

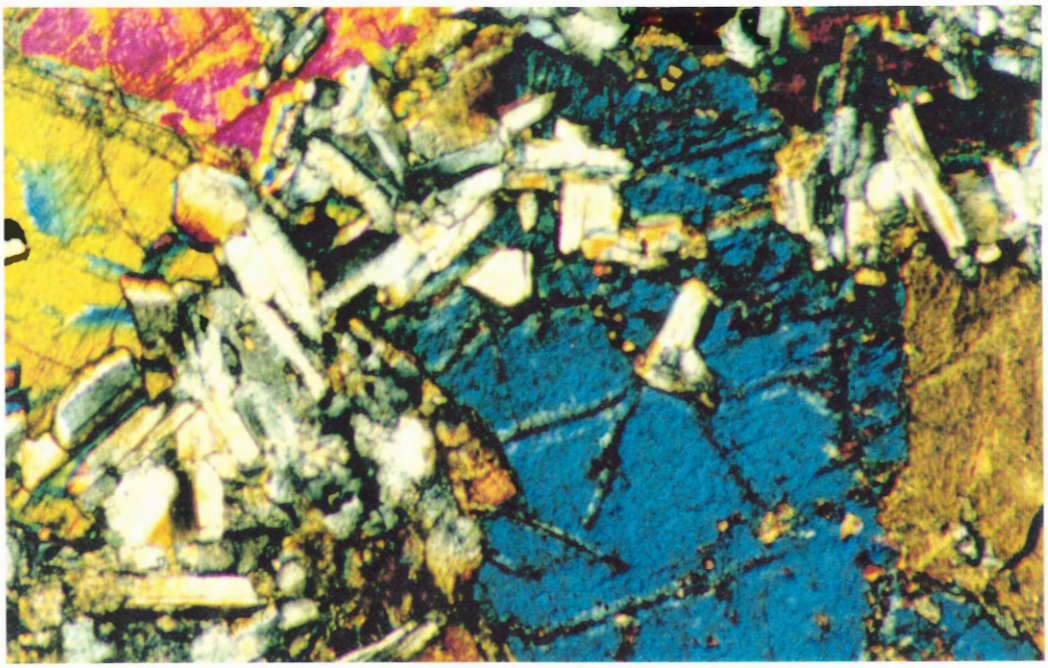

FIGURE 2.15 (MD93-1) Poikilitic texture - plagioclase inside clinopyroxene (width of photo 1 cm.).

The Messejana Dyke extends across the Iberian Peninsula, a distance of 530 km from Odemira in Portugal to Avila in Spain. The dyke cuts through the Volcanic-Siliceous Complex and the Culm Group deposited during the Early Carboniferous Period. Intrusion of the dyke occurred during the Early to Middle Jurassic, also associated with the opening of the north Atlantic Ocean (Schermerhorn et al. 1978). An outcrop of the Messejana Dyke occurs in Cabezuela de Valle; however, the dyke is faulted and covered by fluvial and glacial sediments. The Messejana Dyke is a tholeiite and has a fine-grained margin and a coarse-grained center. Plagioclase and pyroxene are abundant and the dyke has a texture that ranges from subophitic to ophitic. The dyke intrudes a body of sillimanite-bearing two-mica granite.

2.5 Comparison

Although the Shelburne and the Messejana Dykes are now on different continents, separated by the Atlantic Ocean, striking similarities exist:

(i) Both the Shelburne and Messejana Dykes are extensive vertical sheets of intrusive rock that average around 100 m in thickness and extend northeast-southwest at a latitude of 44° N.

(ii) The emplacement of the two dykes occurred roughly between the Late Triassic and the Middle Jurassic Periods, associated with the early phases of the formation of the North Atlantic Ocean.

(iii) Petrologically, the Shelburne and Messejana Dykes are also similar. Both are tholeiites and contain an abundant plagioclase and pyroxene, with minor opaque

minerals, olivine and biotite. Both have subophitic to ophitic textures and the center of the Messejana dyke also has a poikilitic texture.

Further comparisons follow in the chapters on geochemistry and geochronology.

3.1 Introduction

This chapter presents the major, trace, and rare earth element geochemistry of the Shelburne and Messejana Dykes, including both previously published data (Papezik and Barr 1981, Alibert 1985) and new analyses. The chemical data permit four types of inferences:

(i) classification of the rocks that comprise the dykes;

(ii) interpretation of within-dyke variations;

(iii) comparison of the Shelburne Dyke and the Messejana Dyke; and

(iv) interpretation of tectonic setting of the dykes based on tectono-magmatic discriminators.

Table 3.1 contains the major element data and CIPW normative mineralogy, and Table 3.2 contains the trace- and rare-earth element data that form the basis for the following descriptions and geochemical variation diagrams.

3.2 Chemical Classification

The alkali-silica plot (Irvine and Barager 1971) (Fig. 3.1a) shows that all data fall unequivocally in the subalkaline field. Similarly, the (Na_2O+K_2O)-MgO-FeO plot (Irvine and Barager 1971) (Fig. 3.1b) shows all compositions to be tholeiitic. Figure 3.2 is a projection from clinopyroxene onto the base of the CIPW normative tetrahedron. This plot shows that the majority of the samples lie in the quartz tholeiite field, with two of the published data points for the Messejana Dyke lying in the olivine tholeiite field.

Region	NS	NS	NS	NS	NS	NS	NS	NS	NS	NS	NS	NS	Spain	Spain	Spain	Spain	Spain	Spain
Source	Barr 1981	Barr 1981	Barr 1981	Barr 1981	Barr 1981	Barr 1981	Barr 1981	Barr 1981	Barr 1981	Dunn 1993	Dunn 1993	Dunn 1993	Albert 1985	Albert 1985	Albert 1985	Albert 1985	Albert 1985	Dunn 1993
Location										Little Harbour	Little Harbour	Little Harbour						Cabezuola de Valle
Sample	112	G-1	SH-1	P-3	116	120	R-7	S-1	S-3	SD93-1	SD93-6	SD93-7	P2	A1	AL	PO	P3	MD93-1
Major Elements (wt. %)																		
SiO2	52.50	52.80	52.60	52.10	52.60	52.80	51.60	49.70	52.10	52.41	52.09	52.94	50.54	50.16	50.16	52.76	51.26	50.87
TiO2	0.93	0.94	0.99	1.06	1.35	1.12	1.00	1.00	0.96	1.07	1.08	1.13	1.10	1.13	1.00	1.06	1.28	0.85
Al2O3	14.90	14.60	14.20	15.80	14.90	15.10	13.90	14.40	13.60	14.36	15.01	14.31	14.71	14.29	14.47	13.99	15.47	14.67
Fe2O3	2.48	2.98	2.51	3.49	3.63	3.20	3.81	14.05	3.27	11.00	10.78	11.22	11.00	10.95	10.85	11.38	11.55	10.28
FeO	7.37	6.54	7.31	6.14	7.25	7.00	6.54		6.86									
FeOt	9.60	9.22	9.67	9.28	10.62	9.88	9.97	12.64	9.80				9.90	9.85	9.76	10.24	10.39	
MnO	0.17	0.17	0.17	0.16	0.17	0.17	0.17	0.17	0.17	0.18	0.16	0.17	0.18	0.18	0.18	0.18	0.18	0.16
MgO	7.11	7.66	7.13	6.82	5.00	6.16	7.26	6.89	7.66	6.74	6.29	6.83	7.42	7.55	7.55	6.86	6.41	7.89
CaO	10.37	10.92	10.16	10.16	9.33	9.33	9.92	7.61	10.35	9.77	10.11	9.65	11.64	11.57	11.66	10.28	10.33	11.67
Na2O	2.13	1.99	2.08	2.28	2.32	2.33	2.14	2.06	2.04	2.02	2.01	2.13	1.92	1.96	2.03	2.23	2.38	1.61
K2O	0.66	0.66	0.81	0.88	1.01	0.62	0.73	0.41	0.61	0.30	0.69	0.77	0.31	0.44	0.46	0.68	0.65	0.44
P2O5	0.13	0.12	0.16	0.11	0.28	0.16	0.16	0.18	0.12	0.13	0.14	0.14	0.03	0.08	0.08	0.02	0.07	0.08
LOI	1.41	1.45	1.48	1.47	1.85	2.61	1.97	4.20	1.85	1.50	0.8	0	0.67	0.72	0.38	0.59	0.67	0.6
Total	100.16	100.62	99.59	99.45	99.86	100.66	99.18	99.67	99.59	99.49	99.16	98.29	99.32	99.02	98.71	100.02	99.16	98.92
CIPW Norms (mol %)																		
Q	2.29	2.67	2.83	2.39	4.33	4.06	1.72	3.25	2.27	5.22	3.82	5.12	0.67	0	0	2.37	1.59	1.77
Z	0.02	0.02	0.02	0.02	0.03	0.02	0.02	0.02	0.02	0.02	0.02	0.02	0.02	0.02	0	0.02	0.02	0.01
Or	3.85	3.26	4.8	5.21	5.98	3.68	4.33	2.43	3.61	1.78	4.09	4.56	1.84	2.61	2.73	4.03	3.85	2.61
Ab	18.02	16.84	17.6	19.29	19.63	19.71	18.11	17.43	17.26	17.09	17.01	18.02	16.24	16.58	17.18	18.87	20.14	13.62
An	29.19	29.3	27.03	30.3	27.28	28.93	26.18	28.85	26.16	29.24	29.91	27.23	30.61	28.9	29.02	26.16	29.62	31.24
Di	17.78	19.92	18.59	16.17	14.61	13.69	18.32	6.67	20.21	15.28	16.13	16.53	21.87	23.12	22.98	20.62	17.75	21.14
Hy	26.33	24.96	24.82	22.07	22.68	25.16	26.97	33.24	26.83	25.96	23.99	23.28	24.37	22.92	21.09	24.32	21.91	25.13
Ol	0	0	0	0	0	0	0	0	0	0	0	0	0	0.77	2.19	0	0	0
Cm	0.06	0.06	0.06	0.03	0.02	0.03	0.06	0.04	0.06	0.06	0.04	0.03	0.06	0.06	0.06	0.02	0.02	0.04
Il	1.77	1.79	1.88	199	2.56	2.13	1.9	1.9	1.82	2.03	2.06	2.16	2.09	2.16	1.9	1.99	2.43	1.61
Ap	0.31	0.28	0.36	0.26	0.66	0.36	0.36	0.43	0.28	0.31	0.33	0.33	0.07	0.19	0.19	0.06	0.17	0.19
Total	98.6	99.09	97.98	97.74	97.69	97.76	96.94	94.16	97.63	96.98	97.39	97.27	97.73	97.29	97.32	98.36	97.6	97.37

TABLE 3.1 Published and new major element and CIPW normative mineralogy data for the Shelburne and Messejana Dykes

Region	NS	NS	NS	NS	NS	NS	NS	NS	NS	NS	NS	NS	Spain	Spain	Spain	Spain	Spain	Spain
Source	Barr 1981	Barr 1981	Barr 1981	Barr 1981	Barr 1981	Barr 1981	Barr 1981	Barr 1981	Barr 1981	Dunn 1993	Dunn 1993	Dunn 1993	Albert 1985	Albert 1985	Albert 1985	Albert 1985	Albert 1985	Dunn 1993
Location										Little Harbour	Little Harbour	Little Harbour						Cabezuela de Valle
Sample	112	G-1	SH-1	P-3	116	120	R-7	S-1	S-3	SD93-1	SD93-6	SD93-7	P2	A1	AL	PO	P3	MD93-1
Trace Elements(ppm)										Trace elements (ppm) St. Mary's								
Ba	194	207	205	242	269	158	176	134	205	72	179	238	89	129	161	166	175	83
Rb	25	22	33	36	36	28	30	17	22	10	26	27	22	21	20	23	25	28
Sr	197	199	208	231	223	211	198	177	183	187	211	195	120	113	109	89	146	176
Ga	20	20	19	23	21	22	22	22	20	13	15	14						13
V	256	218	247	247	277	274	259	252	252	263	249	268						219
Cr	227	273	251	143	105	125	234	193	286	253	199	143	235	224	222	116	108	174
Ni	83	88	87	62	64	73	87	74	90	81	68	60	99	99	86	72	56	81
Cu	105	103	110	107	136	112	131	100	99	95	114	114						97
Zn	80	67	76	71	86	94	75	95	74	109	71	84						65
Pb	7	7	7	10	9	13	8	11	5	14	< 10	< 10						< 10
Nb	10	11	9	10	13	11	9	11	9	7	8	8						5
Zr	97	91	100	100	132	112	102	106	95	100	103	121	76	79		83	94	67
Y	23	22	23	23	30	26	25	26	23	24	24	27						20
U																		
Th	5	4	6	6	4	5	4	6	4	< 10	< 10	< 10						< 10
Rare Earth Elements (ppm)										Rare Earth Elements (ppm) MUN								
La	22	27	20	26	22	26	20	24	23	11.73	11.31	13.13	7.9	7.9	8.6	9.7	11	6.01
Ce	28	30	29	31	36	29	26	25	25	26.01	25.28	29.35	16.8	16.6	18	18.3	23.4	14.12
Pr										3.36	3.22	3.77						1.89
Nd										14.19	14.11	16.16	10.4	10.4	10.2	11.8	14	8.84
Sm										3.61	3.26	3.85	2.69	2.64	2.6	2.84	3.37	2.26
Eu										1.16	1.12	1.18	0.92	0.94	0.94	0.98	1.16	0.90
Gd										4.30	3.61	4.06	3.27	3.09	3.46	3.14	3.88	2.92
Tb										0.67	0.59	0.69						0.46
Dy										4.24	4.14	4.27	3.42	3.39	3.26	3.69	4.28	2.86
Ho										0.85	0.86	0.90						0.59
Er										2.52	2.41	2.67	1.87	1.85	2.03	2.01	2.31	1.76
Tm										0.38	0.34	0.38						0.26
Yb										2.19	2.18	2.41	1.93	1.84	1.78	2.14	2.3	1.67
Lu										0.34	0.37	0.35						0.25
Hf										2.88	2.99	3.29						1.60
Ta										0.48	0.77	0.88						0.54
Th										2.65	2.60	2.91						1.05

TABLE 3.2 Published and new trace and rare-earth element data for the Shelburne and Messejana Dykes

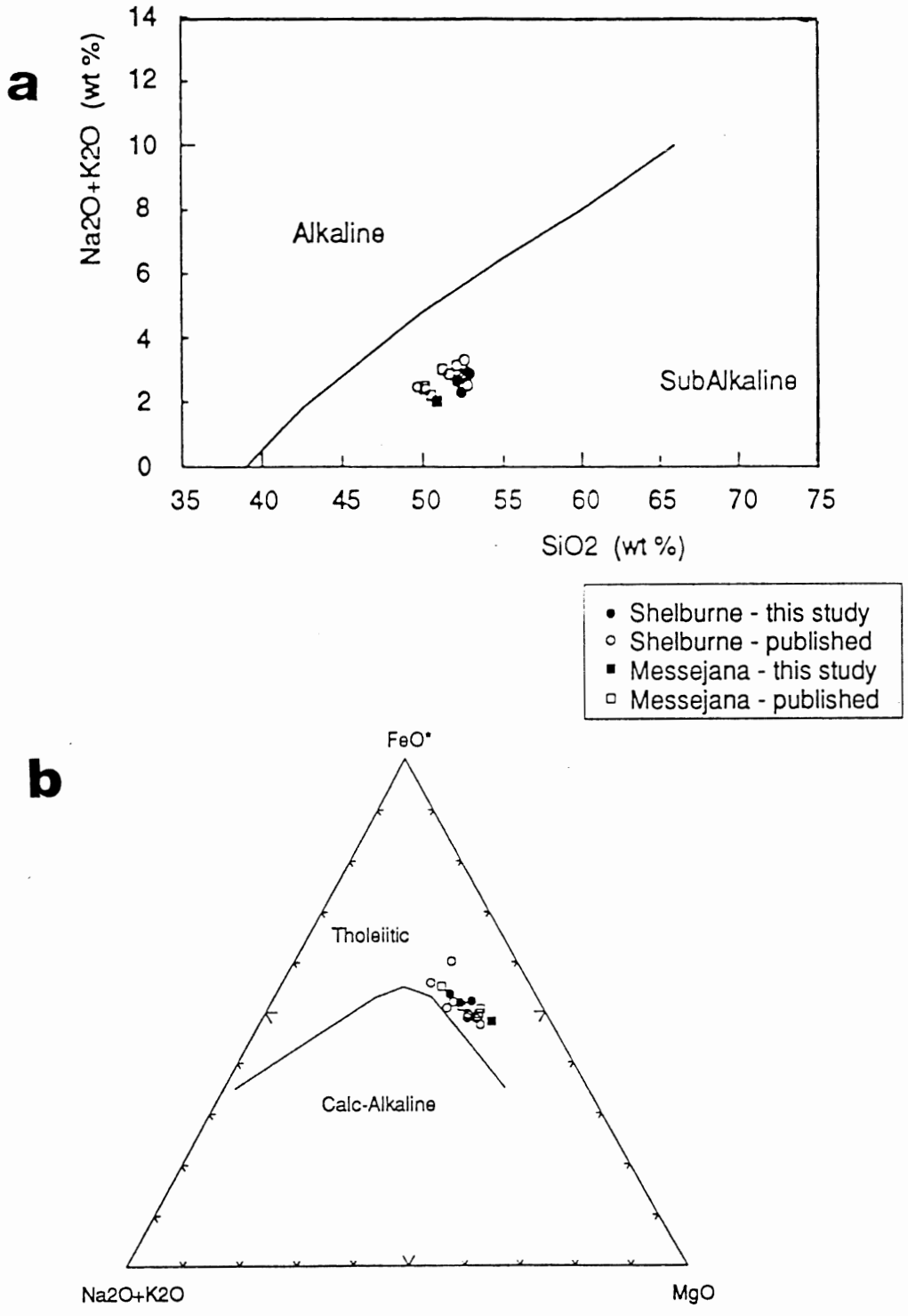

FIGURE 3.1 a. Alkali-silica plot (Irvine and Baragar 1971) b. Na_2O+K_2O-MgO-FeO plot (Irvine and Baragar 1971)

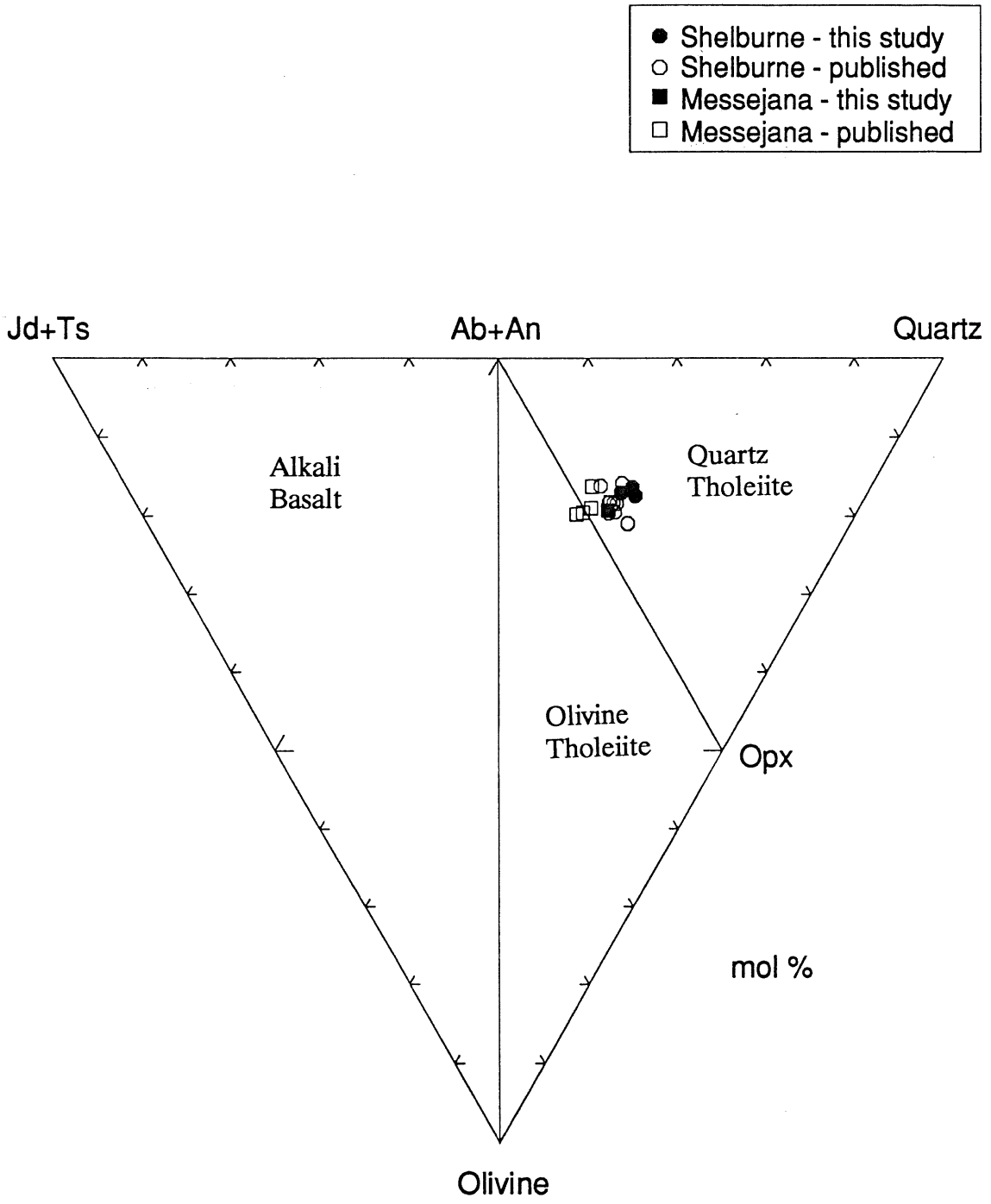

FIGURE 3.2 A projection from clinopyroxene onto the base of the CIPW normative tetrahedron.

3.3 Major Elements

3.3.1 Within-Suite Variation

Figure 3.3a shows total iron content (Fe_2O_3*0.9+FeO) plotted against MgO for the Shelburne Dyke. The data points cluster, suggesting no extensive differentiation, at least involving these elements. The clustering may indicate that the liquid composition is confined at, or close to, a eutectoid or invariant point, i.e. a point where the temperature, pressure, and composition of a phase assemblage cannot change without the loss of one or more phases (Hall 1987). The data points for the Messejana Dyke in Fig. 3.3a also suggests no extensive variation of Fe or Mg. All the samples cluster together and show little evidence of a trend or correlation.

Titanium (Ti^{4+}, 0.68 Å) and phosphorus (P^{5+}, 0.34 Å) are present in minor amounts and, as with the major elements, they cluster (Fig. 3.3b). The single sample with high values of TiO_2 and P_2O_5 is anomalous, but may indicate that these elements underwent extensive passive enrichment. Passive enrichment refers to the increased abundance of incompatible elements, such as Ti and P, resulting from the extraction of compatible elements during fractional crystallization. Titanium may eventually enter titaniferous-magnetite or ilmenite, and phosphorus enters apatite. Phosphorus values for the Messejana Dyke are very low (Fig. 3.3b).

Figure 3.3c shows titanium (Ti^{4+}, 0.68 Å) plotted against another incompatible element, zirconium (Zr^{4+}, 0.80 Å). Like the Ti-P pair, these two elements may also undergo passive enrichment, but they compete for the same octahedral sites in suitable minerals. Although there are only five new data points, the general trend may also

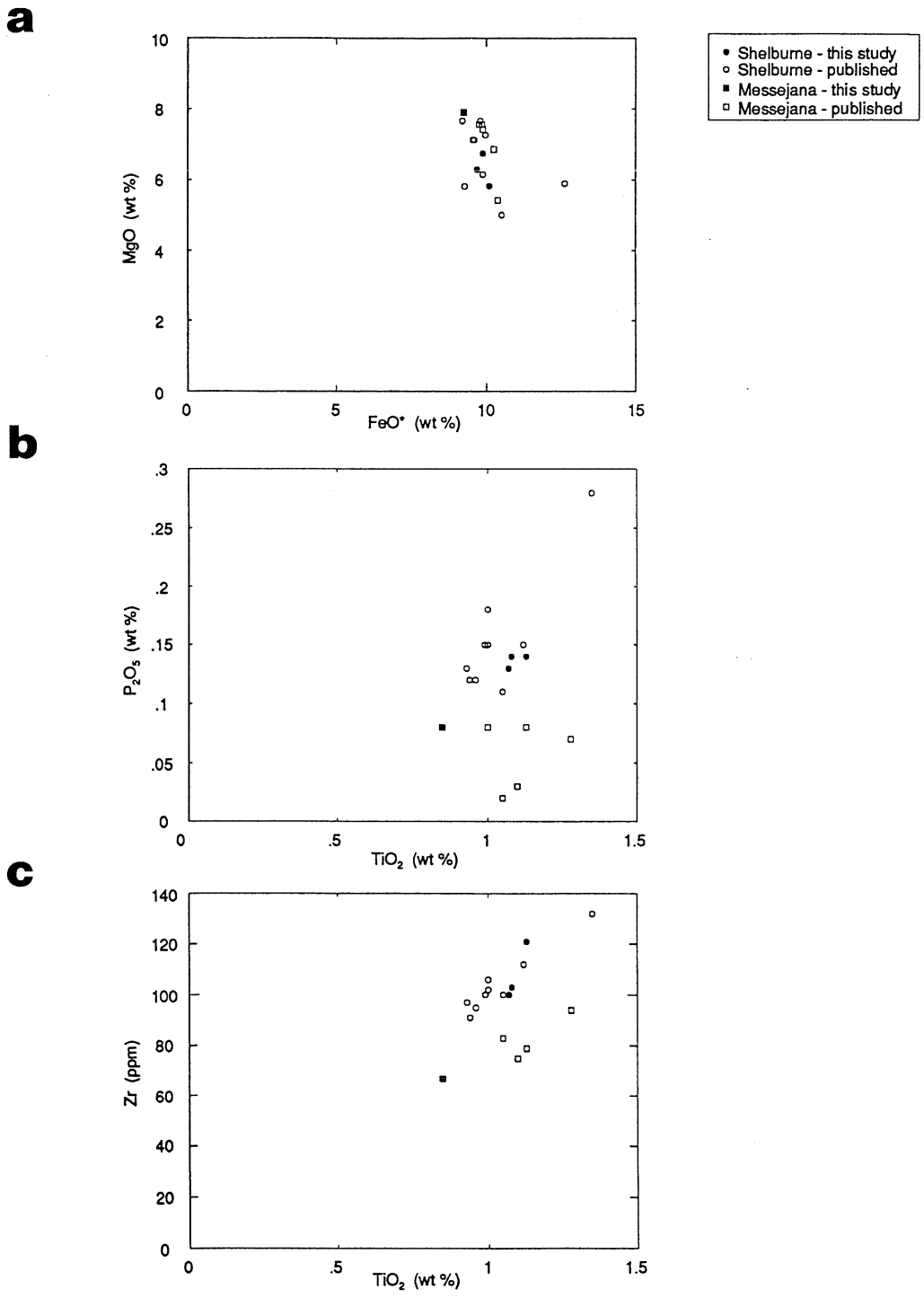

FIGURE 3.3 Major element variation diagrams a. FeO*-MgO plot ($FeO^*=Fe_2O_3*0.9 + FeO$) b. TiO_2-P_2O_5 plot c. TiO_2-Zr plot

indicate passive enrichment. The more primitive rocks contain lower concentrations of TiO_2 and Zr than the evolved or late-forming rocks. These elements may eventually enter into ilmenite or zircon.

The potassium (K^{1+}, 1.33 Å) versus rubidium (Rb^{1+}, 1.48 Å) plot (Fig. 3.4a) shows another example of passive enrichment of incompatible elements. The average K/Rb ratio for the Shelburne Dyke is 221 (± 27). The samples cluster, but appear to record a pattern of passive enrichment. The average K/Rb ratio for the Messejana Dyke is 179 (± 45); the lower K/Rb values may be the result of alteration.

3.4 Trace Elements

3.4.1 Within-Suite Variation

Figure 3.4b plots nickel (Ni^{3+}, 0.62 Å) against chromium (Cr^{3+}, 0.69 Å). Both the Shelburne and Messejana Dykes show a positive correlation between nickel and chromium. The early, primitive rocks contain higher concentrations of Ni and Cr than the late, evolved rocks. The positive trend is probably the result of the fractional crystallization of ferromagnesian minerals, particularly olivine and chrome spinel, which incorporate nickel and chromium respectively, replacing magnesium, iron, and aluminum in those minerals. The early, primitive rocks contain higher concentrations of Ni and Cr than the late, evolved rocks.

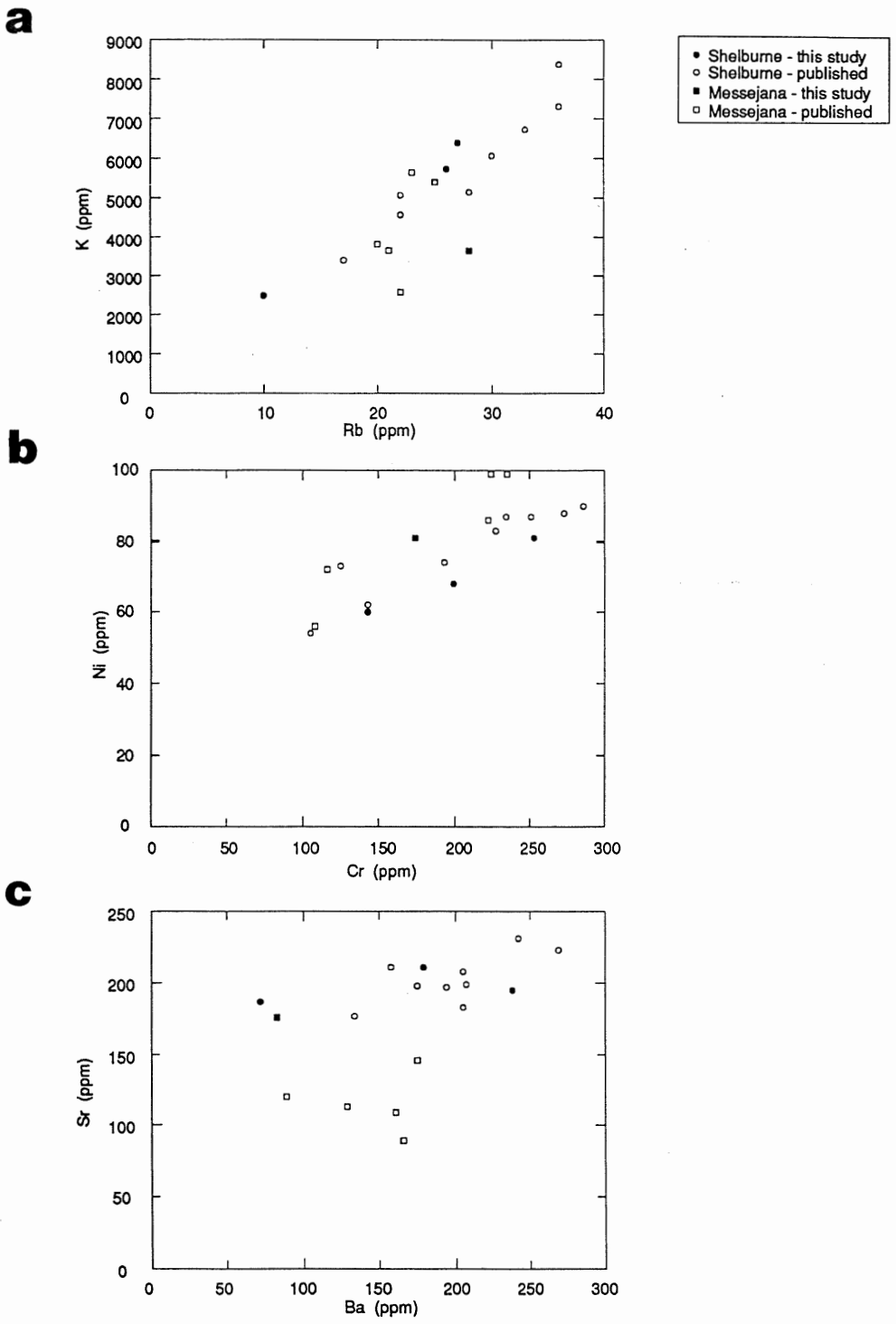

FIGURE 3.4 Trace element variation diagrams a. Rb-K plot b. Cr-Ni plot c. Ba-Sr plot

The plot of strontium (Sr^{2+}, 1.13 Å) versus barium (Ba^{2+}, 1.35 Å) (Fig. 3.4c) demonstrates that, as olivine and pyroxene crystallize, passive enrichment of incompatible Sr and Ba occur. The data for the Shelburne Dyke displays a positive correlation typical for incompatible elements, whereas the data for the Messejana Dyke are erratic, possibly due to other processes.

Figure 3.5a, which is a plot of strontium (Sr^{2+}, 1.13 Å) and rubidium (Rb^{1+}, 1.48 Å), also shows a correlation between two incompatible elements that is another example of passive enrichment. Both the dykes display positive correlations but with two different trends.

The plot of (Ni+Cr)-(Sr+Ba) (Fig. 3.5b) also demonstrates a pattern of passive enrichment for the Shelburne Dyke. The diagram shows a weak antipathetic relationship between the compatible and incompatible parameters, respectively. The data points for the Messejana Dyke display the same trend; the passive enrichment of the incompatible Sr and Ba caused by the removal of Ni and Cr from the melt.

Figure 3.5c, (Ni+Cr)-(Sr+Rb), displays a patterns of passive enrichment for both the Shelburne and Messejana Dykes similar to the patterns seen in Fig. 3.5b. A decrease in nickel and chromium leads to a general increase in strontium and rubidium.

3.5 Rare-Earth Elements

3.5.1 Within-Suite Variation

Figure 3.6 shows the chondrite normalized rare-earth patterns for the Shelburne and Messejana Dykes. The light-REE concentrations range between 30 to 40 x

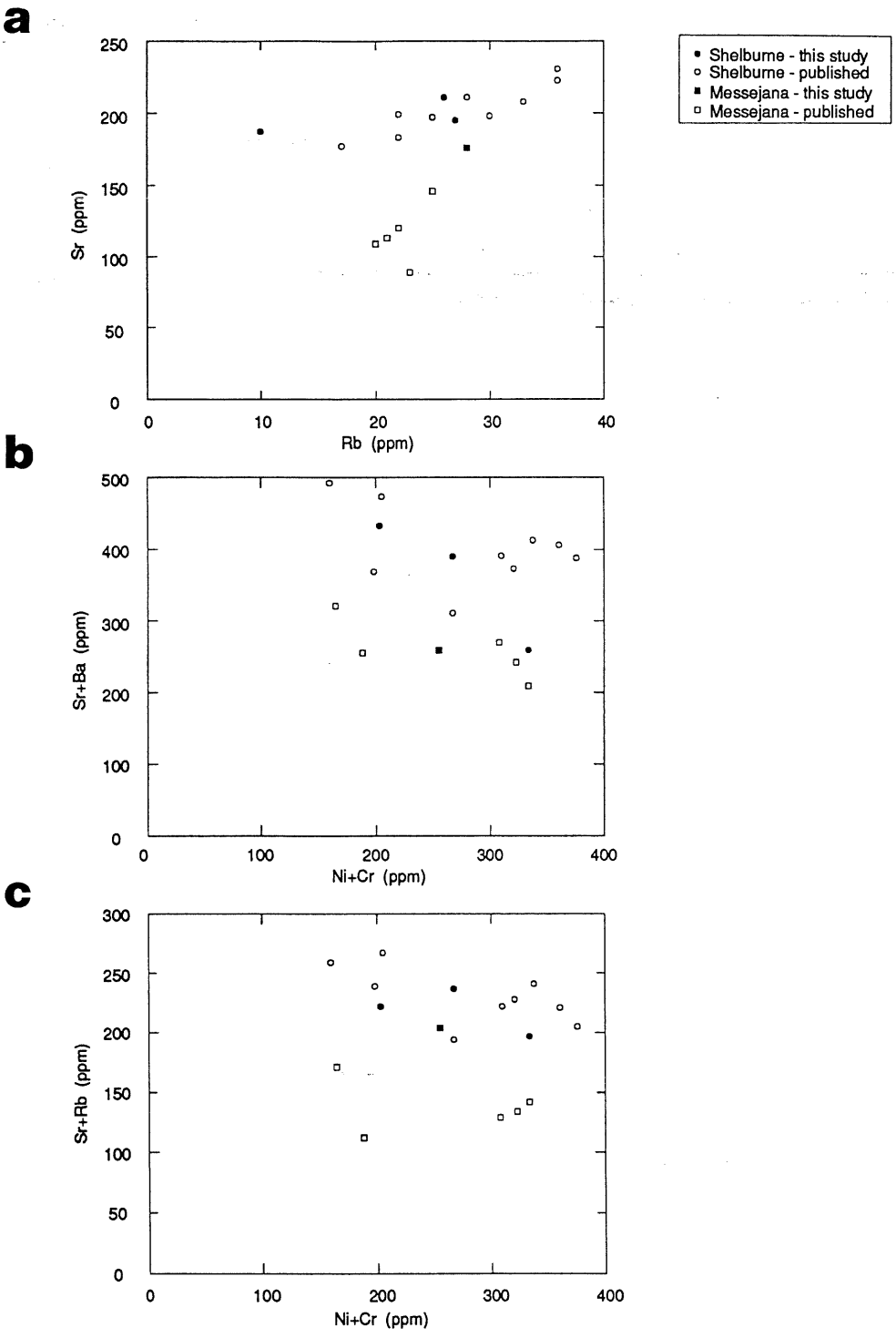

FIGURE 3.5 Trace element variation diagrams a. Rb-Sr plot b. (Ni+Cr)-(Sr+Ba) plot c. (Ni+Cr)-(Sr+Rb) plot

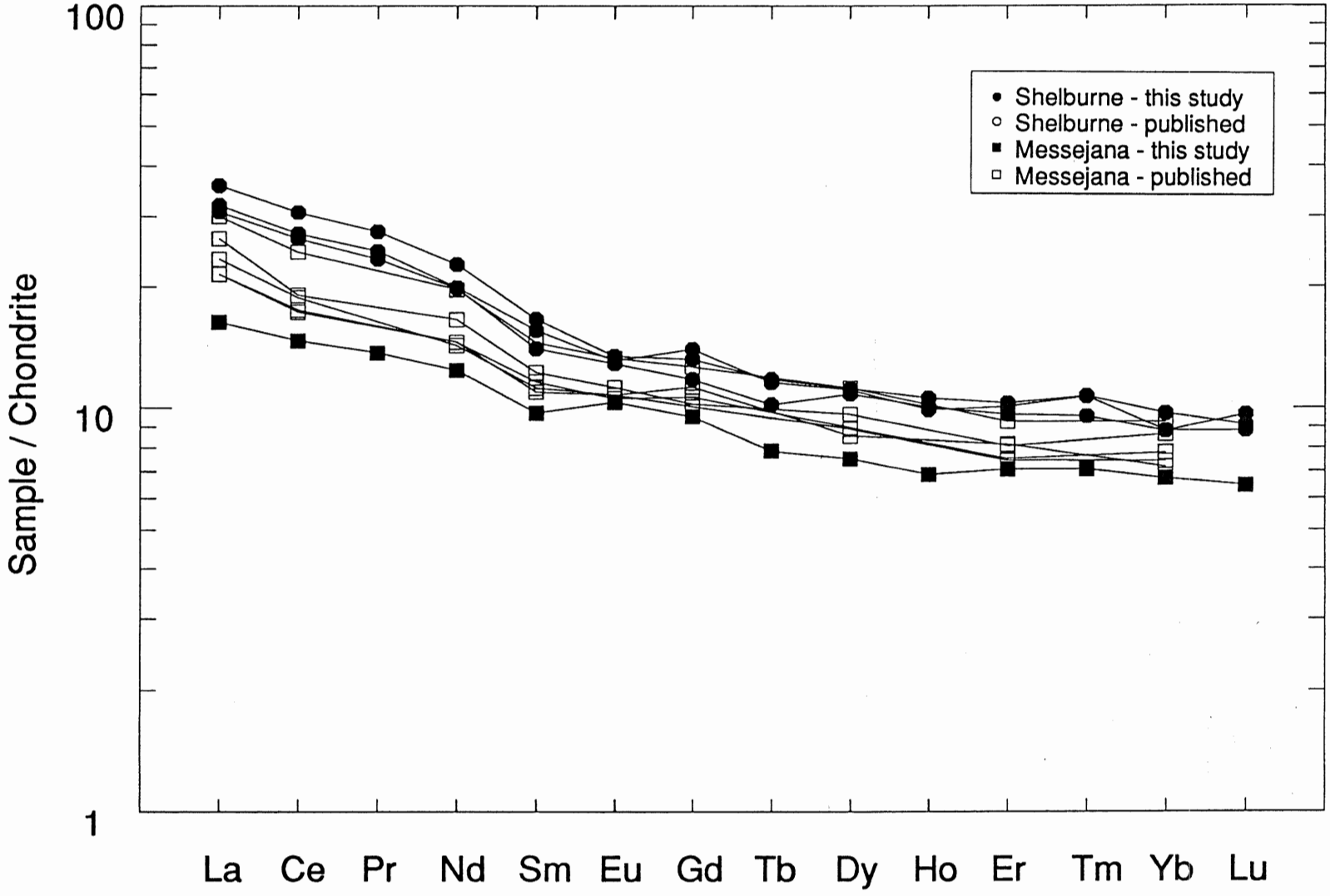

FIGURE 3.6. Rare-earth element plot for Shelburne and Messejana Dykes.

chondrite and the heavy-REE concentrations cluster around 10 x chondrite. The slight enrichment of LREEs (La/Yb_N- 3.5-3.7) could indicate that the Shelburne Dyke formed from small degrees of partial melting or from a LREE-enriched source (Wilson 1989). The weak negative Eu anomalies (Eu/Eu*= 0.89-0.99) in the Shelburne Dyke suggest that it may have undergone some fractional crystallization of plagioclase, or was in equilibrium with a plagioclase-bearing mantle source (Wilson 1989).

The Messejana Dyke is also slightly enriched in light-REEs, with the LREE concentrations ranging from 18 to 30 x chondrite and the heavy-REE concentrations ranging from 5 to 10 x chondrite (Fig. 3.6). The Messejana Dyke also shows slight LREE enrichment (La/Yb_N- 2.9-3.3). The depletion of the HREEs suggests that garnet was absent from the source melt. The previously published REE patterns display weak negative and positive Eu anomalies (Eu/Eu*= 0.95-1.02), but the new REE pattern shows a slightly greater positive Eu anomaly (Eu/Eu*= 1.08). This range of Eu/Eu* values suggests both the removal and accumulation of plagioclase in various parts of the Messejana Dyke.

3.6 Comparison of Shelburne Dyke with the Messejana Dyke

The Shelburne and Messejana Dykes only differ considerably in three respects:

(i) The P_2O_5 concentrations for the Messejana Dyke do not overlap those for the Shelburne Dyke. The difference may reflect influences of sources, or of processes other than high-level fractionation (Clarke 1970, Clarke et al. 1988).

(ii) The Shelburne Dyke exhibits a positive correlation, whereas the data points

for the Messejana Dyke are erratic.

(iii) The REE patterns for the Messejana Dyke are generally lower than for the Shelburne Dyke, and have more variable Eu/Eu* anomalies. The restricted range of Eu/Eu* in the Shelburne Dyke simply reflects the single sampling locality.

3.7 Tectonic Setting

In this section, ten different tectono-magmatic discriminator diagrams provide some insight into the tectonic setting for the Shelburne and Messejana Dykes.

Figure 3.7a is the Ti/100-Zr-Y*3 (Pearce and Cann 1973) tectono-magmatic discriminator diagram. The data points for the Shelburne dyke all cluster in the C (calc-alkali basalt) field very close to the boundary of the B (ocean-floor basalt, low-potassium tholeiite, and calc-alkali basalt) field. The single data point for the Messejana Dyke lies in the B field.

The Ti/100-Zr-Sr/2 plot (Pearce and Cann 1973) (Fig. 3.7b) shows all the data for the Shelburne Dyke in the calc-alkali basalt field. The previously published data for the Messejana Dyke fall into the ocean-floor basalt field, whereas the single new sample lies on the boundary between the calc-alkali and island-arc basalt region. The published data (Alibert 1985) have higher Ti and Zr values and lower Sr values than the new sample from Cabezuela de Valle. The differences may be a result of analytical methods, or real differences in the samples.

Figure 3.7c is the TiO_2-(MnO*10)-(P_2O_5*10) discriminator diagram (Mullen 1983). All the data points for both the Shelburne and Messejana Dykes fall in the island-arc

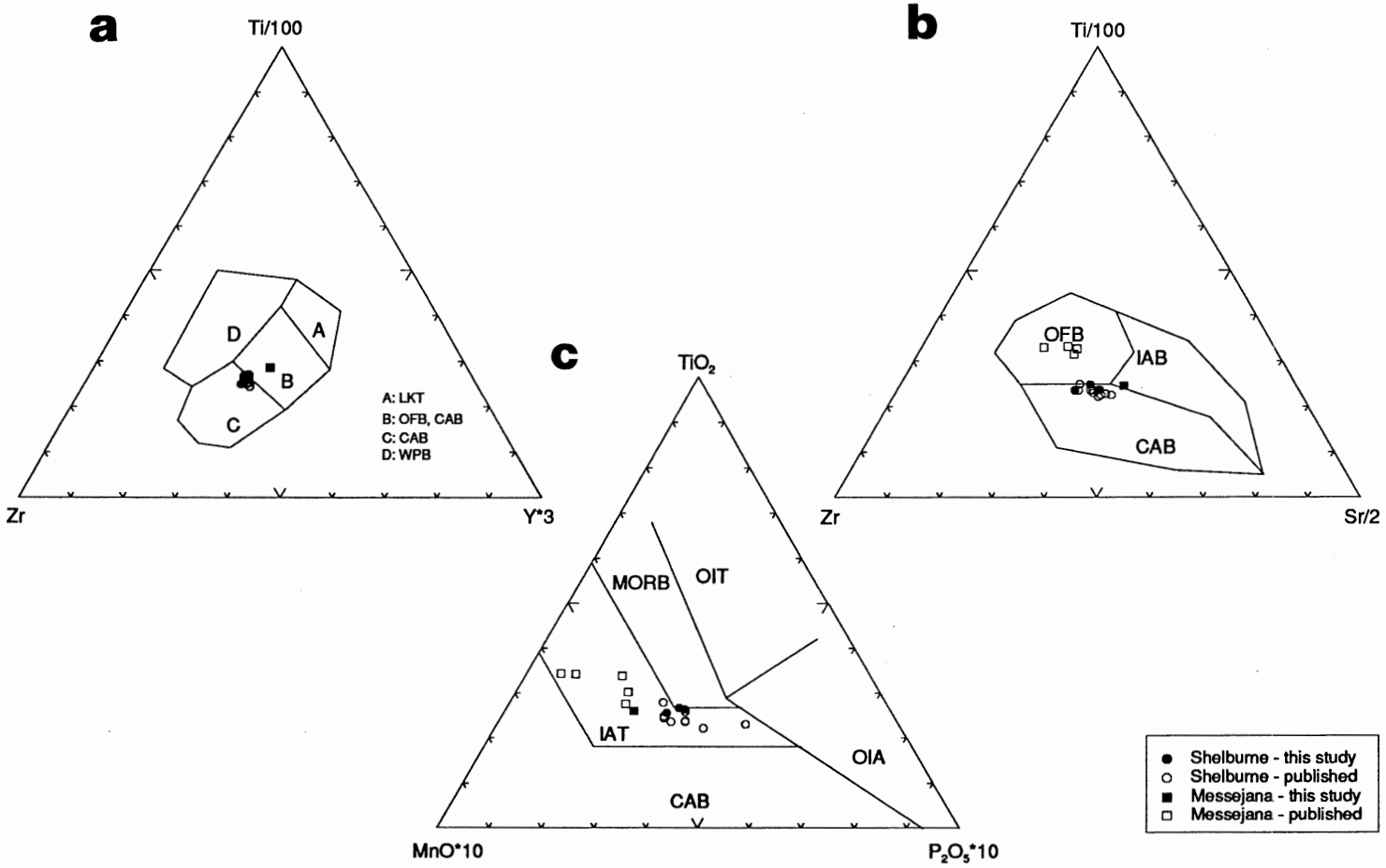

FIGURE 3.7 Tectono-magmatic discriminator diagrams a. Ti/100-Zr-Y*3 plot (Pearce & Cann 1973) b. Ti/100-Zr-Sr/2 (Pearce & Cann 1973) c. TiO_2- MnO*10-P_2O_5 (Mullen 1983)

tholeiite (IAT) field of the plot, or close to the boundary of the mid-ocean ridge basalt field (MORB). This diagram may not be appropriate for the present study because it contains no fields for within-plate basalt or ocean-floor basalt fields.

Figure 3.8a is the Hf/3-Th-Nb/16 diagram (Wood 1980). Only the new data points plot on the graph, because no published Hf, Th, and Nb are available for the Shelburne and Messejana Dykes. All samples fall in the destructive plate margin basalt field, a result not expected from what is known from field relations and other geochemical indicators.

No single tectonic environment for the Shelburne and Messejana Dykes is evident from the FeO-MgO-Al_2O_3 plot (Pearce et al. 1977) (Fig. 3.8b). The data points cluster on the boundaries of three of the five fields. According to this discriminator diagram, the Shelburne and Messejana Dykes were not formed in an oceanic island or in an orogenic setting, but any of the other three fields (ocean ridge and floor, ocean island, and continental) are possible.

Figure 3.8c shows the Nb*2-Zr/4-Y discriminator diagram (Meschede 1986). The samples from the Shelburne Dyke fall in the volcanic-arc basalt and passive-type mid-ocean ridge basalt fields. The single Messejana Dyke sample falls in the normal-type mid-ocean ridge basalt and volcanic basalt field.

Figure 3.9a is the Ti/1000-V plot (Shervais 1982). All the data points for both the Shelburne and Messejana Dykes fall in the ocean-floor basalt region of the graph.

Figure 3.9b shows the Ti-Zr diagram (Pearce and Cann 1973). All but one of the samples from the Shelburne Dyke fall in the calc-alkali basalt region of the plot. The

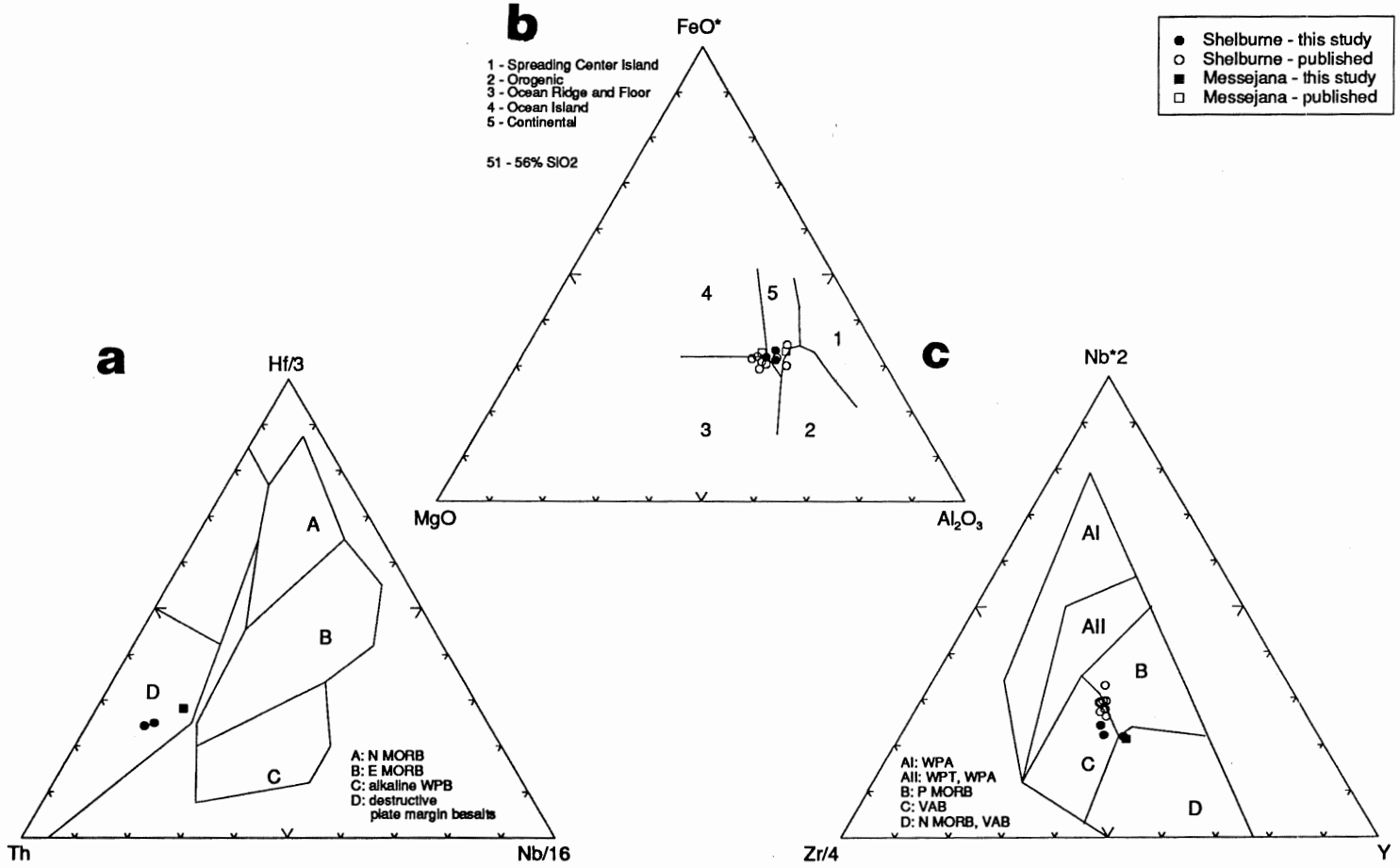

FIGURE 3.8 Tectono-magmatic discriminator diagrams a. Hf/3-Th-Nb/16 (Wood 1980) b. FeO-MgO-Al_2O_3 (Pearce et al. 1977) c. Nb*2-Zr/4-Y (Meschede 1986)

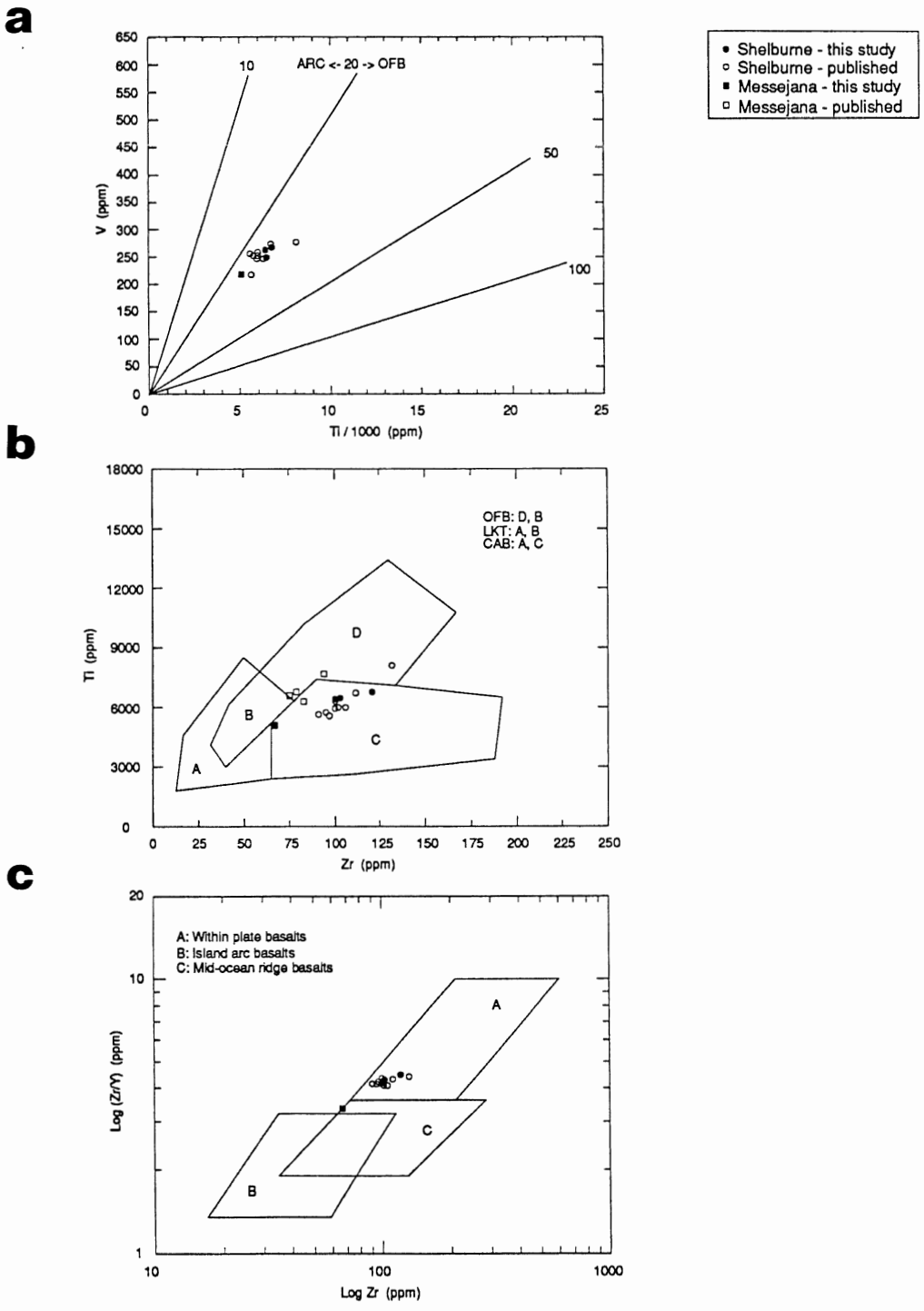

FIGURE 3.9 Tectono-magmatic discriminator diagrams a. Ti/1000-V plot (Shervais 1982) b. Ti-Zr plot (Pearce and Cann 1973) c. Log Zr-Log (Zr/Y) (Pearce and Norry 1979)

remaining sample falls in the ocean-floor basalt field. Three of the data points from the Messejana Dyke also fall in the ocean-floor basalt field, whereas the remaining two samples lie in the calc-alkali basalt region.

In the log Zr-log (Zr/Y) discriminator diagram (Pearce and Norry 1979) (Fig. 3.9c), the Shelburne Dyke samples plot in the within-plate basalt field, whereas the single Messejana Dyke sample falls in the mid-ocean ridge basalt field.

Figure 3.10a shows the log (Ta/Yb)-log (Th/Yb) plot (Pearce 1983). The four data points fall in the subduction area of the continental-arc field, again contrary to the general belief that these dykes formed in a non-subduction setting. Because both Ta and Th are difficult to measure accurately by ICP-MS, the values may be erroneous, yielding inaccurate information about the tectonic setting. The "pseudo-Ta" values are Nb/17.

The final discriminator diagram is Figure 3.10b, the log Cr-log Ti plot (Pearce 1975). All the data points fall in the ocean-floor basalt field of the graph.

3.8 Summary and Conclusions

The alkali-silica, AFM and CIPW normative mineralogy plots establish the tholeiitic nature of the Shelburne and Messejana Dykes. The clustering of the data in FeO*-MgO plot shows little or no fractionation of the major elements. The trends of the TiO_2-P_2O_5, TiO_2-Zr, Rb-K, Sr-Ba, and Sr-Rb plots show passive enrichment of incompatible elements as compatible elements like Ni and Cr are fractionated into olivine and spinel.

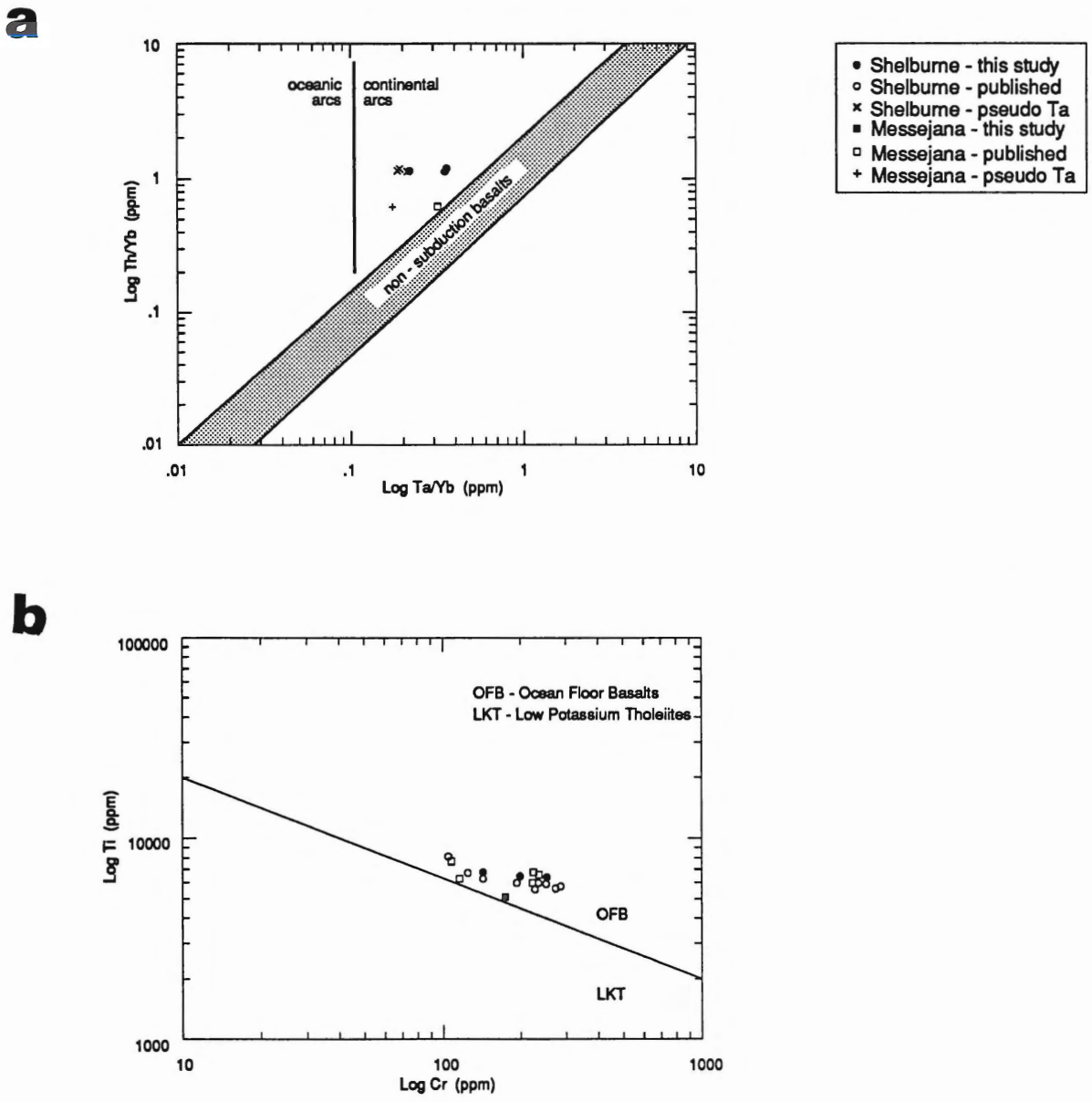

FIGURE 3.10 Tectono-magmatic discriminator diagrams a. Log (Ta/Y)-Log(Th/Y) (Pearce 1983) b. Log Cr-Log Ti (Pearce 1975)

The REE patterns for the Shelburne and Messejana Dykes, excluding the new pattern for the Messejana Dyke, are almost identical. This similarity suggests that both dykes were created from a similar source and underwent similar processes prior to solidification.

The compositional overlap in many cases, and degree of similarity in others, suggests that the Shelburne and Messejana Dykes may have shared a common source and petrogenetic history.

Table 3.2 summarizes the results of all the tectono-magmatic discriminator diagrams. The results from the Ti/100-Zr-Y*3, Ti/100-Zr-Sr/2, FeO-MgO-Al_2O_5, Nb*2-Zr/4-Y, Ti/1000-V, Zr-Ti, log Zr-log(Zr/Y), and log Cr-log Ti all generally fit the previous field and tectonic deductions that the Shelburne and Messejana Dykes are within-plate transitional to ocean-floor basalts. The TiO_2-MnO*10-P_2O_5*10, Hf/3-Th-Nb/16, and log (Ta/Y)-(Th/Y) discriminators yield unexpected results, a discussion of which will follow in Chapter 5.

Discriminator	Shelburne Dyke	Messejana Dyke	Reference	Figure Number
Ti/100-Zr-Y*3	CAB	CAB,OFB	Pearce and Cann 1973	3.7a
Ti/100-Zr-Sr/2	CAB	OFB,IAB	Pearce and Cann 1973	3.7b
TiO_2-MnO*10-P_2O_5*10	IAT	IAT	Mullen 1983	3.7c
Hf/3-Th-Nb/16	DPMB	DPMB	Wood 1980	3.8a
FeO-MgO-Al_2O_3	ORF,OI,C	ORF,OI,C	Pearce et al. 1977	3.8b
Nb*2-Zr/4-Y	VAB,P-MORB	VAB,N-MORB	Meschede 1986	3.8c
Ti/1000-V	OFB	OFB	Shervais 1982	3.9a
Zr-Ti	CAB,OFB	CAB,OFB	Pearce and Cann 1973	3.9b
Log Zr-Log (Zr/Y)	WPB	MORB	Pearce and Norry 1979	3.9c
Log (Ta/Yb)-Log (Th/Yb)	CA-S	CA-S	Pearce 1983	3.10a
Log Cr-Log Ti	OFB	OFB	Pearce 1975	3.10b

Key: C-continental; CAB-calc-alkali-basalt; CA-S-continental arc-subduction zone; DPMB-destructive plate margin basalt; IAB-island-arc basalt; IAT-island-arc tholeiite; N-MORB-normal type mid-ocean ridge basalt; OFB-ocean-floor basalt; OI-ocean island; ORF-ocean-ridge and floor; P-MORB-primitive type mid-ocean ridge basalt; VAB-volcanic-arc basalt; WPB-within-plate basalt

TABLE 3.3 Summary of tectono-magmatic discriminator diagrams

CHAPTER 4: GEOCHRONOLOGY

4.1 Introduction

Following a brief description of the theory behind $^{40}Ar/^{39}Ar$ dating and the argon lab procedure, this chapter presents four new age determinations for the Shelburne and Messejana Dykes. Also included is a new date for a pelitic band in the Goldenville Formation adjacent to the Shelburne Dyke. The chapter concludes with an interpretation and comparison of the new data.

4.2 Theory

The ages of rocks can be determined through the use of radioactive parent isotopes and their stable daughters, including such systems as U-Pb, Th-Pb, Rb-Sr, and Sm-Nd. The system of interest in this document is potassium (K) and argon (Ar). Radioactive decay of parent ^{40}K produces daughter ^{40}Ar. The decay rate of ^{40}K to ^{40}Ar is constant, so by measuring the ratio between the two isotopes, an age can be determined for the time at which the system became closed to isotope diffusion (Dallmeyer 1979).

The equation that describes the half-life of a radioactive element is:

$$t_{1/2} = \log_e/\lambda \qquad (4.1)$$

Where λ = decay constant of the parent isotope.

The decay constant for ^{40}K is 5.54×10^{-10}/year and the half-life of ^{40}K is 1.3×10^{9} years. However, because two different elements are involved, separate techniques are required to analyze for K and Ar.

To avoid the problem of using two such different analytical procedures, the $^{40}Ar/^{39}Ar$ method has replaced the conventional K/Ar technique. In the $^{40}Ar/^{39}Ar$ technique, ^{39}Ar is a proxy for ^{40}K, because irradiation of a sample with fast neutrons in a nuclear reactor converts a portion of the ^{39}K to ^{39}Ar (Dallmeyer 1979). The production of ^{39}Ar by irradiation is given by the following equation:

$$^{39}Ar_K = {}^{39}K \, \Delta \, T \int \varphi \, (\epsilon) \, \sigma \, (\epsilon)^{d\epsilon} \qquad (4.2)$$

Where $^{39}Ar_K$ = ^{39}Ar produced from ^{39}K

^{39}K = ^{39}K present in sample

Δ T = duration of irradiation

φ (ϵ) = flux of neutrons of energy ϵ

σ (ϵ) = capture cross-section for neutrons of energy ϵ

Also, in the $^{40}Ar/^{39}Ar$ method, the sample is heated during the analysis so that an age spectrum is produced in addition to a total gas age (York 1984).

The age of a sample is determined by the following formula:

$$t = 1/\lambda \log_e (^{40}Ar^*/^{39}Ar \, J + 1) \qquad (4.3)$$

where λ = decay constant

$^{40}Ar^*$ = radiogenic ^{40}Ar produced in sample

^{39}Ar = ^{39}Ar present in sample

J = an irradiation parameter that can be evaluated experimentally as long as a sample of known age is irradiated along with unknowns (Faure 1977).

Ages determined by the $^{40}Ar/^{39}Ar$ technique may be influenced by geological events which affected the rock over time. The ages are a measure of the decay of parent

to daughter isotopes; therefore, they represent times at which the daughter isotope becomes immobile and accumulates in the mineral or rock (Dodson 1973). The temperature at which an isotope begins to accumulate in a system is its "closure" temperature (Dodson 1973). The closure temperature of a mineral can vary as a function of compositional differences of the minerals and the type of minerals, e.g., the closure temperatures for biotite and K-feldspar are 280-300°C and 200°C, respectively (Harrison 1981; McDougall and Harrison 1988).

An age spectrum represents the complete stepwise heating procedure of a mineral(s) sample (Section 4.3). These age spectra often yield important information on the history of cooling and gas retention of a sample (Fleck et al 1977). To assign an age to these spectra, two methods are used. The most common is to use the total gas age which represents the weighted average of ages from all heating steps (Fleck et al 1977). The second method is to determine a "plateau age" (the age from the flat, concordant part of the age spectrum) (Fleck et al. 1977). A plateau must represent at least 50% of the gas released in contiguous steps. In addition, no two of the age steps used can have age differences greater than the "critical value" (C V). The C V can be calculated with the following formula:

$$C\,V = 1.960\,(\delta_1^2 + \delta_2^2)^{1/2} \qquad (4.4)$$

Where δ_1 and δ_2 = Standard deviation of the two steps used.

Each step represents a temperature increase of 50°C at which the sample is heated to release the argon gas.

Interpretation of an age spectrum can be straightforward (if it is concordant or

flat), or can be complex (if it is discordant or not flat). The plateau age generally represents the cooling age of a mineral through its closure temperature (Fleck et al. 1977). Occasionally concordant spectra, such as those for some biotite, yield anomalously old ages. The cause of this discordance may be the presence of excess argon; argon which was not present in a sample initially but subsequently incorporated (Foland 1983). Discordant ages for some minerals may also indicate partial resetting of argon caused by a metamorphic event or slow cooling.

4.3 Argon Lab Procedure

The following description of the dating procedure is paraphrased from Check (1989).

Argon gas is extracted from the samples by placing them into an evacuated tantalum resistance furnace. Gas released from the sample is admitted to a VG 3600 mass spectrometer after: (i) the sample is outgassed for approximately fifty minutes at each temperature increment of 50°C; and (ii) the impurities in the gas are separated by cleaning the gas with the titanium "getter". The sample moves through the system by a system of valves. Gas in the mass spectrometer is analyzed for ^{40}Ar, ^{39}Ar, ^{37}Ar, and ^{36}Ar. Measurements of ^{37}Ar and ^{36}Ar are used for elemental and atmospheric contamination corrections. The computer attached to the mass spectrometer prints out the isotope ratios, correction factors, and age for the step. All the gas release steps for a sample are plotted together on a diagram showing apparent age versus % ^{39}Ar released, yielding an age spectrum (Fig. 4.1).

4.4 Sample Description

Five samples were analyzed for this thesis: two from the Shelburne Dyke (Little Harbour), two from the Messejana Dyke (Cabezuela de Valle), and one from the Meguma Group adjacent to the Shelburne Dyke.

The two samples from the Shelburne Dyke are SD93-1 and SD93-6. Sample SD93-1 (whole-rock) was taken from the margin of the dyke. A whole-rock sample is used for this analysis because no K-rich phase, such as biotite, could be separated from the rock. Sample SD93-6 contains 5-10% modal biotite that was separated from the rest of the rock.

The single hand specimen of the Messejana Dyke (MD93-1) yielded two mineral separates (biotite and felsics) for age determination. These mineral separates present two opportunities to determine the age of the dyke and potentially its thermal history.

Sample SD93-4 (biotite) was taken from the country rock (Meguma) less than 2 metres from the Shelburne dyke. Intrusion of the adjacent dyke should have reset the argon in the biotites to yield the age of dyke emplacement.

Table 4.1 lists selected mineral compositions for the Shelburne Dyke, the Meguma Group, and the Messejana Dyke.

4.5 Sample Preparation

To obtain the mineral separates, the hand samples were first crushed, sieved and washed to produce a 60-120 mesh fraction. From this fraction the biotite and feldspar separates were obtained by the following methods.

Region	NS (rim)	NS (rim)	NS (core)	NS (core)	NS (core)	NS (Meguma)	Spain (core)	Spain (core)	Spain (core)
Sample	SD93-1	SD93-7	SD93-6	SD93-6	SD93-6	SD93-4	MD93-1	MD93-2	MD93-3
Mineral	Plagioclase	Plagioclase	Plagioclase	Biotite	Ilmenite	Biotite	Plagioclase	Biotite	Magnetite
Structural Formula	CaAl2Si2O8	CaAl2Si2O8	CaAl2Si2O8	K2(Mg,Fe)3AlSi3O10(OH)2	FeTiO2	K2(Mg,Fe)3AlSi3O10(OH)2	CaAl2Si2O8	K2(Mg,Fe)3AlSi3O10(OH)2	FeFe2O4
Sio2	50.92	51.89	53.35	36.1	5.62	35.05	53.71	35.33	30.98
TiO2	0	0	0	4.3	17.45	1.64	0	1.81	0
Al2O3	29.64	29.46	28.36	11.96	1.12	17.4	28.32	17.7	0
FeO	0.57	0.59	0.76	27.52	64.89	22.62	0.77	21.55	46.91
MnO	0	0	0	0	1.49	0	0	0	0.49
MgO	0	0.23	0	6.87	0.25	7.92	0	7.96	1.88
CaO	14.02	13.87	12.13	0	1.31	0	11.86	0	12.62
Na2O	3.57	3.81	4.74	0.57	0.46	0	4.69	0	0.31
K2O	0.16	0	0.23	8.69	0.41	9.42	0.36	9.57	0
ClO	0	0	0	0.33	0	0	0	0	0
Total	98.89	99.86	99.57	96.33	93.01	94.05	99.72	93.92	93.19

TABLE 4.1 Select mineral compositions for the Shelburne Dyke, Meguma Group, and the Messejana Dyke

The samples were run through the Frantz magnetic separator which separates the mafic from the felsic fractions by their magnetic susceptibilities; quartz and feldspar are less magnetic than biotite and other ferromagnesian minerals. To obtain the biotite samples, the mafic fraction was further separated by the paper-panning technique. The sample was placed on a sheet of paper that was then inclined. The platy biotites adhered to the sheet while the other minerals rolled off.

The biotite, felsic, and whole-rock samples were then sent to McMaster University where they were irradiated, returned to Dalhousie and analyzed in the mass spectrometer.

4.6 Results

4.6.1 Shelburne Dyke

The biotite from sample SD93-6 shows a discordant age spectrum (Fig. 4.1a). The discordant nature of the spectrum could be caused by the low percentages of ^{39}Ar released from the biotite which, in turn, could be caused by the alteration of biotite (K-rich) to chlorite (K-poor). A true plateau age cannot be determined from this spectrum, but a pseudo-plateau age of 207 ± 2 Ma can be determined from the eighth and ninth heating steps. These two steps are the most reliable and form the only concordant section of the age spectrum. The total gas age for this sample is 206 Ma.

The age spectrum for the whole-rock sample SD93-1 is very discordant, probably because a variety of minerals (plagioclase, pyroxene, and cryptocrystalline groundmass phases) released argon gas (Fig. 4.1b). Because the spectrum is so discordant, a plateau

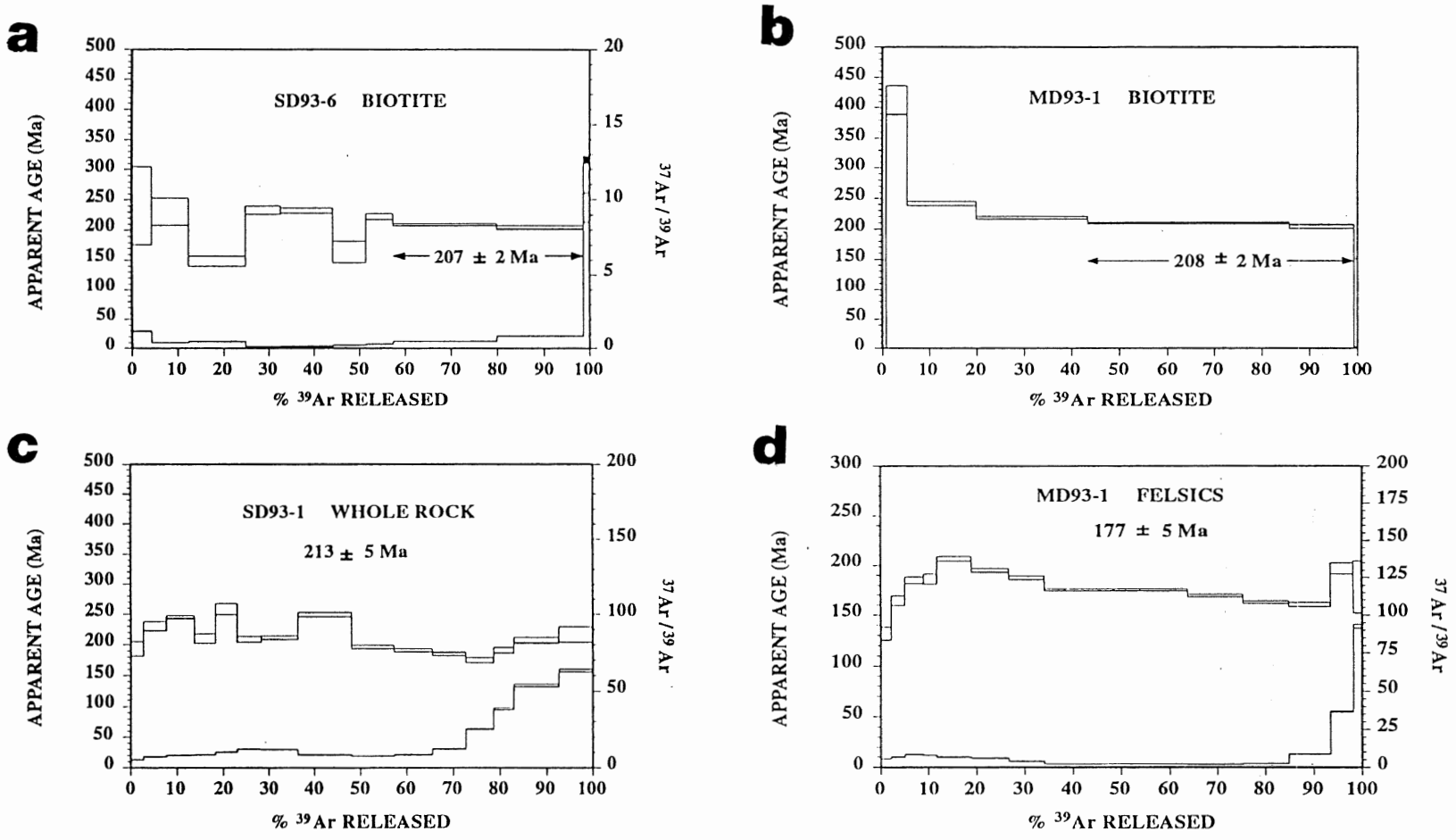

FIGURE 4.1 Age spectra for the Shelburne and Messejana Dykes a. SD93-6, Shelburne Dyke biotite sample b. SD93-1, Shelburne Dyke whole-rock sample c. MD93-1, Messejana Dyke biotite sample d. MD93-1, Messejana Dyke felsic sample

age cannot be determined; however, the total gas age for this sample is approximately 213 ± 5 Ma. The second curve on the graph is the $^{37}Ar/^{39}Ar$ plot. The ratio of these two isotopes of argon is related to the ratio of calcium to potassium (Ca/K) in the rock. The first 70% of the argon release curve has low (Ca/K) values, suggesting a mineral containing a much higher abundance of K than Ca, such as biotite or sericite (an alteration product of plagioclase). At the high-temperature heating steps, the increase in the Ca/K curve indicates that a more calcic mineral, such as plagioclase, released gas. X-ray maps from the electron microprobe showed that the K is primarily in the very fine-grained matrix, and that the most likely mineral in the matrix that contained the potassium is K-feldspar (Fig. 4.2-4.3).

4.6.2 Messejana Dyke

Biotite provided an additional total gas age of 222.2 Ma for the sample from the Messejana Dyke. This high age could be the result of excess argon in the biotites. A plateau age of 208 ± 2 Ma can be calculated from the fifth and sixth steps of the age spectrum (Fig. 4.1c). The amount of biotite used to determine an age was considerably smaller than the other samples, so the heating increments were 100°C, rather than the usual 50°C, to accumulate the necessary amount of argon gas to measure.

Feldspars were used to determine a date for sample MD93-1, yielding total gas age of 194.1 Ma. A plateau age of 177 ± 5 Ma can be calculated from the seventh to the tenth step of the age spectrum (Fig. 4.1d). Subsequent alteration could be the cause of this lower age, as suggested by $^{37}Ar/^{39}Ar$ plot. The plateau corresponds to the section

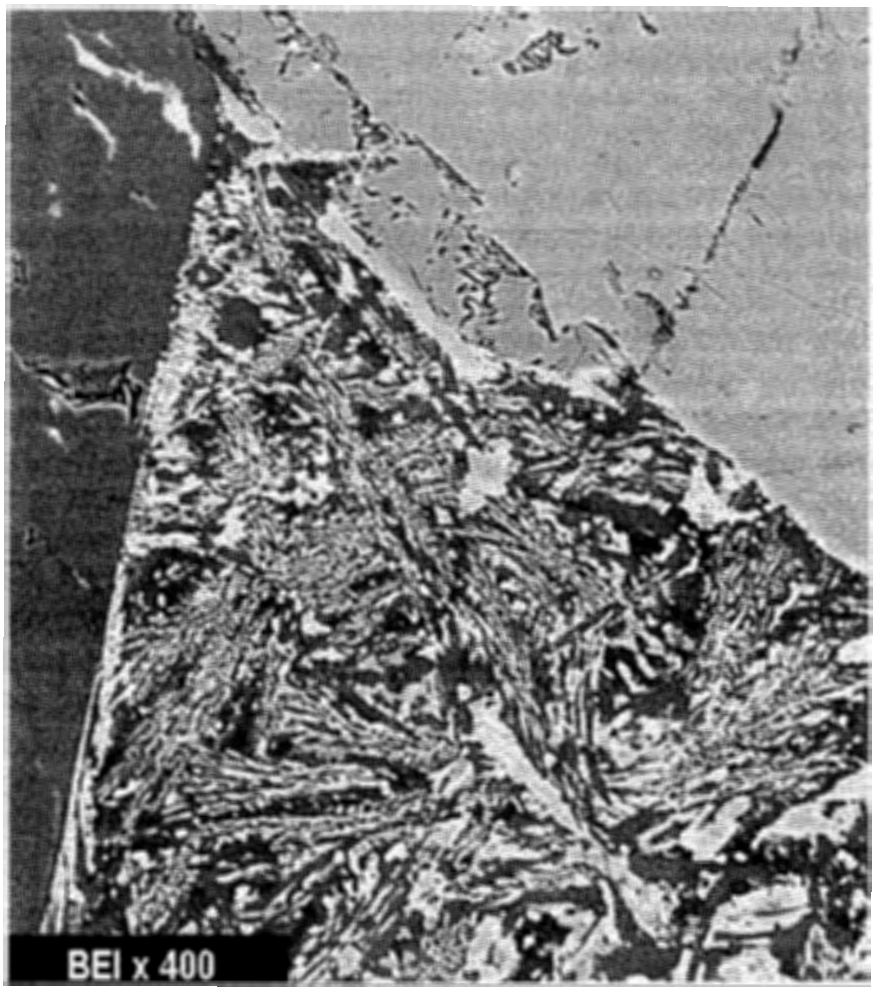

FIGURE 4.2 Backscattered electron image (BEI) showing a plagioclase crystal (left), a pyroxene crystal (right), and the fine-grained matrix containing skeletal quench crystals of sample SD93-1. This area was analyzed to produce the X-ray element maps in Figure 4.3.

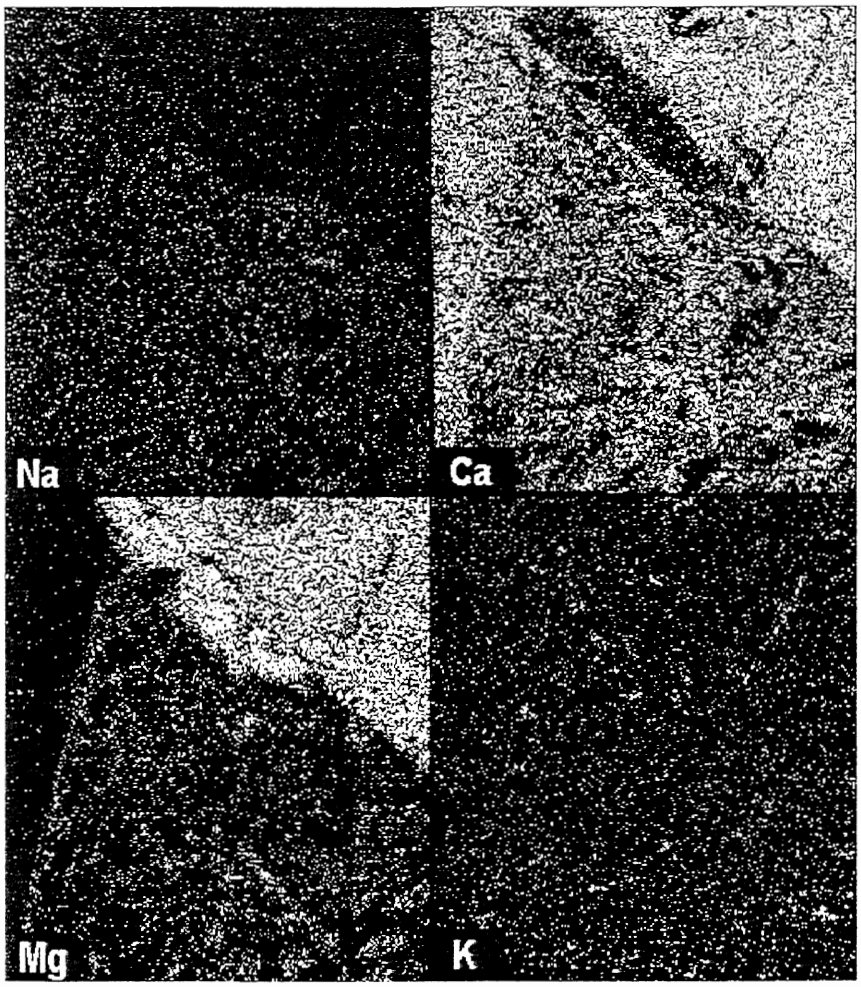

FIGURE 4.3 X-ray maps showing where the elements Na, Ca, Mg, and K are located in Figure 4.2. The light areas indicate places where the element is most abundant. The potassium analyzed to determine the age of sample SD93-1 was probably released from K-feldspar in the fine-grained matrix.

of argon release spectrum that shows a low Ca/K ratio. Sericite, an alteration product of plagioclase, contains more K than plagioclase, and is probably the mineral responsible for producing the lower plateau age. The total gas and plateau ages for this sample are considerably lower than the age determined from the biotite.

4.6.3 Meguma Group

Sample SD93-4 is biotite from the Meguma Group. The rationale for selecting this sample is that, should the dyke itself not contain any datable phases, intrusion of the Shelburne Dyke should have reset the ages of the biotites in the adjacent country rocks (Fig. 4.5). The total gas age, and also the plateau age (because the spectrum is so concordant), is 372 ± 2 Ma. This determination is neither the age of the Acadian metamorphism (ca. 400 Ma), nor is it the age of the Shelburne Dyke (ca. 208 Ma); however, it is identical to the age of granitic intrusion in the Meguma Zone (Clarke et al. 1993). Complete resetting, or even formation of the biotite porphyroblasts in sample SD93-4 at the time of the granite intrusion is probably a better explanation for this age than either excess argon or partial resetting by the dyke. A question remains as to why the dyke did not reset the biotites. The country rock is less than 2 metres away from the dyke, whereas the nearest exposed body of granite is about 10 kilometres distant. This question could form the basis of future work in this area.

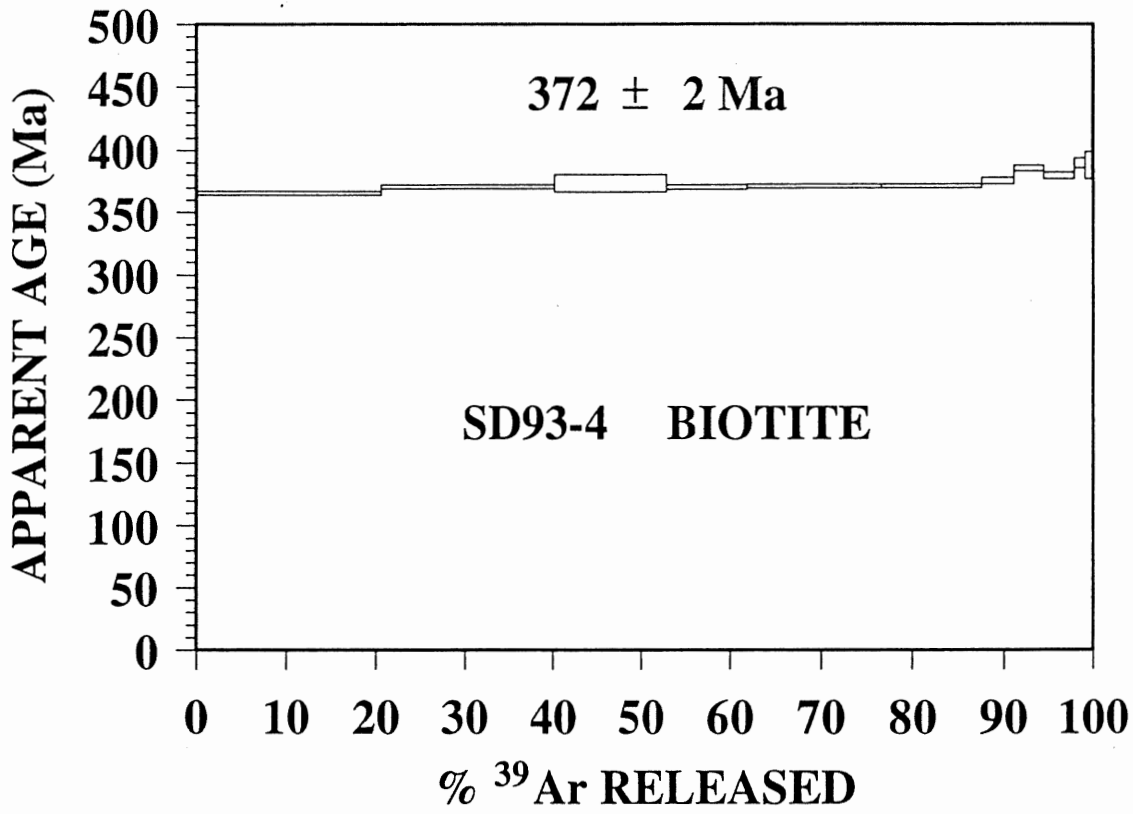

FIGURE 4.4 Age spectrum of the Meguma Group adjacent to the Shelburne Dyke.

4.7 Comparisons

The average total gas age for the two samples from the Shelburne Dyke is 209.3 Ma, and the average total gas age for the two samples from the Messejana Dyke is 208.2 Ma. These determinations place the intrusion of both the dykes on the boundary of the Triassic-Jurassic Periods (Harland et al. 1990).

Table 4.1 summarizes all the ages determined for the Shelburne and Messejana Dykes. The total gas ages for the biotites from the Shelburne Dyke (SD93-6) and the Messejana Dyke (MD93-1) differ by 16.2 Ma. However, the plateau age for MD93-1 (208 ± 2 Ma) is not statistically different from the plateau age for SD93-6 (207 ± 2 Ma).

The ages determined by the whole-rock sample (SD93-1) and the felsic sample (MD93-1) differ from the biotite ages and are not very reliable. Obtaining reliable ages from these types of samples is difficult because of the presence of so many minerals in each sample that release argon gas. Some of the minerals could contain more gas, and some may be alteration products or younger phases. Clear evidence of alteration or younger phases is evident in the $^{37}Ar/^{39}Ar$ plot on the age spectra: the low flat areas were formed by K-rich minerals such as biotite or sericite, and the higher regions were formed by minerals with lower values of K and high values of Ca.

Sample Number	Total Gas Age	Plateau Age
SD93-1 (whole rock)	213 ± 5 Ma	N/A
SD93-6 (biotite)	206 Ma	207 ± 2 Ma
MD93-1 (felsics)	194.1 Ma	177 ± 2 Ma
MD93-1 (biotite)	222.2 Ma	208 ± 2 Ma

TABLE 4.2 Summary table for geochronological data from the Shelburne and Messejana dykes.

4.8 Conclusions

All previously published ages for the two dykes were determined from the analysis of whole-rock, plagioclase, and pyroxene samples. Why biotites were not used for geochronological analysis is unknown, unless the small modal proportions escaped notice or prohibited concentration.

The $^{40}Ar/^{39}Ar$ plateau ages from the biotite show that the Shelburne and Messejana Dykes were emplaced on the boundary of the Triassic-Jurassic Periods (Harland et al. 1990). Because these ages were obtained from concordant plateaus, they are probably the most reliable of the new age determinations. The ages from the analysis of the whole-rock and felsic samples are not reliable because the argon gas was probably released from a variety of minerals, some of them secondary.

The plateau age from the Shelburne Dyke (207 ± 2 Ma) is identical to the plateau age of the Messejana Dyke (208 ± 2 Ma). These ages are significantly older than any of the previously published ages. The implications of these older ages are examined in the following chapter.

CHAPTER 5: DISCUSSION

5.1 Introduction

This chapter synthesizes the data and information from the earlier parts of this paper. In particular, it discusses the important aspects of the petrology, geochemistry, and geochronology of the Shelburne and Messejana Dykes. The final section considers three tectonic hypotheses or models to explain the formation and setting of the Shelburne and Messejana Dykes. The chapter ends with an evaluation of the hypothesis which best fits the existing data.

5.2 Field Relations and Petrology

Table 5.1 summarizes the important points of Chapter 2. The Shelburne Dyke and the Messejana Dyke are very similar in their physical dimensions, attitude, and position with respect to the axis of the Atlantic Ocean. The dykes also share the common mineral assemblages of basaltic rocks, but significantly they both contain biotite, a rare mineral in tholeiites. That the dykes contain biotite is important because the analysis of the biotite to determine ages for the dykes provided the most reliable data.

5.3 Geochemistry

5.3.1 Comparison of the Shelburne and Messejana Dykes

Based on their whole-rock geochemistry, the Shelburne and Messejana Dykes are also similar. Both are tholeiites with similar major element, trace element, and rare-earth element compositions.

Field Relations and Petrology	Shelburne Dyke	Messejana Dyke
Location of Outcrop	Little Harbour 44°10' N, 64°29' W	Cabezuela de Valle 44°12' N, 5°48' W
Length/width	140 km/100 m	530 km/300 m (max.) 20 m at outcrop
Host rock	metawacke and metapelite from the Goldenville Formation	sillimanite-bearing two-mica granite
Mineralogy of margins	microphenocryts of plagioclase, orthopyroxene and minor olivine	microphenocryts of plagioclase, orthopyroxene and minor olivine
Texture of margins	fine-grained, inequigranular, glomeroporphyritic, subophitic	fine-grained, subophitic to ophitic
Mineralogy of interior	plagioclase, clinopyroxene, biotite, opaque minerals and minor olivine	plagioclase, clinopyroxene, biotite, opaque minerals and minor olivine and chlorite
Texture of interior	coarse-grained, equigranular, holocrystalline and subophitic to ophitic	medium to coarse-grained, sub-ophitic to ophitic and poikiolitic

FIGURE 5.1 Summary table of the field relations and petrology of the Shelburne and Messejana Dykes

Based on this high degree of chemical similarity, the Shelburne and Messejana Dykes are possibly related and may have formed from comparable magma sources.

5.3.2 Tectonic Setting

The results from the tectono-magmatic discriminator diagrams fall into three different groups:

(i) both the analytical data and the discriminator appear reliable,

(ii) both the analytical data and the discriminator appear unreliable; and

(iii) the analytical data are reliable but the discriminator yields unexpected results.

The first group of diagrams (Ti/100-Zr-Y*3, Ti/100-Zr-Sr/2, FeO-MgO-Al_2O_3, Nb*2-Zr/4-Y, Ti/1000-V, Zr-Ti, log Zr-log (Zr/Y), and log Cr-log Ti) suggests that the Shelburne and Messejana Dykes are ocean-floor basalts, within-plate basalts, and mid-ocean ridge basalts. All these environments are consistent with other dykes that have the same chemistry as the Shelburne and Messejana Dykes. Some of these diagrams (the Ti/100-Zr-Y*3, Ti/100-Zr-Sr/2, and Zr-Ti plots) however, describe the Shelburne Dyke as being a calc-alkali basalt; normally considered a product of a subduction. The reason for subduction signature may be subduction components in the mantle underneath the Meguma Group residual from the Devonian Period (Tate and Clarke 1994 in preparation). The source of the subduction-enriched mantle may be the destruction of Iapetus lithosphere during the Early Devonian, or Theic crust during the Middle Devonian. The initial rifting that preceded the formation of the Shelburne Dyke allowed some of the enriched mantle to contribute to the formation of the first igneous products of the formation of the Atlantic Ocean. More primitive mantle material quickly

followed, to form the ocean floor.

Two discriminators are not reliable; the Hf/3-Th-Nb/16 and log (Ta/Yb)-log (Th/Yb) plots. The two diagrams suggest that the dykes were formed in a destructive plate margin and continental arc-subduction zone respectively. The results from these plots are odd, probably because of analytical problems with the Th and Ta determinations by ICP-MS. Inaccurate values for these two elements may result in erratic deductions about the tectonic environment; however, these results are similar to those above that yield subduction signatures.

The analytical data for the TiO_2-MnO*10-P_2O_5*10 plot are reliable, but the deduced tectonic environment is not. This diagram suggests the Shelburne and Messejana Dykes were formed in island arcs; however, the TiO_2-MnO*10-P_2O_5*10 plot does not contain a within-plate basalt or ocean-floor basalt field. The WPT and OFB fields could possibly occupy the same area as the IAT field.

5.4 Geochronology

The biotite plateau ages from the Shelburne and Messejana Dykes (207 ± 2 Ma and 208 ± 2 Ma, respectively) are identical, and they straddle the Triassic and Jurassic boundary (Harland et al. 1990). This age is significantly older than any of the previously published ages. Figure 5.1 is a histogram showing the published and new ages for the Messejana Dyke. The plateau age for the felsic sample falls in the region of the plot with the highest frequency data points (median of the histogram). The average

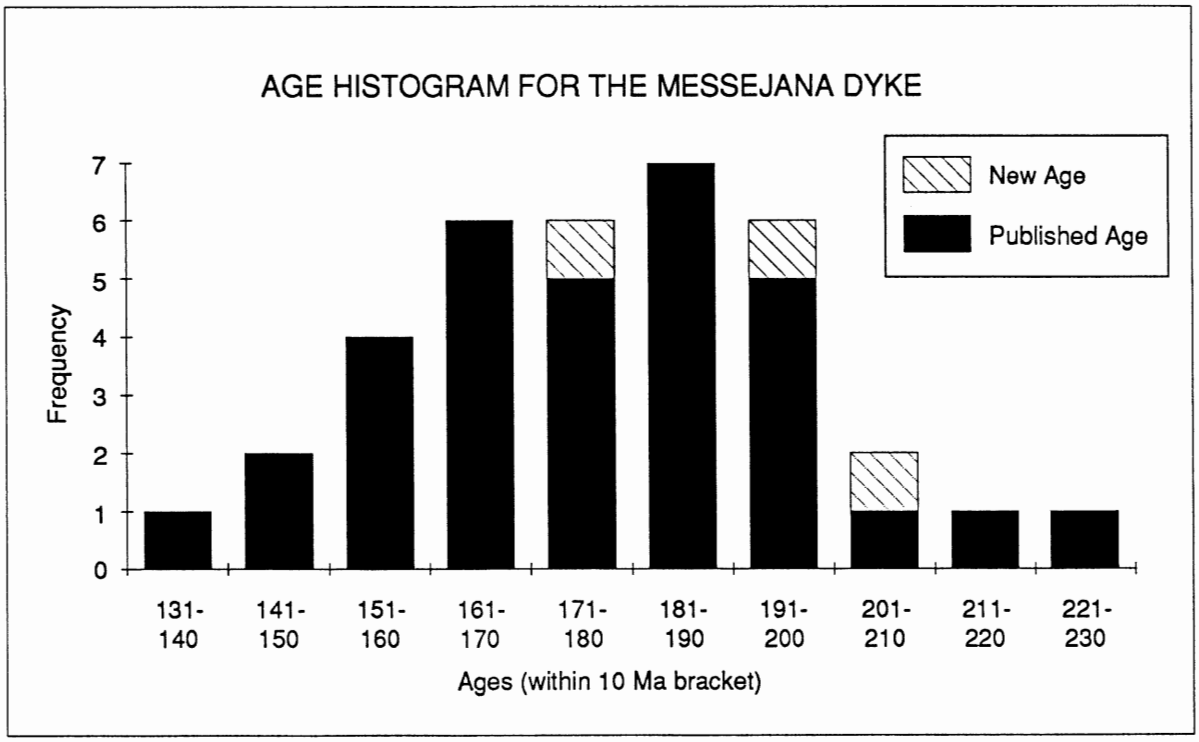

Mean- 178.8 Ma
Median- 171 - 180 Ma

FIGURE 5.1 Histogram showing the published and new ages for the Messejana Dyke

published age for the Messejana Dyke is 178.8 Ma; and the plateau age for the new felsic sample is 177 ± 5 Ma. This coincidence suggests that many previously published ages for the Messejana Dyke recorded the alteration event, not the intrusive age of the dyke.

5.5 Tectonic Models for the Shelburne and Messejana Dykes

Although the Shelburne and Messejana Dykes are contemporaneous, the question that still remains is, how the two dykes are related to each other with respect to tectonic setting and position. Three simple, but plausible, models are:

(i) *one dyke*- the Messejana Dyke is an extension of the Shelburne Dyke;

(ii) *two parallel dykes*- the Shelburne and Messejana Dykes are rift-parallel on opposite sides of the Atlantic Ocean; and

(iii) *two perpendicular dykes*- the Shelburne Dyke is rift-parallel whereas the Messejana Dyke is rift-perpendicular, emplaced instead in a transform fracture zone.

Figure 5.2 illustrates these three models schematically.

5.5.1 One-Dyke Model

This model considers that the Messejana Dyke is equivalent to, i.e. an extension of, the Shelburne Dyke. Figure 5.3 (Ziegler 1988) is a paleotectonic and paleogeographical map showing the North Atlantic Ocean in the Early Jurassic Period. According to this reconstruction, the Messejana Dyke could be an extension of the Shelburne Dyke.

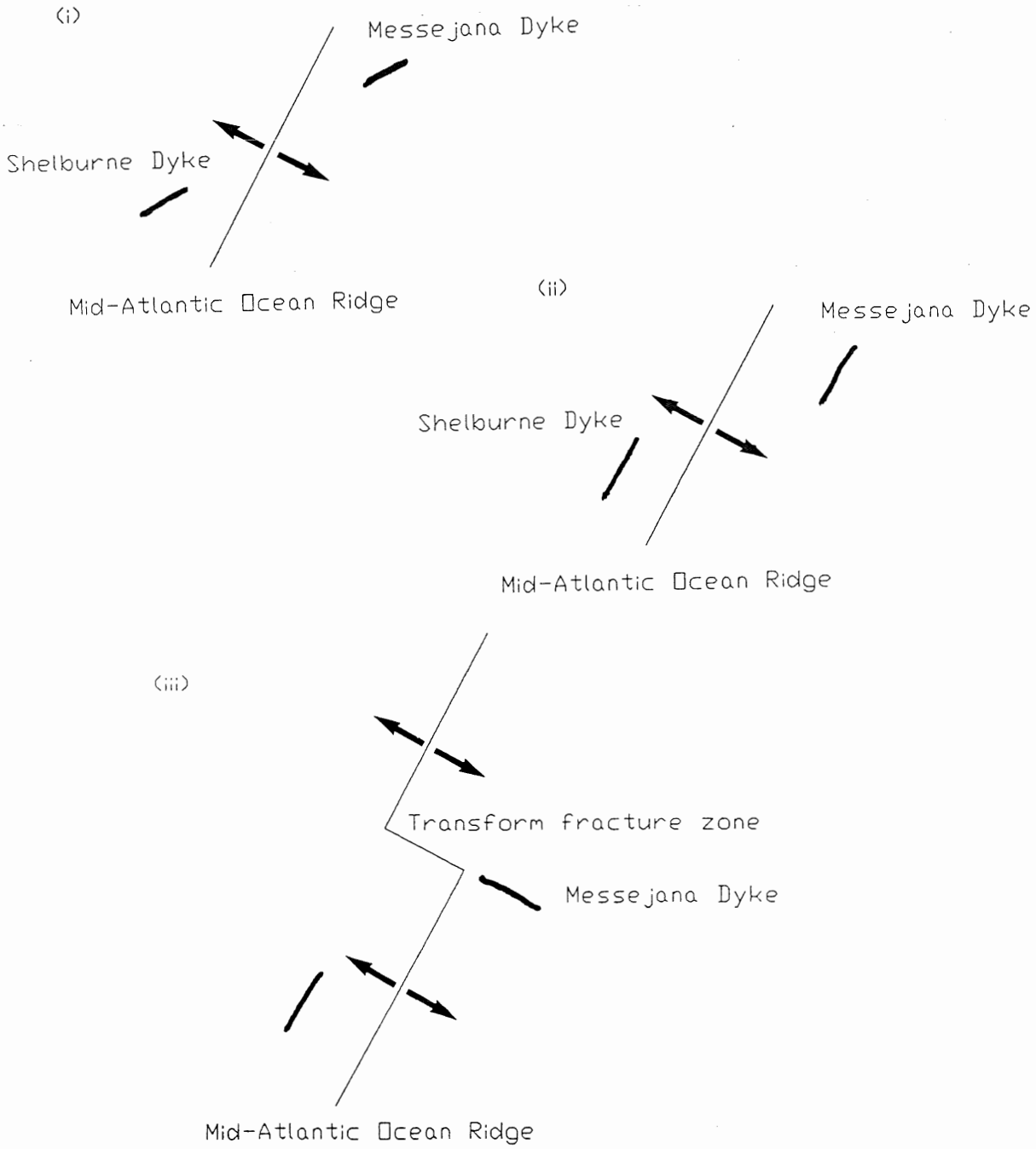

FIGURE 5.2 Three models for the relationship between the Shelburne and Messejana Dykes: (i) the Messejana Dyke is an extension of the Shelburne Dyke; (ii) the Shelburne and Messejana Dykes are rift-parallel; and (iii) the Shelburne Dyke is rift-parallel and the Messejana Dyke is rift-perpendicular, emplaced in a transform fracture zone.

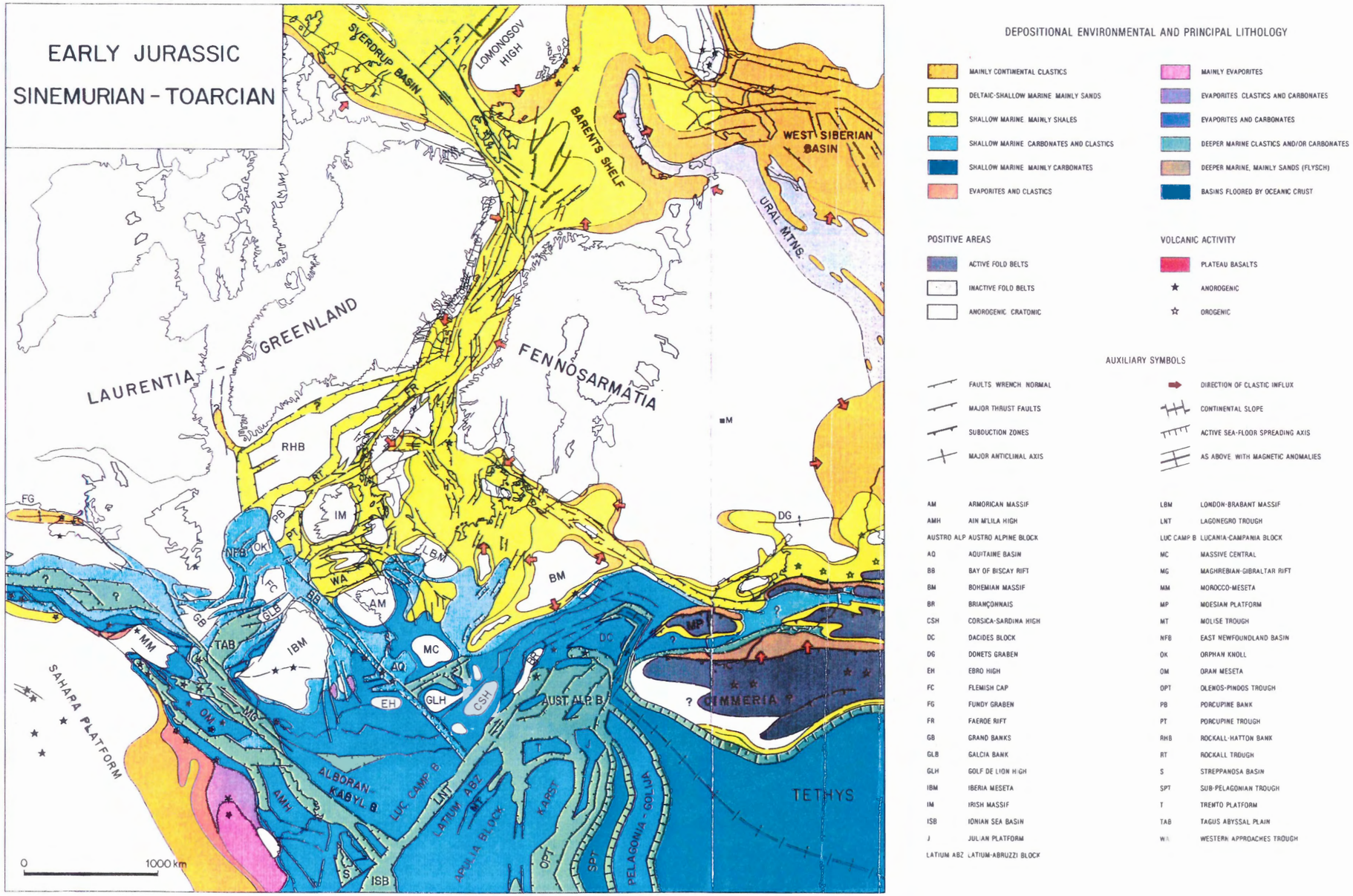

DEPOSITIONAL ENVIRONMENTAL AND PRINCIPAL LITHOLOGY

- MAINLY CONTINENTAL CLASTICS
- DELTAIC-SHALLOW MARINE MAINLY SANDS
- SHALLOW MARINE MAINLY SHALES
- SHALLOW MARINE CARBONATES AND CLASTICS
- SHALLOW MARINE MAINLY CARBONATES
- EVAPORITES AND CLASTICS
- MAINLY EVAPORITES
- EVAPORITES CLASTICS AND CARBONATES
- EVAPORITES AND CARBONATES
- DEEPER MARINE CLASTICS AND/OR CARBONATES
- DEEPER MARINE, MAINLY SANDS (FLYSCH)
- BASINS FLOORED BY OCEANIC CRUST

POSITIVE AREAS

- ACTIVE FOLD BELTS
- INACTIVE FOLD BELTS
- ANOROGENIC CRATONIC

VOLCANIC ACTIVITY

- PLATEAU BASALTS
- ★ ANOROGENIC
- ☆ OROGENIC

AUXILIARY SYMBOLS

- FAULTS WRENCH NORMAL
- MAJOR THRUST FAULTS
- SUBDUCTION ZONES
- MAJOR ANTICLINAL AXIS
- DIRECTION OF CLASTIC INFLUX
- CONTINENTAL SLOPE
- ACTIVE SEA-FLOOR SPREADING AXIS
- AS ABOVE WITH MAGNETIC ANOMALIES

AM	ARMORICAN MASSIF
AMH	AIN M'LILA HIGH
AUSTRO ALP	AUSTRO ALPINE BLOCK
AQ	AQUITAINE BASIN
BB	BAY OF BISCAY RIFT
BM	BOHEMIAN MASSIF
BR	BRIANÇONNAIS
CSH	CORSICA-SARDINA HIGH
DC	DACIDES BLOCK
DG	DONETS GRABEN
EH	EBRO HIGH
FC	FLEMISH CAP
FG	FUNDY GRABEN
FR	FAEROE RIFT
GB	GRAND BANKS
GLB	GALCIA BANK
GLH	GOLF DE LION HIGH
IBM	IBERIA MESETA
IM	IRISH MASSIF
ISB	IONIAN SEA BASIN
J	JULIAN PLATFORM
LATIUM ABZ	LATIUM-ABRUZZI BLOCK
LBM	LONDON-BRABANT MASSIF
LNT	LAGONEGRO TROUGH
LUC CAMP B	LUCANIA-CAMPANIA BLOCK
MC	MASSIVE CENTRAL
MG	MAGHREBIAN-GIBRALTAR RIFT
MM	MOROCCO-MESETA
MP	MOESIAN PLATFORM
MT	MOLISE TROUGH
NFB	EAST NEWFOUNDLAND BASIN
OK	ORPHAN KNOLL
OM	ORAN MESETA
OPT	OLENOS-PINDOS TROUGH
PB	PORCUPINE BANK
PT	PORCUPINE TROUGH
RHB	ROCKALL-HATTON BANK
RT	ROCKALL TROUGH
S	STREPPANOSA BASIN
SPT	SUB-PELAGONIAN TROUGH
T	TRENTO PLATFORM
TAB	TAGUS ABYSSAL PLAIN
WA	WESTERN APPROACHES TROUGH

FIGURE 5.3 Early Jurassic paleotectonic-paleogeographical map showing the positions of the Shelburne Dyke (★ on Nova Scotia) and the Messejana Dyke (★-★ on Iberia Meseta- IBM)

Compositional, geochronological, and spatial constraints permit this hypothesis, however no further support exists. In particular, a strong aeromagnetic signature for an extension of the Shelburne Dyke across the Scotian Shelf is needed to substantiate this particular hypothesis. The Shelburne Dyke does have such a signature offshore (Papezik et al. 1975), but it only extends for a few kilometres. This result could mean that the areomagmatic signature is lost underneath younger offshore sediments. To test the one-dyke model, drilling and core analysis could be done along the Continental Shelf.

5.5.2 Two Parallel Dykes Model

The second hypothesis states that the Shelburne and Messejana Dykes are parallel to each other and to the present-day Mid-Atlantic Ridge. Again, geochemical and geochronological data indicate that the two dykes are similar and related, but says nothing about their positions. According to Schermerhorn et al. (1978), the Messejana Dyke is parallel to the Mid-Atlantic rift between Northwest Africa and North America. Investigations into the Shelburne Dyke by Papezik and Barr (1981) and Pe-Piper et al. (1992) demonstrate that it is also parallel to the Mid-Atlantic Ridge. Modern and paleo-reconstruction geological maps, such as the ones published by Ziegler (1988) (Fig. 5.3), provide support for this model.

5.5.3 Two Perpendicular Dykes Model

This model considers that the Shelburne Dyke is rift-parallel, as the previous hypothesis does, but that the Messejana Dyke is rift-perpendicular, meaning it was intruded into a transform fracture zone caused by faulting along the Mid-Atlantic Ridge. The opening of the Bay of Biscay caused Iberia to be rotated during the Cretaceous

Period (Sibuet 1989). This rotation may have moved a formerly perpendicular Messejana Dyke to become parallel with the Shelburne Dyke. In support of this hypothesis, the Messejana Dyke has also experienced a high degree of deformation in the Messejana fault zone unlike the Shelburne Dyke. The Mid-Atlantic Ridge shows many transform faults, however, none of these occurs close to the Messejana Dyke.

5.6 Conclusions

The geochemical and geochronological data presented in this paper show that the Shelburne and Messejana Dykes were comparable and probably related, thus allowing the formation of three hypotheses to explain their relationship to each other and the Mid-Atlantic Ridge.

The simplest model, which suggests the Shelburne and Messejana Dykes are parallel to each other and to the Mid-Atlantic Ridge, bests explains the relationship between the two dykes. Figure 5.4, a cross-section of one of the initial phases of the rifting in the Mid-Atlantic, shows the parallel association between the Shelburne and Messejana Dykes.

The sequence of events that led to the formation of the Shelburne and Messejana Dykes and the proto-Atlantic Ocean is interpreted to be the following.

The creation of the North Atlantic Ocean started with a phase of continental stretching and rifting, and as North America split from Africa and later Europe, new oceanic crust formed between the continents by seafloor spreading (Schermerhorn et al. 1978).

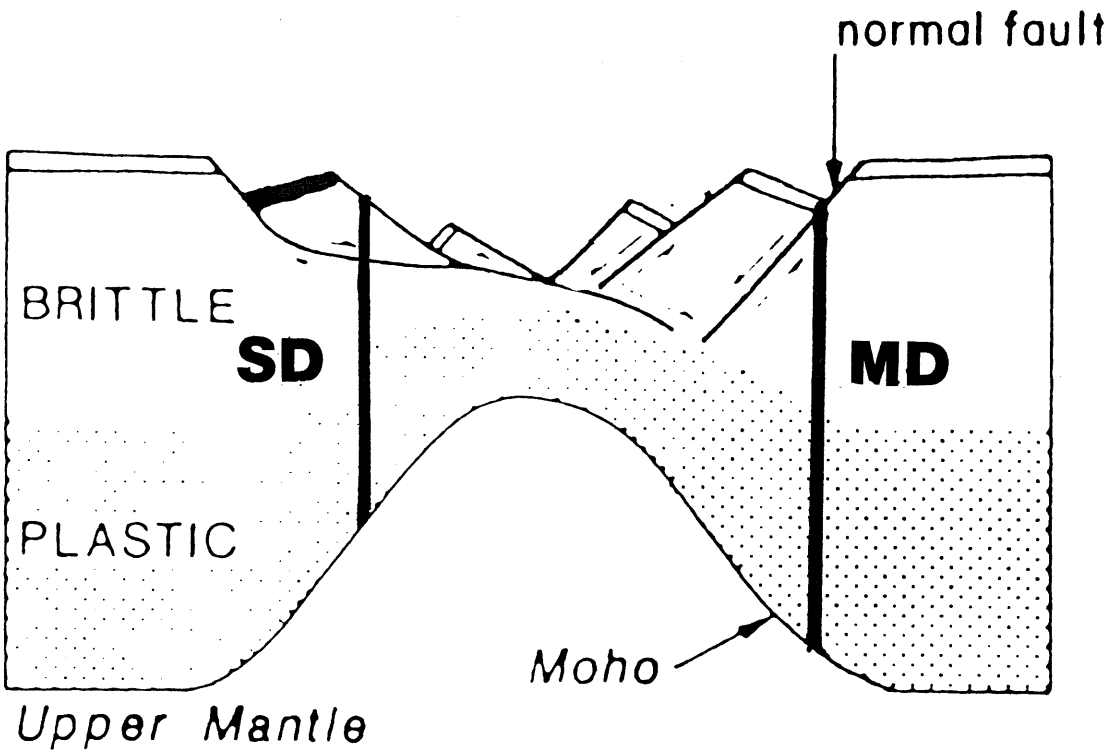

FIGURE 5.4 Hypothetical Late Triassic-Early Jurassic rifting of the North Atlantic Ocean. (SD=Shelburne Dyke MD=Messejana Dyke) (after Sibuet 1992)

The initial fracturing and rifting that led to the breakup of the continents occurred around the Triassic-Jurassic boundary (Schermerhorn et al. 1978). In the axial parts of the Central Atlantic Rift, rapid crustal extension induced regional stresses that caused the intrusion of tholeiitic dykes and other magmatic rocks around the North Atlantic Ocean (Ziegler 1988). The Shelburne and Messejana Dykes are examples of these tholeiitic dykes.

Around 180 Ma, the Early Jurassic, seafloor spreading, lithosphere separation, and generation of oceanic crust began (Schermerhorn et al. 1978).

CHAPTER 6: CONCLUSIONS AND SUGGESTIONS FOR FURTHER WORK

6.1 Conclusions

Following are the most significant findings and conclusions from this study of the Shelburne and Messejana Dykes.

(i) The Shelburne and Messejana Dykes are extensive vertical sheets of intrusive rock that are over 100 kilometres in length, average around 100 metres in thickness, and extend in the northeast-southwest direction at a latitude of 44°N.

(ii) The Shelburne and Messejana Dykes contain an abundance of plagioclase and pyroxene, with minor opaque minerals, olivine, and biotite. Both have subophitic to ophitic textures.

(iii) The alkali-silica and Na_2O+K_2O-MgO-FeO plot show that the two dykes are tholeiites. The projection from clinopyroxene out of the base of the CIPW normative tetrahedron shows the majority of the samples lie in the quartz tholeiite field with two of the published data points for the Messejana Dyke lying in the olivine tholeiite.

(iv) There is little or no fractionation of the major elements in the Shelburne and Messejana Dykes.

(v) Fractional crystallization of compatible elements such as Ni and Cr causes elements such as Sr, Ba, and Rb to become passively enriched.

(vi) The rare-earth element patterns for the Shelburne and Messejana Dykes

are similar, suggesting that they originated from a similar mantle source.

(vii) According to the tectono-magmatic discriminator diagrams, the Shelburne and Messejana Dykes are within-plate basalts, ocean-floor basalts, or mid-ocean ridge basalts.

(viii) The most reliable ages for the Shelburne and Messejana Dykes were obtained from the plateaus of the biotite samples: 207 ± 2 Ma and 208 ± 2 Ma, respectively. These dates place the intrusion of the two dykes on the boundary of the Triassic and Jurassic Periods.

(ix) The Shelburne and Messejana Dykes are parallel to each other and the Mid-Atlantic Ridge.

(x) The Shelburne and Messejana Dykes are related to the opening of the North Atlantic Ocean.

6.2 Suggestions for Further Work

Although this paper on the geochemistry and geochronology of the Shelburne and Messejana Dykes has answered many questions, it has also posed some new ones that could be the basis for future projects. The most intriguing question is, why the intrusion of the Shelburne Dyke did not reset the argon in the biotites from the Meguma Group.

Another interesting problem is why some of the tectono-discriminator diagrams suggest the Shelburne Dyke was formed by subduction processes. Further geochemical work might resolve the origin of the subduction component.

REFERENCES

Alibert C (1985) A Sr-Nd isotope and REE study of the Late Triassic dolerites from the Pyrenees (France) and the Messejana Dyke (Spain and Portugal). Earth Planet Sci Lett 73:81-90

Brak-Lamy J (1949) A composicao quimica do dolerito pigeonitico da Derroca (Odemira). Bol Mus Lab Min Geol 17:11-18

Check G (1989) $^{40}Ar/^{39}Ar$ Thermochronology of the Britt Domain Grenville Province-Georgian Bay, Ontario. BSc Thesis, Dalhousie University, Halifax, Nova Scotia, 55p

Clarke DB, Chatterjee AK, Giles PS (1993) Petrochemistry, tectonic history, and Sr-Nd systematics of the Liscomb Complex, Meguma Lithotectonic Zone, Nova Scotia. Can J Earth Sci 30:449-464

Clarke DB, Cameron BI, Muecke GK, Bates JL (1988) Early Tertiary basalts from the Labrador sea floor and Davis Strait region. Can J Earth Sci 26:956-968

Clarke DB, Halliday An (1985) Sm/Nd isotopic investigation of the age and origin of the Meguma Zone metasedimentary rocks. Can J Earth Sci 22:102-107

Clarke DB (1970) Tertiary basalts of Baffin Bay: possible primary magma from the mantle. Contr Mineral Petrol 25:203-224

Cummins L, Arthur J, Ragland P (1992) Classification and Tectonic Implications for Early Mesozoic Magma types of the Circum-Atlantic. In: Eastern North American Mesozoic Magmatism. Puffer JH, Ragland PC (eds) Geological Society of America, Boulder, Colorado, pp 119-135

Dallmeyer RD (1979) $^{40}Ar/^{39}Ar$ Dating: Principles, techniques and applications in orogenic terranes. In: Lectures in Isotope Geology. Springer-Verlag, Berlin pp 77-100

Dalrymple GB, Lanphere, MA (1969) Potassium-Argon Dating, Principles, techniques and applications to geochronology. WH Freeman and Company, San Francisco

Dodson MH (1973) Closure temperatures in cooling geochronological and petrological systems. Contr Mineral Petrol 40:259-274

Dostal J, Grenough JD (1992) Geochemistry and Petrogenesis of the Early Mesozoic North Mountain basalts of Nova Scotia, Canada. In: Eastern North American Mesozoic Magmatism. Puffer JH, Ragland PC (eds) Geological Society of America, Boulder, Colorado, pp 149-159

Faribault ER (1919) Investigations in Southwestern Nova Scotia. Geological Survey of Canada, Summary Report 1919, Part F:2-20

Faribault ER (1913) Geology of the Port Mouton area, Queen's County, Nova Scotia. Geological Survey of Canada Summary Report 1913, Sessional paper 26:251-258

Faribault ER (1911) Gold-bearing series of the basins of Medway River, Nova Scotia. Geological Survey of Canada Summary Report 1911 Sessional Paper 26:334-340

Faure G (1977) Principles of Isotope Geology. J. Wiley and Sons, Inc. New York

Feio M (1951) A evolucao do relevo do Baixo Alentejo e Algarve. Com Serv Geol Portugal 32:303-477

Fleck RJ, Sutter JF, Elliot DH (1977) Interpretation of discordant $^{40}Ar/^{39}Ar$ age spectra of Mesozoic tholeiites from Antarctica. Geochim et Cosmochim 451:15-32

Fukuzawa M (1988) K/Ar dating of the Messejana Dike, Spain and Portugal. BSc Thesis, University of Western Ontario, London, Ontario, 53 p

Garcia de Figuerola (1965) La continuacion hacia el SW del dique basico de Plasencia (Caceres). Not Com Inst Geol Minero Espana 69:1129-164

Hall A (1987) Igneous Petrology. John Wiley and Sons, New York

Harland Brian et al. (1990) A geologic time scale 1989. Cambridge University Press, New York

Harrison TM (1981) Diffusion of ^{40}Ar in hornblende. Contr Mineral Petrol 78:324-331

Hawkesworth CJ, Norry MJ (eds) (1983) Continental Basalts and Mantle Xenoliths. Shiva Publishing Limited, United Kingdom

Hess HH and Poldervaart A (eds) (1967) Basalts: The Poldervaart Treatise on rocks of basaltic composition v1. John Wiley and Sons, New York

Hodych JP and Hayastu A (1980) K-Ar isochron age and paleomagnetism of diabase along the trans-Avalon aeromagnetic linement-evidence of Late Triassic rifting in Newfoundland. Can J Earth Sci 17:491-499

Hozik J (1992) Paleomagnetism of Igneous Rocks in the Culpeper, Newark, and Deerfield Basins. In: Eastern North American Mesozoic Magmatism. Puffer JH, Ragland PC (eds) Geological Society of America, Boulder, Colorado pp 279-308

Irvine TN, Baragar WRA (1971) A guide to the chemical classification of the common rocks. Can J Earth Sci 8:523-548

Keppie JD, Dallmeyer RD (1987) Dating transcurrent terrane accretion: an example from the Meguma and Avalon composite terranes in the northern Appalachians. Tectonics 6:831-847

Keppie JD (1979) Geological Map of the Province of Nova Scotia, 1:500,000. Nova Scotia Department of Mines, Halifax, Nova Scotia

Larochelle A, Wanless RK (1966) The paleomagnetism of a Triassic diabase dike in Nova Scotia. J Geophys Res 71:4949-4953

Lawrence DE (1966) A contribution to the Great Dike of Nova Scotia. MSc Thesis, Dalhousie University, Halifax, Nova Scotia 108p

McDougall I, Harrison TM (1988) Geochronology and thermochronology by the $^{40}Ar/^{39}Ar$ method. Oxford University Press, New York

Meschede MS (1986) A method of discriminating between different types of mid-ocean ridge basalts and continental tholeiites with Nb-Zr-Y diagram. Chem Geol 56:207-218

Mohr P (1982) Musings on Continental Rifts. In: Continental and Oceanic Rifts Palmason G (eds) American Geophysical Union Washington D.C. pp 293-309

Muecke GK, Elias P, Reynolds PH (1988) Hercynian/Alleghanian overprinting of an Acadian terrane: $^{40}Ar/^{39}Ar$ studies in the Meguma Zone, Nova Scotia, Canada Chem Geol 73:153-167

Mullen ED (1983) $MnO-TiO_2-P_2O_5$: a minor element discriminant for basaltic rocks of oceanic and environments and its implications for petrogenesis. Earth Planet Sci Lett 62:53-62

Papezik VS, Barr SM (1981) The Shelburne dike, an Early Mesozoic diabase dike in Nova Scotia: mineralogy, chemistry, and regional significance. Can J Earth Sci 18:1346-1355

Papezik VS, Hodych JP, Goodacre AK (1975) The Avalon magnetic linement-a possible continuation of the Triassic dike system of New Brunswick and Nova Scotia. Can J Earth Sci 12:332-335

Pearce JA (1983) The role of sub-continental lithosphere in magma genesis at destructive plate margins. In: Continental basalts and mantle xenoliths. Hawkesworth CJ, Norry MJ (eds) Shiva Publishing Limited, United Kingdom pp 230-249

Pearce JA, Norry MJ (1979) Petrogenetic implications of Ti, Zr, and Nb variations in volcanic rocks. Contr Mineral Petrol 69:33-47

Pearce JA, Gorman BE, Birkett TC (1977) The relationship between major element chemistry and tectonic environment of basic and intermediate volcanic rocks. Earth Planet Sci Lett 36:121-132

Pearce JA, Cann JR (1973) Tectonic setting of basic volcanic rocks determined using trace element analysis. Earth Planet Sci Lett 19:290-300

Pe-Piper G, Jansa L, Lambert R (1992) Early Mesozoic magmatism on the Eastern Canadian Margin: petrogenetic and tectonic significance. In: Eastern North American Mesozoic Magmatism. Puffer JH, Ragland PC (eds) Geological Society of America, Boulder, Colorado pp 13-36

Puffer H (1992) North American flood basalts in the context of the incipient breakup of Pangea. In: Eastern North American Mesozoic Magmatism. Puffer JH, Ragland PC (eds) Geological Society of America, Boulder, Colorado pp 95-118

Quesada Garcia A (1960) Falla de desgarre en el S-W de la Peninsula Iberica. Not Com Inst Geol Minero Espana 58:163-182

Schenk PE (1991) Events and sea-level change on Gondwana's margin: the Meguma Zone (Cambrian-Devonian) of Nova Scotia, Canada. Geol Soc of American Bull 103:512-521

Schenk PE, Lane TE (1982) Pre-Acadian sedimentary rock of the Meguma Zone, Nova Scotia- a passive continental margin juxtaposed against a volcanic island arc. International Association of Sedimentologists, Excursion 5B Guidebook 85p

Schermerhorn LSB et al. (1978) Age and origin of the Messejana dolerite fault-dike system (Portugal and Spain) in the light of the opening of the North Atlantic Ocean. J of Geol 86:294-304

Schott M, Thuizat (1981) Paleomagnetism and potassium-argon of the Messejana Dike (Portugal and Spain): angular limitation to the rotation of the Iberian Peninsula since the Middle Jurassic. Earth Planet Sci Lett 53:457-470

Shervais JW (1982) Ti-V plots and the petrogenesis of modern and ophiolitic lavas. Earth Planet Sci Lett 57:101-118

Sibuet JC (1992) Formation of non-volcanic passive margins: A composite model applies to the conjugate Galicia and Southeastern Flemish Cap Margins. Geophys Res Lett 19:769-772

Sibuet JC (1989) Paleoconstraints during rifting of the Northeast Atlantic passive margins. J Geophys Res 94:7265-7277

Soares De Andrade AA (1972) Sur l'age Permien inferieur d'une intrusion doleritique a Portel, Alentejo (filon de Messejana). Revista Fac Cienc 17:237-242

Tate M, Clarke DB (1994 in preparation) Petrogenesis and regional significance of Late Devonian mafic intrusions in the Meguma Zone, Nova Scotia Canada

Teixeria C, Torquato JR (1975) Nouvelles donnees sur l'age du grand filon doleritique de Vila do Bispo-Placencia. Bol Soc Geol Portugal 19:99-101

Torre De Assuncao, Correia Perdigao J (1962) Sobre o prolongamento do alinhamento filoniano doleritico de Odemira-Vidigueira ate Ouguela. Com Serv Geol Portugal 46:349-363

Torre De Assuncao C (1957) Rochas gabroicas e anortositicas do Alto Alentejo. Assoc Portuguesa Progresso Cienc 5:23-28

Torre De Assuncao C (1951a) Os doleritos pigenoniticos de quimismo pacifico do sul de Portugal. Bol Mus Lab Min Geol 19:109-117

Torre De Assuncao C (1951b) Doleritos da regiao de Aljustrel. Bol Mus Lab Min Geol 19:119-122

Torre De Assuncao C (1949) Sobre uma intrusao doleritica no Antracolitico do Baixo-Alenjo. Bol Soc Portuguesa Cienc Naturais 2:66-74

Wark JM, Clarke DB (1980) Geochemical discriminators and petrogenesis of the North Mountain basalts, Nova Scotia. Can J of Earth Sci 17:1740-1745

Wood DA (1980) The application of a Th-Hf-Ta diagram to problems of tectonomagmatic classification and to establishing the nature of crustal contamination of basaltic lavas of the British Tertiary volcanic province. Earth Planet Sci Lett 50:11-30

York D (1984) $^{40}Ar/^{39}Ar$ Dating: Principles, techniques, and applications in orogenic terranes. In: Lectures in Isotope Geology. Springer-Verlag pp 77-100

Zbyszewski G, Freire de Andrade R (1957) Nota preliminar sobre a geologia da regiao de Aljustrel. Assoc Portuguesa Progresso Cienc 5:5-13

Ziegler PA (1989) Evolution of the North Atlantic Ocean- An overview. In: Extensional tectonics and stratigraphy of the North Atlantic Margins. Innkard AJ, Balkwill HR (eds) American Association of Petroleum Geologists and the Canadian Geological Foundation pp 110-130

Ziegler PA (1988) Post Hercynian plate reorganization in the Tethys and Arctic-North Atlantic. In: Triassic-Jurassic rifting events leading to continental break-up and the origin of the Atlantic passive margin. Manspeizer (ed) Elsevier Amsterdam

Ziegler PA (1982) Geological Atlas of Western and Central Europe. Elsevier Amsterdam

Appendix A- Thin Section Description

The following petrological description is based on the analysis of five thin sections. The label 'SD' denotes a sample from the Shelburne Dyke and 'MD' denotes a sample from the Messejana Dyke.

SD93-1

Minerals- Plagioclase- An_{47}- 15-20% of minerals
- Pyroxene- Orthopyroxene- 10-15%
  - Augite - 5%
- Olivine- Altered to iddingsite- < 5%

Texture- Subophitic
- Glomeroporphyritic (groups of minerals)

Groundmass- Cryptocrystalline texture

Comments- Fine-grained (from chilled margin)
- Minerals are microphenocrysts
  - Minerals are inequigranular
  - Minerals comprise 30-40% of rock
  - Subhedral to euhedral crystals
- Oscillatory zoning and twinning seen

SD93-4

Minerals- Biotite- 20-30% of minerals
- Chlorite- 5-10%
- Opaques- 5-10%
- Muscovite- < 5%

Texture- Foliated metapelite

Groundmass- Micro-cryptocrystalline texture

Comments- Meguma sample
- Biotites are ovoid porphyroblasts
- Minerals comprise 40-50% of rock

- Anhedral to subhedral crystals

SD93-6

Minerals- Plagioclase- An_{55-59}- 35-40% of minerals
- Pyroxene- Clinopyroxene- 40-45%
- Biotite- 5-10%
- Opaques- 5-10%
- Olivine- < 5%

- Micrographic intergrowth of quartz and feldspar < 1%

Texture- Subophitic to ophitic

Groundmass- None

Comments- Coarse-grained (from center of the dyke)
- Minerals are equigranular
- Subhedral to euhedral crystals
- Oscillatory zoning and twinning seen

SD93-7

Minerals- Plagioclase- An_{47}- 15-20% of minerals
- Pyroxene- Orthopyroxene- 10-15%
  - Augite - 5%
- Olivine- Altered to iddingsite- < 5%

Texture- Subophitic
- Glomeroporphyritic (groups of minerals)

Groundmass- Cryptocrystalline texture

Comments- Same as slide SD93-1
- Fine-grained (from chilled margin)
- Minerals are microphenocrysts
  - Minerals are inequigranular
  - Minerals comprise 30-40% of rock
  - Subhedral to euhedral crystals
- Oscillatory zoning and twinning seen

MD93-1

Minerals- Plagioclase- An_{52}- 60-70% of minerals
- Pyroxene- Clinopyroxene- 20-30%
- Opaques- 5%
- Biotite- 5%
- Chlorite- < 5%

Texture- Subophitic to ophitic
- Late poikilitic- small plagioclase enclosed by pyroxene

Groundmass- None

Comments- Medium to coarse-grained (from center region of dyke)
- Minerals are inequigranular
- Subhedral to euhedral crystals
- Oscillatory zoning and Carlsbad twinning seen

Appendix B- $^{40}Ar/^{39}Ar$ Analysis Summary Sheets

SD93-6 BIOTITE SUMMARY

oC	mV 39	% 39	AGE (Ma)	% ATM	37/39	36/40	39/40	% IIC
650	3.1	4.3	240.3 +/- 63.9	83.5	1.19	.002826	.002386	.2
700	5.6	8	230.4 +/- 22.3	71	.39	.002403	.004388	.07
750	8.8	12.5	148 +/- 8.5	72.2	.47	.002446	.006685	.11
800	5.4	7.7	232.8 +/- 6.3	29.8	.14	.00101	.010504	.02
850	8.1	11.5	232.1 +/- 4.2	28.2	.16	.000955	.010782	.02
900	5.1	7.2	163.7 +/- 18.2	40	.24	.001355	.013022	.05
950	4.2	6	221.7 +/- 4.8	20.4	.3	.000692	.012547	.05
1000	15.8	22.3	208.5 +/- 2	7.3	.49	.000248	.015603	.09
1100	13.3	18.8	204.1 +/- 2.9	11.1	.85	.000377	.015303	.16
1200	.9	1.3	237.3 +/- 23.9	75.4	12.66	.002552	.003608	2.23

TOTAL GAS AGE = 206 Ma

J = .002064

ERROR ESTIMATES AT ONE SIGMA LEVEL

37/39,36/40 AND 39/40 Ar RATIOS ARE CORRECTED FOR INTERFERING ISOTOPES

% IIC - INTERFERING ISOTOPES CORRECTION

SD93-1 WHOLE ROCK SUMMARY

oC	mV 39	% 39	AGE (Ma)	% ATM	37/39	36/40	39/40	% IIC
550	4.3	2.7	193.5 +/- 11.8	44.6	5.21	.00151	.010091	1.05
600	7.8	4.9	230.4 +/- 7.2	37.4	7.21	.001268	.009468	1.29
650	9.5	6	245.5 +/- 2.5	29	8.33	.000984	.010037	1.43
700	7.4	4.6	209.9 +/- 7.5	32.4	8.57	.001098	.011294	1.64
750	7.3	4.6	258.5 +/- 9.1	37.8	10.19	.001281	.008319	1.69
800	8.4	5.2	208.8 +/- 4.8	41.8	12.16	.001416	.009777	2.33
850	12.8	8	211.3 +/- 2.9	29.9	11.81	.001014	.011625	2.25
900	18.5	11.6	249.7 +/- 3.3	31.2	8.46	.001056	.009556	1.44
950	14.7	9.2	196.3 +/- 3.1	31.6	7.77	.001071	.012261	1.56
1000	13.1	8.2	191.2 +/- 2.6	24.7	8.61	.000836	.013891	1.76
1050	11.2	7.1	185.4 +/- 2.4	25.9	12.36	.000878	.014112	2.59
1100	9.4	5.9	175.3 +/- 3.9	34.3	25.27	.001162	.013279	5.51
1150	6.8	4.3	191 +/- 4.3	27.2	38.75	.000925	.013432	7.94
1250	15.3	9.6	207.4 +/- 4.4	48.9	53.74	.001656	.008647	10.38
1350	11.6	7.3	217 +/- 12.4	74.2	63.5	.002513	.004153	11.89

TOTAL GAS AGE = 212.6 Ma

J = .002064

ERROR ESTIMATES AT ONE SIGMA LEVEL

37/39,36/40 AND 39/40 Ar RATIOS ARE CORRECTED FOR INTERFERING ISOTOPES

% IIC - INTERFERING ISOTOPES CORRECTION

MD-93-1 BIOTITE SUMMARY

oC	mV 39	% 39	AGE (Ma)	% ATM	37/39	36/40	39/40	% IIC
600	.7	.8	10 +/- 138.9	98.1	.57	.003321	.006841	1.64
700	3.7	4.4	412.5 +/- 23.5	26.6	.14	.0009	.005893	.01
800	12.4	14.6	241.4 +/- 3	13.9	.04	.000472	.012397	0
900	20	23.4	217.9 +/- 2.2	10.2	.02	.000345	.014427	0
1000	36.1	42.3	209.3 +/- 1.2	4.6	.04	.000157	.015986	0
1100	11.4	13.4	203.6 +/- 3	12.9	.17	.000439	.015022	.03
1200	.5	.6	76.8 +/- 74	92.2	6.37	.003123	.003656	2.7

TOTAL GAS AGE = 222.2 Ma

J = .002064

ERROR ESTIMATES AT ONE SIGMA LEVEL

37/39,36/40 AND 39/40 Ar RATIOS ARE CORRECTED FOR INTERFERING ISOTOPES

% IIC - INTERFERING ISOTOPES CORRECTION

MD93-1 FELSICS SUMMARY

oC	mV 39	% 39	AGE (Ma)	% ATM	37/39	36/40	39/40	% IIC
550	6.5	2.2	131.6 +/- 6.5	56.3	5.53	.001908	.011885	1.5
600	8	2.7	164.6 +/- 4.7	47.9	6.79	.001621	.011248	1.55
650	11.6	4	185.1 +/- 3.2	39.6	8.48	.001342	.011515	1.77
700	7.9	2.7	186.4 +/- 5	34	7.86	.001152	.012501	1.64
750	20.7	7.1	206.8 +/- 2.3	29.6	6.8	.001004	.011943	1.31
800	22.6	7.7	195 +/- 1.9	22	6.09	.000747	.014081	1.23
850	21.3	7.3	187.6 +/- 1.7	14.8	4.09	.000501	.016036	.85
900	41.6	14.3	175.2 +/- 1	10.5	2.23	.000357	.018086	.48
950	44.5	15.3	175.3 +/- 1	10.1	2.19	.000344	.018158	.47
1000	33.8	11.6	169.5 +/- 1.2	11.4	1.98	.000386	.01855	.44
1050	27.5	9.4	162.9 +/- 1.3	14.2	2.45	.000483	.018714	.56
1125	24.9	8.5	160.8 +/- 1.9	26.4	8.75	.000896	.016268	2.03
1200	14	4.8	196.9 +/- 5.8	57.8	37.05	.001959	.007533	7.43
1300	5.1	1.7	940.7 +/- 87.1	22.8	92.65	.000773	.002325	8.14

TOTAL GAS AGE = 194.1 Ma

J = .002064

ERROR ESTIMATES AT ONE SIGMA LEVEL

37/39,36/40 AND 39/40 Ar RATIOS ARE CORRECTED FOR INTERFERING ISOTOPES

% IIC - INTERFERING ISOTOPES CORRECTION

SD93-4 BIOTITE SUMMARY

oC	mV 39	% 39	AGE (Ma)	% ATM	37/39	36/40	39/40	% IIC
650	204.4	20.5	365.9 +/- 1.6	1.7	0	.000059	.009015	0
700	194.8	19.6	371 +/- 1.6	.8	0	.000027	.008965	0
750	125.8	12.6	373.5 +/- 7	1.2	.01	.000043	.008854	0
800	89.8	9	370.5 +/- 1.7	1.2	.01	.000042	.008935	0
850	145.1	14.6	371.6 +/- 1.6	.8	.02	.000029	.008944	0
900	110	11	371.5 +/- 1.6	1.5	.02	.000051	.008886	0
950	35.2	3.5	375.5 +/- 2.4	2.7	.03	.000094	.008667	0
1000	32.4	3.2	385.7 +/- 2.4	1.4	.01	.00005	.008526	0
1050	34.8	3.5	379.6 +/- 2.5	1.8	.02	.000064	.008644	0
1100	11.8	1.1	389.9 +/- 3.8	3.8	.06	.000128	.008227	0
1150	6.7	.6	388.1 +/- 10.8	17.4	.07	.000589	.007096	.01
1250	2.6	.2	480.7 +/- 52	40.4	.08	.001369	.004024	.01

TOTAL GAS AGE = 371.9 Ma

J = .002064

ERROR ESTIMATES AT ONE SIGMA LEVEL

37/39,36/40 AND 39/40 Ar RATIOS ARE CORRECTED FOR INTERFERING ISOTOPES

% IIC - INTERFERING ISOTOPES CORRECTION